DROSOPHILA MUSCLE COFILIN MAINTAINS NEUROMUSCULAR JUNCTION STRUCTURE FOR PROPER NEUROTRANSMISSION

A Dissertation

Presented to the Faculty of the Weill Cornell Graduate School

of Medical Sciences

in Partial Fulfillment of the Requirements for the Degree of

Doctor of Philosophy

by

Briana Christophers

May 2024

DROSOPHILA MUSCLE COFILIN MAINTAINS NEUROMUSCULAR JUNCTION STRUCTURE FOR PROPER NEUROTRANSMISSION

Briana Christophers, Ph.D.

Cornell University, 2024

The actin-severing protein cofilin plays pivotal roles in actin cytoskeletal dynamics. Previously, our lab has shown that muscle-specific knockdown of *Drosophila* cofilin (*DmCFL*) leads to a progressive decline in larval muscle structure and function due to defective addition and maintenance of sarcomeres during growth. A similar deterioration is seen in the muscle disorder nemaline myopathy (NM) resulting from cofilin mutations. Given the importance of actin throughout the cell, I hypothesized that *DmCFL* knockdown would impact other aspects of muscle development. Consequently, I conducted an RNA sequencing analysis, which showed upregulation of genes associated with the neuromuscular junction (NMJ). The NMJ is the site of communication between the presynaptic motor neuron and postsynaptic muscle membrane. In this work, I found that DmCFL is enriched at the postsynaptic compartment, and its loss precipitates disorganization of F-actin prior to sarcomeric defects seen in the *DmCFL* KD model. Surprisingly, I did not observe significant changes in gross presynaptic Bruchpilot active zones or overall postsynaptic glutamate receptor levels. There is, however, a reduction and mislocalization of GluRIIA-containing glutamate receptors in *DmCFL* KD, resulting in a pronounced impairment in neurotransmission strength. These findings expand our understanding of cofilin's roles in muscle to include NMJ structural development and suggest that NMJ defects may contribute to NM pathophysiology.

BIOGRAPHICAL SKETCH

Briana (Bri) Christophers was born in Miami, Florida in 1995. She is the daughter of Marlene and Franklin Christophers and older sister to Jeffrey and David Christophers. She discovered her love of biology during her first year of high school at Ransom Everglades School.

She earned her Bachelor of Arts in Molecular Biology from Princeton University, where she developed a passion for developmental biology and social justice. From sophomore to senior year, she worked in the laboratory of Rebecca Burdine, PhD. Her senior thesis work was an examination of FGF signaling in heart development using a zebrafish model. In this work, she found that FGF signaling is important for proper cardiac tissue morphogenesis, including during looping and ballooning. Briana served as co-president and advocacy chair of Princeton Latinos y Amigos and co-founded Project Welcome Mat: A Guide for First-Generation Students. Her advocacy work at Princeton was recognized with the Frederick Douglass Service Award, the Spirit of Princeton Award, and the Santos-Dumont Award for Innovation. After Princeton, Briana pursued further scientific training in developmental biology as a research technician at the Children's Hospital of Philadelphia (CHOP) Research Institute. Under the guidance of Robert Heuckeroth, MD, PhD, she studied enteric nervous system (ENS). The work focused on potential therapeutics for ENS regeneration at the distal colon in a mouse model of Hirschsprung Disease, a birth defect with unknown etiology.

Blending her scientific interests with her growing ideas on how to transform the scientific and medical landscape for marginalized black, indigenous, and other people of color (BIPOC), she decided to pursue dual MD-

PhD training at the Weill Cornell/Rockefeller/Sloan Kettering Tri-Institutional Program (Tri-I) in New York City. She pursued her thesis research in the lab of Mary Baylies, PhD, at Sloan-Kettering Institute. In 2023, Briana was awarded the National Institutes of Health F30 individual trainee fellowship for her research. She also orchestrated and participated in community efforts as a co-leader of the Association of Diverse Physician-Scientists in Training (ADePT), a former committee chair in the American Physician Scientists Association (APSA), and a volunteer in student-led clinics and migrant shelters.

Since she joined the Tri-I community in 2018, Briana has honed her voice in academic medicine to consistently engage and empower other trainees, medical and scientific professionals, and patients. In response to disparities in access to information and preparedness for medical school admissions, she co-created “The Free Guide to Medical School Admissions,” and, during the COVID-19 pandemic, she helped develop a national virtual summer research program for undergraduate students through APSA. Briana has collaborated with medical trainees and physicians nationwide to determine how medical education and, specifically, physician-scientist training can be more socially equitable. She has become an expert in the medical education field, conducting up-to-date studies revealing inequities in medical school admissions for low-income and BIPOC applicants, while putting forth actionable steps for institutes to achieve an inclusive admissions process and supportive training environment for first-generation and marginalized people. Her work has been published in *JAMA*, *Nature Medicine,* and *Journal of Clinical Investigation,* among other journals. Fueled by chocolate, an unwavering purpose, and naps, Briana is a leader in academic medicine who aims to represent and supports others throughout her career as a physician-scientist.

ACKNOWLEDGMENTS

I have many people to thank for their support and guidance throughout my life and training thus far.

First, there are no words to convey the thanks that I owe to my family and friends for everything. To my parents and brothers: your love, guidance, and nurturing of my curiosity have shaped who I am today. Thank you to Edwin for being my anchor, and I am endlessly grateful for his unwavering support as we navigate life together. Thanks to my friends Kauribel, Nick, Sam, Adalberto, Debby, and Rocío for making me a better person and for your understanding even after I repeatedly disappear off the face of the planet. A deep and heartfelt thank you to Victoria for being my scientific advisor, sounding board, co-chef, and cherished friend.

I am indebted to the Baylies lab for fostering a supportive and encouraging environment, providing the space for my growth as a scientist over the past few years. Special thanks to Dr. Carolina Zapater i Morales and Therandë Jashari for their invaluable advice, astute observations, motivational pep talks, and daily doses of quick wit. Thank you to David Soffar for teaching me everything I know about fly genetics and care, for his laughter, and for keeping all of us up to date on the latest news. I extend my appreciation to Dr. Bianca Borchin, Cassie Manrique, Exequiel Sisso, Isabelle Top, Marco Gualtieri, Nicole Torres-Santiago, Dr. Patrick Busch, Ruth Silimon, and Dr. Stefanie Windner for making my time in the Baylies lab a positive experience and for always being inquisitive. Thanks to Rishi Ravichandran and Miguel Gomez for keeping our flies healthy,

well fed, and happy. I also value Meg Distinti for always being there to lend a helping hand. I am incredibly grateful for Dr. Mary Baylies for her guidance as my advisor, for how she has pushed me to keep going during the ups and downs of this project, and for her support in my growth as a developmental biologist and physician-scientist. I also appreciate the insightful questions and guidance from my thesis committee members—Drs. Amy Shyer, Geoffrey Pitt, and Jennifer Zallen.

Thanks to my pre-PhD advisors who helped me find my way to becoming a scientist. Thank you to Dr. Rebecca Burdine for inspiring me to continue in developmental biology and to Dr. Meagan Grant for taking me under your wing to teach me everything you know. Thanks to Dr. Robert Heuckeroth for seeing my potential as a future physician-scientist and to Dr. Sabine Schneider for being a teacher and role model. Additionally, I extend my gratitude to the Tri-Institutional MD-PhD program and to my cohort for being there every step of the way as we make it along this long training path.

This work was funded by the Medical Scientist Training Program grant from the National Institute of General Medical Sciences of the National Institutes of Health under award number T32GM007739 to the Weill Cornell-Rockefeller-Sloan Kettering Tri-Institutional MD-PhD Program; the Training Program in Developmental and Stem Cell Biology grant from the National Institute of Child Health and Human Development under award number T32HD060600; and the National Research Service Award (NRSA) Individual Fellowship award from the National Institute of Child Health and Human Development under award number F30HD111309-01.

TABLE OF CONTENTS

LIST OF FIGURES

LIST OF TABLES

LIST OF ABBREVIATIONS

Abbreviation	Term
ABP	Actin-binding protein
Ach	Acetylcholine
AchE	Acetylcholinesterase
AchR	Acetylcholine receptor
ADF	Actin depolymerizing factor
AIP	Actin-interacting protein
AMPAR	AMPA receptors
Brp	Bruchpilot
CFL2	Cofilin-2
Cora	Coracle
Dlg	Discs-large
DmCFL	*Drosophila* cofilin
DSHB	Developmental Studies Hybridoma Bank
ECC	Excitation-contraction coupling
EJC	Excitatory junction current
EMG	Electromyogram
F-actin	Filamentous actin
FCM	Fusion competent myoblast
G-actin	Globular actin
GFP	Green fluorescent protein
GluR	Glutamate receptor
GO	Gene ontology
GSEA	Gene set enrichment analysis
HRP	Horseradish peroxidase
ISN	Intersegmental nerve
KD	Knockdown
LIMK	LIM kinase
Mhc	Myosin heavy chain
Mrf	Myogenic regulatory factor
NCS	Nerve conduction studies
NM	Nemaline myopathy
NMJ	Neuromuscular junction
ORA	Overrepresentation analysis
p-DmCFL	Phosphorylated DmCFL
PSD	Postsynaptic density
PTM	Post-translational modification

RNAi	RNA interference
RNAseq	RNA sequencing
Ssh	Slingshot
SSR	Subsynaptic reticulum
TEM	Transmission electron microscopy
TEVC	Two-electrode voltage clamping
Tmod	Tropomodulin
Tsr	Twinstar
VL	Ventral longitudinal

CHAPTER 1:
INTRODUCTION

I. OVERVIEW

Proper skeletal muscle function is critical for daily life, as muscle contraction and relaxation are required for movement, posture, respiration, and energy metabolism. Coordinated muscle contraction and relaxation are required for gross and fine motor functions. Myopathies, or diseases that affect skeletal muscle, have serious negative impacts on these functions and, as such, quality of life. To identify the molecular underpinnings of these myopathies and find new ways to treat, we turn to model organisms.

In a screen for regulators of muscle development, our lab identified *twinstar* (*tsr*) also known as *Drosophila* cofilin (*DmCFL*), as important for proper muscle formation, patterning, and maintenance. *DmCFL* is the *Drosophila* homolog of *Cofilin-2* (*CFL2*), which encodes an actin-severing protein known to work at the muscle sarcomere, and mutations in this gene have been linked to nemaline myopathy (NM). NM is a skeletal muscle disorder that results in muscle weakness and is characterized by actin accumulations throughout the muscle which can be appreciated on histopathology. Previous work in our lab found that manipulating *DmCFL* levels specifically in muscle led to defective sarcomeric addition, resulting in a progressive loss of muscle cell integrity that mimics the degeneration in human NM.

The overarching purpose of my thesis work has been to expand our understanding of cofilin's role in muscle biology which may, in turn, provide new insights to the mechanism of NM. By mining an RNA sequencing data set, I compared gene expression changes seen in *DmCFL* knockdown larvae relative to control. This analysis highlighted changes in pathways related to the neuromuscular junction (NMJ), the site where the muscle receives signals from the motor neuron to contract. I confirmed the localization of DmCFL protein at the muscle-side of the NMJ (i.e. postsynapse) and observed a striking progressive actin accumulation phenotype at the NMJ when *DmCFL* is reduced in muscle. *DmCFL* KD produced structural and functional postsynaptic NMJ changes, which I found is related to changes in glutamate receptor GluRIIA subunit levels. This work furthers our understanding of cofilin in a disease model and what we know about actin at the NMJ.

Below, I introduce as context a comparison of vertebrate and *Drosophila* muscle and NMJ development. Additionally, I discuss the biochemical functions of actin and cofilin in addition to the results of affecting these in muscle. Finally, I include a more detailed description of the larval *DmCFL* knockdown model.

II. VERTEBRATE SKELETAL MUSCLE BIOLOGY AND PATHOLOGY

A. Muscle structure

Vertebrate muscle has marked complexity in order to produce maximum force for contraction (Figure 1.1). Skeletal muscle attaches to bone as an anchor point via its tendon. The muscle comprises various grouped fascicles held together

by the elastic epimysium. Each fascicle is made up of a bundle of muscle fibers (i.e. myofibers) ensheathed by the perimysium connective tissue. The fascicles also contain branches of the vascular and nervous systems. Each myofiber contains interconnected arrays of myofibrils, which are longitudinal chains of sarcomeres.

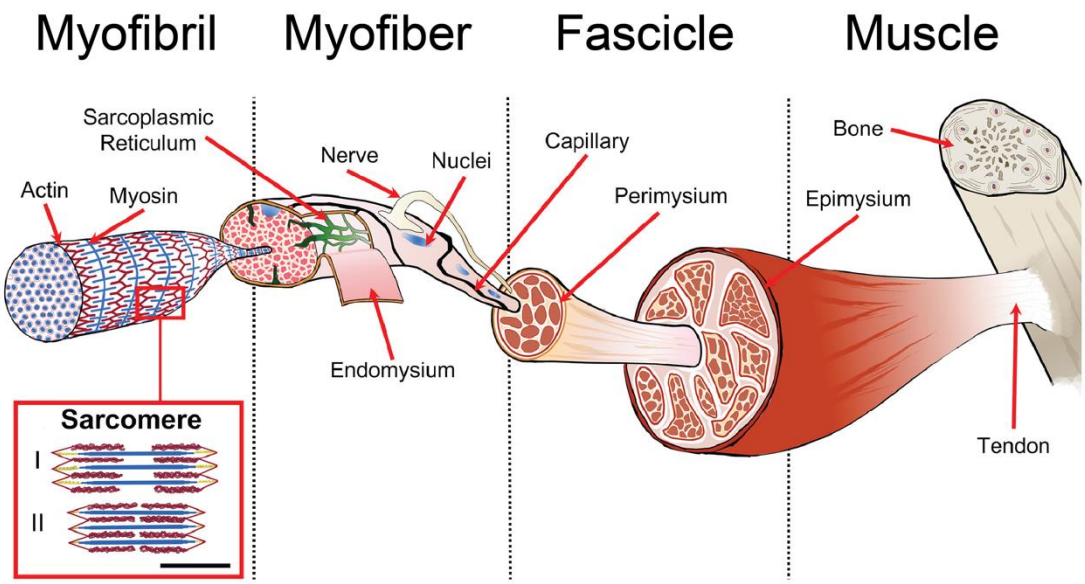

Figure 1.1: Layers of vertebrate skeletal muscle complexity. Reproduced with permission from (Gotti et al., 2020).

The sarcomere is the smallest contractile unit, whose contraction is a result of coordinated motion of the myosin thick filament along the actin thin filament (Figure 1.2). The Z-disc (also known as Z-disk or Z-band) binds to the muscle membrane at the costamere and serves as the border of the sarcomere since it is the anchor point for the thin filament. The thin filaments comprise F-actin filaments and actin-binding proteins necessary for anchoring and maintaining the filament's length. The barbed ends of the actin filament interact with the proteins at the Z-disc, while the pointed end faces the M-line and is the site of

both polymerization and depolymerization of the filament. The thick filament contains the myosin motors that bind the actin thin filament. Through their calcium-regulated powerstroke, myosins pull the filament toward the M-line at the middle of the sarcomere in a process called the “cross-bridge cycle” described by Huxley as the sliding model (A. F. Huxley & Niedergerke, 1954; A. F. Huxley, 1957; H. Huxley & Hanson, 1954). The shortening of the sarcomeres in the longitudinal direction leads to a pulling of the cell membrane by the Z-disc’s attachment to the costamere, causing the entire muscle cell to shorten and contract.

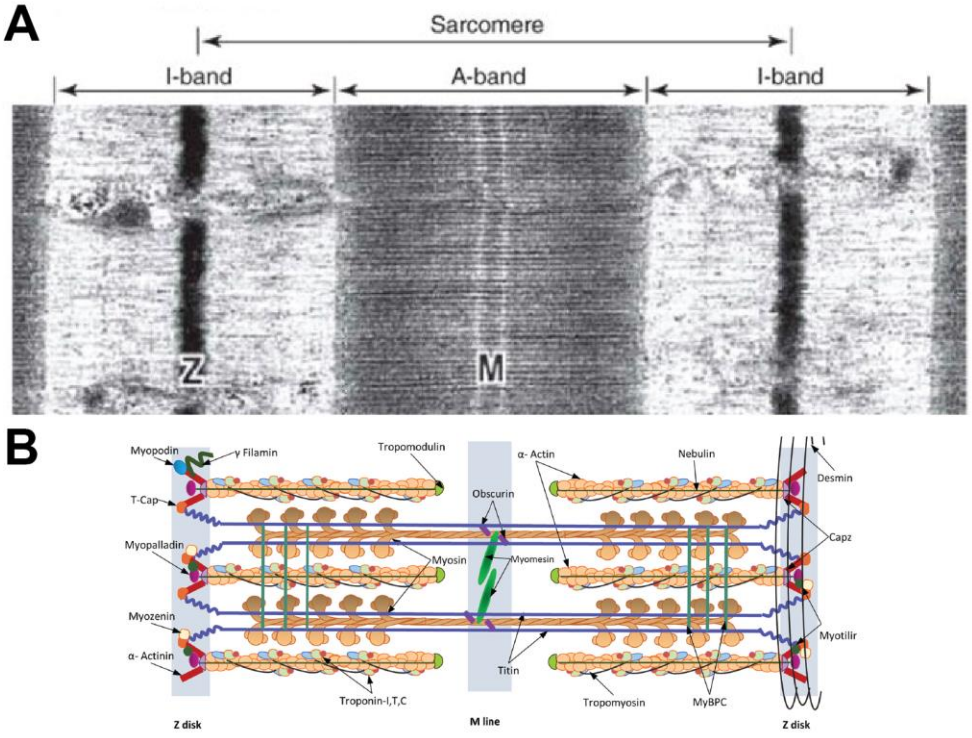

Figure 1.2: The sarcomere is the smallest contractile unit of muscle. (A) Electron micrograph of sarcomere. Z = Z-disc; M = M-line. Reproduced with permission (Henderson et al., 2017). (B) Schematic of single sarcomere, showing various proteins that comprise the Z-disc, thin filament, and thick filament. Reproduced with permission (Mukund & Subramaniam, 2020).

Myofibers belong to one of two classes: slow-twitch (Type I) or fast-twitch (Type II), which is further subdivided into Types IIA, IIB, and IIX. Fiber type is determined by several properties, including contraction time, speed of fatigue, metabolic profile, and myosin heavy chain expression [reviewed in (Talbot & Maves, 2016)]. Type I fibers are slow to fatigue and contract, and thus generate a low level of force over a longer period of time. To maintain this long period of activation, Type I fibers are highly vascularized and rely on oxidative metabolism requiring a high concentration of mitochondria. Meanwhile, Type II fibers contract and fatigue quickly, often relying on glycolytic metabolism, although Type IIA fibers may be oxidative. In humans, the balance of slow-twitch and fast-twitch fibers within a muscle varies by location of and demands on the muscle group. Some muscle diseases show biased deterioration of muscle fiber type. For example, Duchenne muscular dystrophy first targets Type II fibers while muscle inactivity tends to lead to Type I fiber atrophy. In nemaline myopathy, there is a disproportion in fiber types only when some genes are mutated.

B. Excitation-contraction coupling

The neural impulse that instructs muscles to contract originates at the motor cortex of the brain (Figure 1.3). The signal travels along upper motor neurons as they travel through the cerebral cortex, the brainstem, and the corticospinal tract of the spinal cord. The action potential is then propagated to the periphery by the lower motor neurons that branch off the spinal cord.

The lower motor neurons synapse with the muscle fibers, and this pairing is known as the motor unit (Zuccaro et al., 2021). Alpha-motor neurons innervate

the outer extrafusal fibers of the muscle which drive muscle contraction; different types of alpha-motor neurons innervate the slow- and fast-twitch fibers. Meanwhile, gamma-motor neurons play a regulatory role, as they synapse onto the intrafusal of the muscle spindle located in the interior of the muscle. The muscle spindle is sensitive to muscle stretch and tension in order to compensate for muscle length in order to maintain muscle tone over time (Wilkinson, 2021). In addition, the spindle is also sensitive to sensory information that is used for proprioception (Wilkinson, 2021).

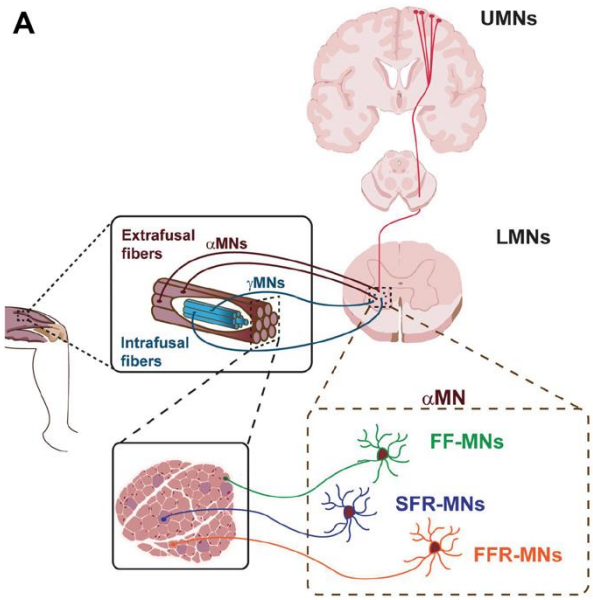

Figure 1.3: Motor system communication pathway. Schematic of central and peripheral motor system. MN = motor neuron, UMN = upper motor neuron, LMN = lower motor neuron. Reproduced with permission (Zuccaro et al., 2021).

Ultimately, communication between the motor neuron and the muscle leads to a process called excitation-contraction coupling [ECC; reviewed in (Shishmarev, 2020) and (Bolaños & Calderón, 2022)]. The site of ECC is at the neuromuscular junction (NMJ; Figure 1.4). The NMJ is a specialized synapse

where the motor neuron axon terminal is the presynaptic side (i.e. bouton) while the muscle is the postsynaptic side [reviewed in (Slater, 2015). In ECC, an electrical signal (i.e. neuron action potential) is transduced into a chemical signal (i.e. neurotransmitter release and binding) and then back to an electrical signal (i.e. muscle action potential) at the NMJ. Acetylcholine (Ach) is the principal excitatory neurotransmitter released at the vertebrate NMJ and its binding to nicotinic acetylcholine receptors (AchR) on the muscle triggers the downstream contraction cascade (Figure 1.5).

The presynaptic motor axon bouton is responsible for release of neurotransmitter. Ach is stored in various pools of synaptic vesicles: a readily-releasable pool, a storage reserve pool, and a recycling pool (Denker & Rizzoli, 2010). The actin cytoskeleton is critical for the formation and stabilization of the presynaptic bouton and forms a scaffold that traffics the synaptic vesicles (J. C. Nelson et al., 2013). The active zone is the site where synaptic vesicles dock and are released at the bouton. Vesicle docking and Ach release by exocytosis rely on SNARE proteins, syntaxin-1, and synaptotagmin in a calcium-dependent process (C.-T. Wang et al., 2006). Inactivation of Ach signal within the synaptic cleft occurs after the neurotransmitter is hydrolyzed by acetylcholinesterase (AchE); Ach is then recycled back into the presynapse (Soreq & Seidman, 2001).

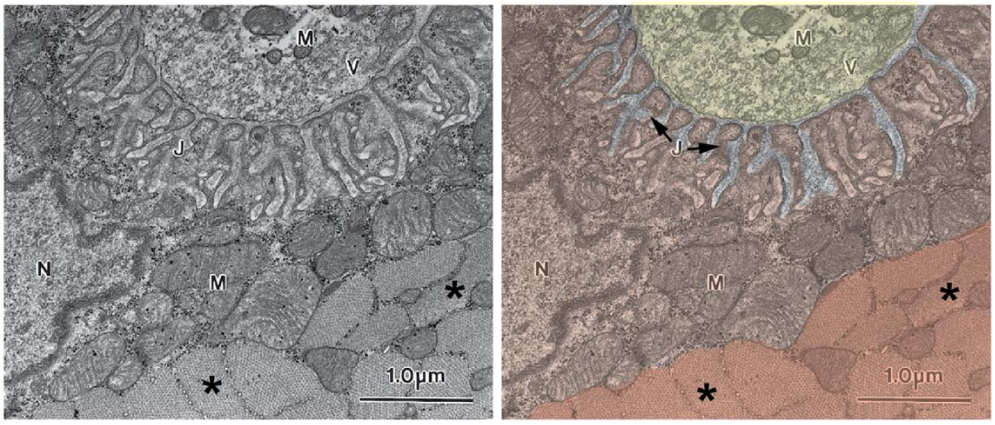

Figure 1.4: NMJ comprises motor neuron and muscle membrane. Left: Electron micrograph of the NMJ synapse. Right: same electron micrograph with structures highlighted. Red highlight = muscle postsynaptic side. Yellow highlight = motor neuron presynaptic side. Reproduced with permission (Fahim et al., 2000).

The muscle membrane is termed the sarcolemma, and, in the vertebrate, the postsynaptic sarcolemma that is in contact with the motor neuron is called the motor end plate. The sarcolemma below the bouton has various invaginations known as junctional folds (Figure 1.4). Components critical for ECC have special localizations at the junctional folds: at the crest are the clustered AchR and at the troughs are voltage-gated sodium channels (Fertuck & Salpeter, 1974; Martin, 1994).

The contraction cascade (Figure 1.5) is triggered by Ach binding to AchR, which as a ligand-gated cation channel allows sodium (and sometimes potassium, calcium, and magnesium) ions to enter the muscle cell. The change in the membrane potential leads to an activation of voltage-gated sodium channels (Na_v1s) to further depolarize the end plate potential (Bailey et al., 2003). The change triggers an action potential along the sarcolemma including the invaginations known as the T-tubules, causing another cascade of ion-driven

events (Rebbeck et al., 2014). Voltage-gated dihydropyridine receptors (DHPR) on the T-tubules let in calcium that then activate the ryanodine receptors (RYR) and STAC3 embedded in the terminal cisternae of the sarcoplasmic reticulum, where pools of calcium are stored (B. R. Nelson et al., 2013; Rebbeck et al., 2014). Calcium is dumped from the sarcoplasmic reticulum into the sarcoplasm (muscle cytoplasm) and taken up again by the SR/ER calcium ATPase (SERCA; B. R. Nelson et al., 2013; Rebbeck et al., 2014). The calcium binds to troponin which allows for access of the myosin-binding site on the actin filament and the formation of the cross-bridge between actin and myosin, which is needed for sarcomeric contraction.

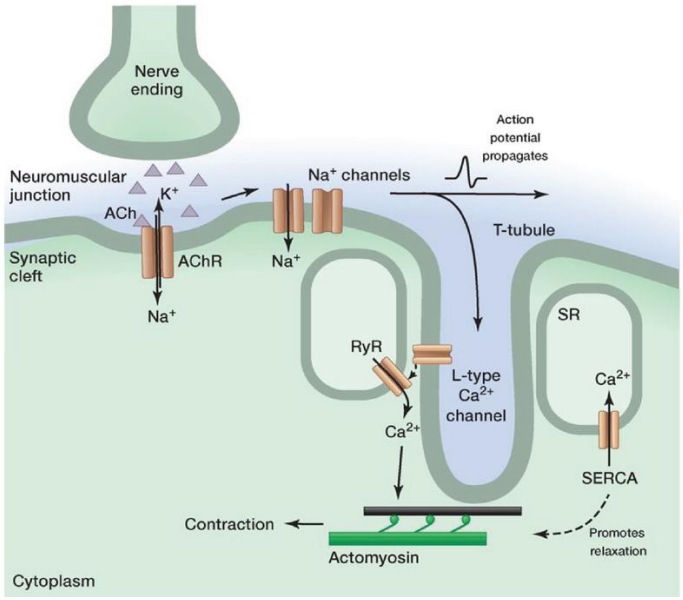

Figure 1.5: Excitation-contraction coupling. Binding of acetylcholine to its receptor on the muscle membrane triggers influx of cations (e.g. Na+) which depolarizes the muscle membrane, producing an action potential with downstream ion channel activation on the T tubule and sarcoplasmic reticulum (SR) and finally contraction. Reproduced with permission (Kuo & Ehrlich, 2015).

C. Muscle development

Vertebrate skeletal muscle development requires a complex coordination of gene expression transitions and cell-cell interactions. During the embryonic stage, different parts of the mesoderm germ layer give rise to the various muscle groups. Truck and limb muscle originate from paraxial mesoderm while head and neck muscles develop from pharyngeal mesoderm (Figure 1.6). The paraxial mesoderm lies lateral to on each side of the neural tube and is specified by Wnt and FGF signaling. The somites—transient structures that become the axial skeleton and skeletal muscle—form through a cycle of overlapping signaling pathways [reviewed in (Musumeci et al., 2015) and (Aulehla & Pourquié, 2006)]. The somites then subdivide into the dermomyotome in response to Wnt activation and BMP4 inhibition by Shh (Marcelle et al., 1997).

Next, myotome precursors from the hypaxial lateral dermomyotome migrate more ventrally, as they express the transcription factor PAX3 and later PAX7 (Figure 1.6B; Kassar-Duchossoy et al., 2005; Relaix et al., 2005; Tajbakhsh & Cossu, 1997). PAX3 and PAX7 also play a role in making the skeletal muscle resident stem cells, called muscle satellite cells, later in development [reviewed in (Buckingham, 2007)]. The activation of bHLH transcription factors triggers the formation of the myoblasts, the muscle progenitor cells (Andrikou & Arnone, 2015). The myogenic regulatory factors (Mrfs) Myf5 and MyoD are the determining factors in specifying myotome cells into myoblasts (Gerhart et al., 2006; Ott et al., 1991; Rudnicki et al., 1993; Tajbakhsh et al., 1997). Further differentiation of myoblasts is driven by MRF4 and myogenin, which are needed

along with MEF2 factors to eventually become myocytes (Hasty et al., 1993; Kassar-Duchossoy et al., 2004; Nabeshima et al., 1993; Venuti et al., 1995).

Myotubes form during embryogenesis by the fusion of myocytes and differentiate during primary myogenesis, resulting in multinucleate syncytial cell. Myotubes assemble a foundation upon which the adult skeletal muscle will be built. A three-step model has been proposed for myoblast fusion that incorporates evidence from *Drosophila*, zebrafish, and mouse studies [reviewed in (Kim et al., 2015)]. The first step is recognition between myocytes via cell adhesion molecules, then when cell membranes are proximal there is invasion and resistance experienced by the myocytes due to changes in the cortical cytoskeleton. Finally, work *in vitro* suggests that the destabilization of the lipid membrane as a necessary step. Fusion has been shown to require the multi-pass transmembrane protein Myomaker and the single-pass transmembrane protein Myomerger (also known as Myomixer and Minion), which are expressed during embryogenesis and needed later for postnatal growth (Bi et al., 2017; Cramer et al., 2020; Millay et al., 2013).

The vertebrate muscle forms during secondary myogenesis in the fetus by a process where more myotubes are added to the scaffold set by the primary myotubes. The growth and increase in muscle mass during this period is kept in check by myostatin (Tobin & Celeste, 2005). It is at this stage when the myotendinous junctions (where muscle attaches to tendon) and the neuromuscular junctions form. Postnatal maturation and growth occurs by hypertrophy by the addition of satellite cells (i.e. muscle stem cells); in mice, this

process only occurs up until P21, after which there is no further nuclear addition (White et al., 2010).

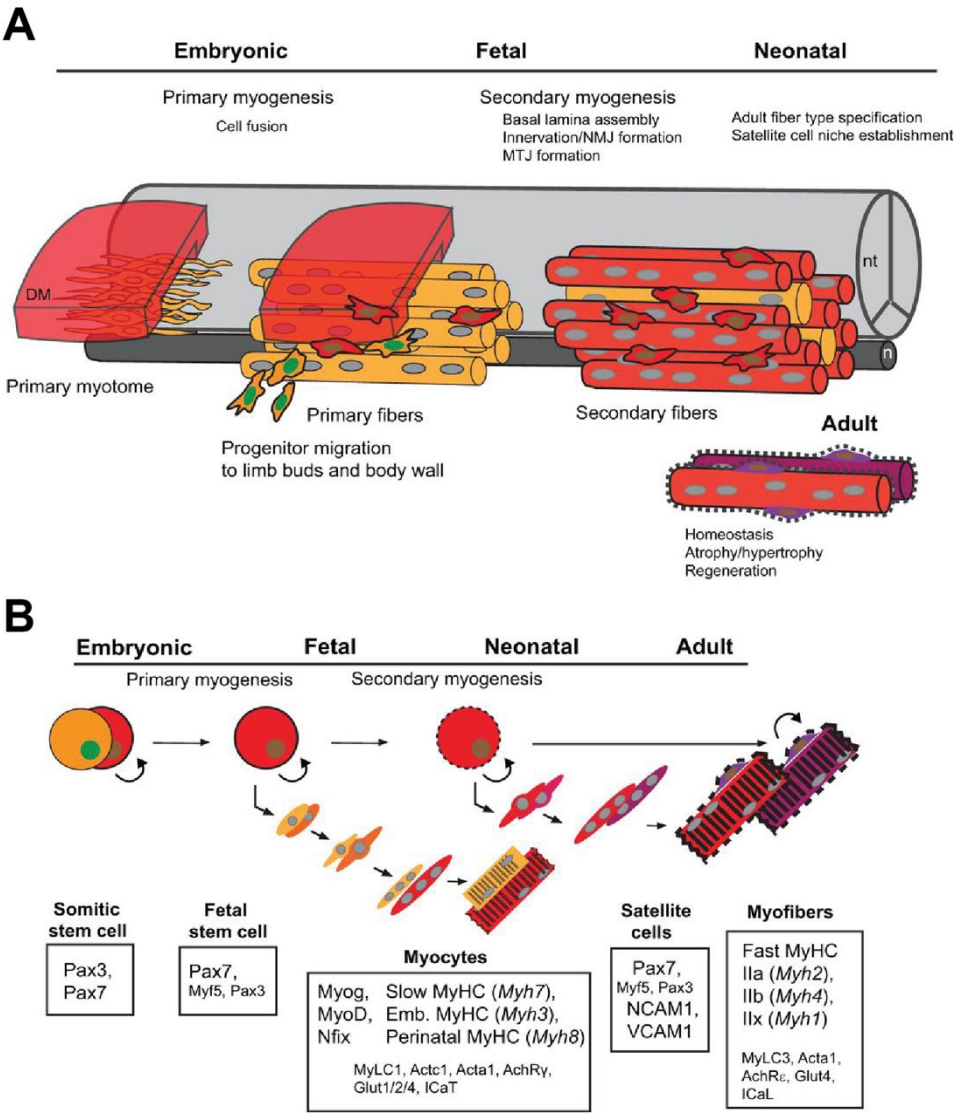

Figure 1.6. Vertebrate trunk muscle differentiation. (A) Schematic of the steps of primary and secondary myogenesis. Primary myotome myoblasts (left, yellow) develop into primary fibers (middle, yellow). Secondary fibers (red, right) are added during secondary myogenesis from myogenic progenitors onto the foundation of the primary fibers. Reproduced with permission (Chal & Pourquié, 2017). (B) Diagram of expression pattern over muscle development. Reproduced with permission (Chal & Pourquié, 2017).

D. Neuromuscular disorders

Neuromuscular disorders are conditions that affect the peripheral nervous system or muscle. Defects could happen at any point along the motor path: upper motor neuron, lower motor neuron, neuromuscular junction, or muscle. They can be inherited or acquired, including injury, cancer, aging, inflammation, autoimmune, medication, or critical illness. Here, I will focus on inherited conditions known to affect the muscle.

Inherited myopathies fall under four overarching categories: (1) congenital genetic myopathies; (2) mitochondrial myopathies; (3) metabolic myopathies; and (4) muscular dystrophies. Congenital myopathies have an overall prevalence of 1.62 per 100,000 and 2.76 per 100,000 in the child population (Huang et al., 2021). The categories of congenital myopathies are core, nemaline, centronuclear, fiber type disproportion, and myosin storage [reviewed in (Claeys, 2020)]. Mitochondrial myopathies are caused by defects in oxidative phosphorylation and are progressive [reviewed in (Ahmed et al., 2018)]. Disruptions in metabolic enzymes that breakdown carbohydrates, lipids, and lysosomes (i.e. inborn errors of metabolism) are termed metabolic myopathies (Finsterer, 2020). Lastly, Duchenne and Becker muscular dystrophies are degenerative muscle disorders (Mercuri et al., 2019).

Clinical workup for inherited myopathies often happens during the neonatal or early childhood period since symptoms typically develop early (Fardeau & Desguerre, 2013; McDonald, 2012; Morrison, 2016). The patient history should cover the distribution and course of weakness, onset of symptoms,

developmental milestones, cardiopulmonary symptoms, functional difficulties, and family history of muscle disorders. On the physical exam, muscle tone, strength, reflexes, sensation, and cranial nerves should be checked. Several laboratory tests could be useful in diagnosing myopathies: enzymes (e.g. transaminases, aldolase, and creatine kinase), neostigmine, and autoantibody testing. Imaging like ultrasound and MRI could be helpful in monitoring disease progression. Electrodiagnostics are critical to understanding whether disease originates from defects at the peripheral nerves, NMJ or muscle. Nerve conduction studies (NCS) focus on the amplitude and velocity of the response in the motor neuron after stimulation. Electromyogram (EMG) studies record muscle electrical activity; oftentimes EMG in myopathy shows small voluntary motor units and increased recruitment. Various modalities—histology, immunohistochemistry, electron microscopy—can be used to visualize various characteristics on tissue from muscle biopsy. Next-generation sequencing can be another useful tool if the clinical algorithm does not yield an obvious diagnosis.

III. NEMALINE MYOPATHY

A. Etiology

Nemaline myopathy (NM), a skeletal muscle disorder and histopathologic diagnosis, affects 0.22 per 100,000 children and has an all age prevalence of 0.20 per 100,000 (Huang et al., 2021). Its hallmarks include muscle weakness—often progressive—and the presence of rods, dubbed nemaline rods or bodies (further described below in diagnosis section) on histopathology.

NM was first described in 1963 in two different case reports of an infant and a child with hypotonia and delayed motor milestones; both had dense "myogranules" of thread-like form throughout the muscle fiber on biopsy examination (Conen et al., 1963; Shy et al., 1963). A few years later, a case report of two teenagers with similar features was published (Gonatas et al., 1966).

NM is mostly considered as a congenital disorder; however, there is an immune-related acquired form that develops in adults called sporadic late-onset NM (Nicolau & Milone, 2023). Twelve genes causative of the congenital form have been identified, most of which are related to the sarcomere (Figure 1.7; further discussed below in diagnosis section).

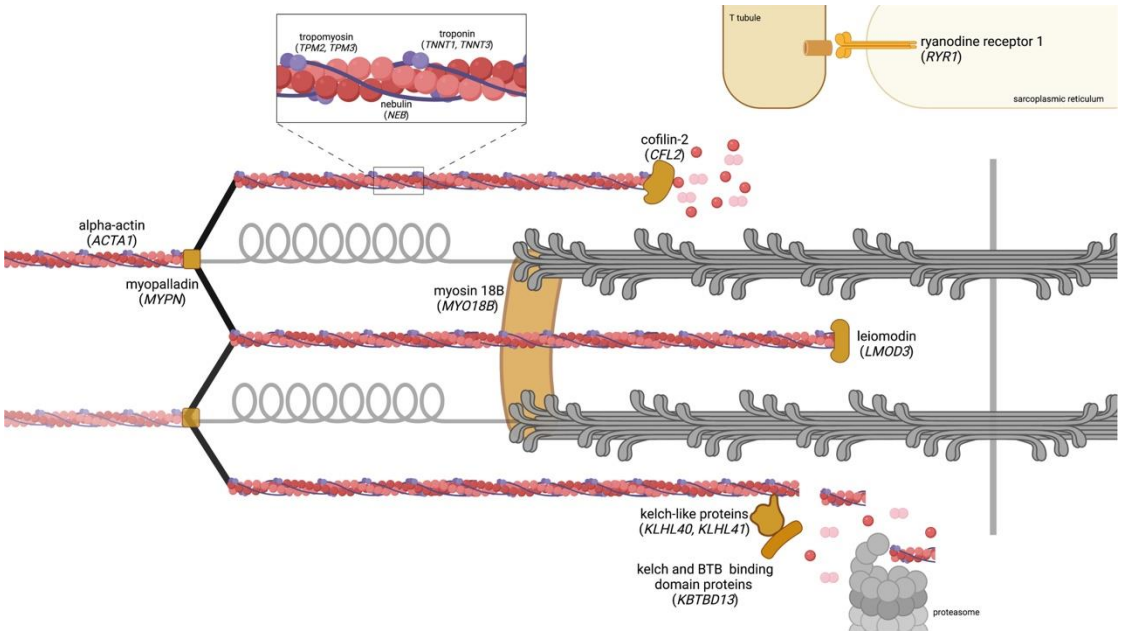

Figure 1.7: Sarcomeric proteins affected in NM. Diagram of a magnified view of sarcomere. Proteins labeled have been implicated in NM. Adapted from (Christophers et al., 2022).

B. Symptomatology and disease course

Initial classification of NM was categorized by causative mutation during a workshop by the European Neuromuscular Center in 1999 (C Wallgren-Pettersson & Laing, 2000). Modern classification of NM has designated seven categories for the disease based on onset, clinical features, and causative genes, since NM is now understood to be phenotypically heterogenous (Table 1.1; Laitila & Wallgren-Pettersson, 2021). In its most severe form, NM severely affects the fetus during intrauterine development, potentially leading to early death or symptoms in the neonatal period. Typical and mild NM become apparent in the neonatal and childhood periods, respectively. Other subtypes are less common or present in a particular community. In a review of pediatric clinical case reports from 2010 to 2020, we found that half of patients showed signs of disease during the fetal or neonatal period and 55% die before age 1 (Table 1.2; Christophers et al., 2022).

As a myopathy, NM patients typically present with muscle weakness in different muscle groups although this may cause symptoms in other organ systems (summarized in Table 1.2). The disease course is progressive. Early signs include neonatal hypotonia, delayed motor development, and respiratory difficulty. Children may go on to develop respiratory insufficiency, kyphoscoliosis, elongated facies with gaped mouth, and joint contractures.

Table 1.1: Classification of genetic NM. Adapted from (Laitila & Wallgren-Pettersson, 2021).

Novel classification of genetically caused nemaline myopathy (NM) and the genes known to cause these forms of the disorder

Category of nemaline myopathy	Clinical features	Causative genes	
Severe NM	Intrauterine onset Neonatal features include at least one of the following - major contractures of large joints - fractures - absence of respiratory effort - absence of movements	***ACTA1, NEB***, *LMOD3, KLHL40, KLHL41, RYR1, TNNT3, TPM2, TPM3*	
Typical NM	Perinatal onset Motor milestones delayed but reached	***NEB, ACTA1,*** *CFL2, TPM2* *LMOD3*	
Mild NM	Childhood or juvenile onset	*ACTA1, NEB, TPM2, TPM3, KBTBD13, MYPN,* dominant, or sometimes recessive mutations in *TNNT1* *LMOD3?*	
Distal NM	Presentation with distal weakness only (or mainly) Presentation with distal arthrogryposis also possible	*NEB, ACTA1, TNNT3, TPM2, FLNC?*	
Childhood onset NM with slowness	Characteristic slowness of movements Core-rod histology	*KBTBD13*	
Recessive *TNNT1* (former Amish) NM	Progressive course Thoracic immobility Restrictive lung disease Early endomysial fibrosis	Recessive mutations in *TNNT1*	Subtype of severe nemaline myopathy
Other (unusual) forms	Unusual distribution of muscle weakness Hypertrophic cardiomyopathy Unusual histological features (e.g. core-rod combination, caps, actin aggregates, intranuclear rods, lipid droplets)	*ACTA1, NEB, RYR1, TPM2, TPM3, MYPN, CFL2, RYR1, MYO18B?, ADSSL?*	

C. Diagnosis

Patient history, physical exam findings, and detailed family history are crucial in understanding the pattern of disease. Absence of altered laboratory findings such creatine kinase may also be a sign to consider myopathies like NM. EMG may show myopathic pattern early in childhood, though neuropathic changes have been noted in NM patients who are older than nine-years of age (C Wallgren-Pettersson et al., 1989).

Table 1.2: NM symptomatology described in pediatric NM case reports. Adapted from (Christophers et al., 2022).

	***n* (%)**	**Associated genes**
Age at first reported signs		
Fetal	31 (31)	*ACTA1, KLHL40, LMOD3, NEB1, RYR1, TNNT3, TNNT1*
Birth	38 (38)	*ACTA1, CFL2, KLHL40, MYO18B, NEB1, TNNT1, TPM2*
Infancy (<1 year)	13 (13)	*CFL2, LMOD3, NEB1, TNNT1*
1-13 years	13 (13)	*ACTA1, CFL2, NEB*
Early signs		
Decreased fetal movements	9 (9)	*ACTA1, KLHL40*
Locked-in state	1 (1)	*KLHL40*
Polyhydramnios	14 (14)	*ACTA1, KLHL40, LMOD3, NEB1, RYR1*
Neonatal hypotonia	64 (64)	*ACTA1, CFL2, KLHL40, LMOD3, MYO18B, NEB1, RYR1, TNNT1, TNNT3*
Delayed motor development	29 (29)	*ACTA1, CFL2, KLHL40, LMOD3, NEB1, RYR1, TNNT1, TPM2*
Abnormal gait/frequent falls	10 (10)	*ACTA1, CFL2, KLHL40, LMOD3, NEB1, TPM2*
Muscle weakness		
Unspecified	22 (22)	*ACTA1, CFL2, KLHL40, LMOD3, NEB1, TNNT1*
Axial and proximal	31 (31)	*ACTA1, CFL2, KLHL40, LMOD3 MYO18B, NEB1, TNNT1, TNNT3, TPM2*
Distal	23 (23)	*ACTA1, CFL2, KLHL40, LMOD3, MYO18B, NEB1, TNNT1*
Tremor	7 (7)	*TNNT1*
Feeding difficulty	16 (16)	*ACTA1, CFL2, KLHL40, MYO18B, NEB1, TNNT3*
Early respiratory difficulty	36 (36)	*ACTA1, CFL2, KLHL40, LMOD3, NEB1, RYR1*
Spinal curvature	37 (37)	*ACTA1, CFL2, LMOD3, NEB1, RYR1, TNNT1, TNNT3*
Scoliosis	15 (15)	*ACTA1, CFL2, LMOD3, NEB1, RYR1, TNNT1, TNNT3*
Kyphosis	11 (11)	*ACTA1, CFL2, LMOD3, TNNT1*
Rigid spine	5 (5)	*ACTA1, LMOD3, NEB1, TNNT1*
Lordosis	5 (5)	*ACTA1, CFL2, LMOD3, NEB1*
Facial Involvement	**55 (55)**	
Facial weakness	29 (53)	*ACTA1, CFL2, NEB1, RYR1, TNNT3, TPM2*
Ptosis	6 (11)	*KLHL40, LMOD3, NEB1, TPM2*
Ophthalmoplegia	1 (2)	*RYR1*
Facial dysmorphias	29 (53)	
High-arched palate	23 (42)	*ACTA1, CFL2, LMOD3, MYO18B, NEB1, RYR1, TNNT1, TNNT3, TPM2*
Micrognathia	4 (7)	*ACTA1, NEB1*
Cleft palate/lip	2 (4)	*KLHL40*

Table 1.2 (cont.)

Myopathic facies	9 (16)	*ACTA1, KLHL40, LMOD3, TNNT1*
Elongated face	7 (13)	*ACTA1, NEB, RYR1*
Macrocephaly	2 (4)	*NEB*
Dysmorphic features	3 (5)	*NEB*
Thoracic deformities		
Pectus excavatum	2 (2)	*ACTA1, MYO18B*
Pectus carinatum	5 (5)	*TNNT1*
Respiratory	**57 (56)**	*ACTA1, CFL2, KLHL40, MYO18B, NEB1, RYR1, TNNT1*
Tracheotomy	15 (27)	*ACTA1, NEB1, RYR1, TNNT1*
Mechanical ventilation	30 (54)	*ACTA1, LMOD3, NEB1, TNNT1, RYR1*
Respiratory insufficiency	6 (11)	*ACTA1, CFL2, NEB1*
Sleep apnea	2 (4)	*NEB1*
Pleural effusion, chylothorax	3 (5)	*ACTA1, KLHL40*
Cardiac	**13 (13)**	
Hypertrophy	2 (15)	*MYO18B*
Ventricular dilatation	4 (31)	*ACTA1, MYO18B, TNNT1*
Sudden cardiac arrest	2 (15)	*NEB1*
Atrioseptal defect	2 (15)	*LMOD3*
Cardiomegaly	1 (8)	
Bradycardia	1 (8)	*RYR1*
Transient supraventricular tachycardia	1 (8)	*MYO18B*
Joints/Skeletal	**39 (39)**	
Contractures	21 (54)	*ACTA1, CFL2, KLHL40, LMOD3, NEB1, RYR1, TNNT1*
Arthrogryposis	10 (26)	*ACTA1, LMOD3, NEB1*
Club feet	7 (18)	*KLHL40, LMOD3, NEB1, TNNT1*
Fractures	3 (8)	*KLHL40*
Hip hyperlaxity	3 (8)	*KLHL40, NEB1, TNNT3*
Gastrointestinal involvement	**3 (3)**	***ACTA1, TNNT1***
Neurological		
Intellectual disability	1 (1)	*NEB1*
Decreased white matter	3 (3)	*ACTA1*
Wheelchair bound	**7 (7)**	**ACTA1, CFL2, KLHL40, NEB1**
Death	**36 (36)**	
0-1 month	5 (14)	*ACTA1, NEB1*
1-6 months	12 (33)	*ACTA1, KLHL40, LMOD3, MYO18B, NEB1, RYR1*
6 months – 1 year	3 (8)	*ACTA1, KLHL40, NEB1, TNNT3,*
1-5 years	7 (19)	*KLHL40, NEB1, TNNT1*
5-10 years	5 (14)	*ACTA1, NEB1, TNNT1*
>10 years	5 (14)	*NEB1, TNNT1*
Cause of death		
Sepsis	3 (8)	*ACTA1, KLHL40, MYO18B*
Respiratory insufficiency	3 (8)	*ACTA1, TNNT3*
Cardiopulmonary arrest	3 (8)	*ACTA1, KLHL40, RYR1*
Infection	2 (6)	*KLHL40, LMOD3,*
Hypoxic-ischemic brain injury	1 (3)	
Terminated Pregnancy	**4 (4)**	*KLHL40, LMOD3*
Pathology features	**65 (64)**	
Cytoplasmic nemaline rods	49 (75)	
Intranuclear rods	5 (8)	*ACTA1*

Table 1.2 (cont.)

Fiber size variation	26 (40)	*ACTA1, CFL2, LMOD3, MYO18B, NEB1, TNNT1*
Internalized nuclei	6 (9)	*ACTA1, CFL2, MYO18B, TNNT1*
Increased fibrous connective tissue	18 (28)	*ACTA1, CFL2, TNNT1, TNNT3*
Inflammatory cell infiltration	3 (5)	*ACTA1, TNNT1*
Atrophic fibers	8 (12)	*ACTA1, MYO18B, TNNT3*
Fingerprint bodies	1 (2)	*LMOD3*
Rods surrounded by halos	1 (2)	*LMOD3*
Mitochondrial aggregates	1 (2)	*NEB1*
Myofibrillar degradation	3 (5)	*ACTA1, CFL2, KLHL40*

Muscle biopsy and sequencing provide the most evidence of NM as the cause of muscle weakness. Muscle biopsy can be examined several ways to visualize pathologic features (Figure 1.8, Table 1.2). The electron-dense aggregates termed nemaline rods/bodies are clear on electron microscopy (Figure 1.8A-B), and in some cases there may be actin thin filament disorganization (Figure 1.8C). On histology, there may be inclusions seen with Gömöri Trichrome or NADH stains, connective and adipose tissue expansion on hematoxylin and eosin stain, fetal or altered proportions of myosin, and focal inclusions positive for actin, alpha-actinin and myotilin (Figure 1.8D).

The increased accessibility of sequencing allows for greater understanding of causative genes (Herman et al., 2021). NM is often seen as a disease of the sarcomere, as mutations in the 12 identified causative genes affect the sarcomere (Table 1.2; Figure 1.7; Christophers et al., 2022; Moreau-Le Lan et al., 2018). Skeletal alpha-actin 1 (ACTA1), cofilin (CFL2), leiomodin 3 (LMOD3), nebulin (NEB1), and kelch repeat and BTB domain containing protein 13 (KBTBD13) are proteins that comprise the actin thin filament (Agrawal et al., 2007; Berkenstadt et al., 2018; Pelin et al., 1997; Sambuughin et al., 2010; Schröder et al., 2004; Carina Wallgren-Pettersson et al., 2002). The other

affected proteins are structural or ECC regulatory proteins: myosin 18B (MYO18B), myopalladin (MYPN), ryanodine receptor 1 (RYR1), slow skeletal muscle troponin T (TNNT1), fast skeletal muscle troponin T (TNNT3), and slow muscle alpha-tropomyosin (TPM2, TPM3; Gommans et al., 2003; Johnston et al., 2000; J. J.-C. Lin et al., 2008; Malfatti et al., 2015; von der Hagen et al., 2008). Lastly, mutations in Kelch-like family member proteins, KLHL40 and KLHL41, disrupt protein turnover (Ravenscroft et al., 2013).

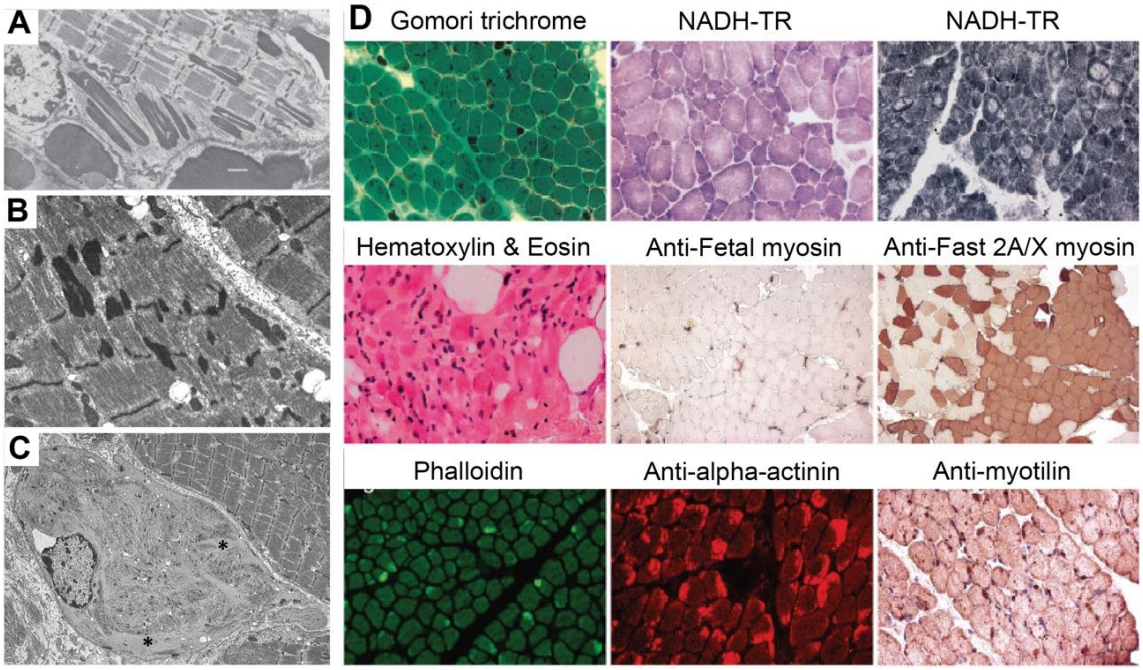

Figure 1.8: Nemaline rods on histology and EM. (A) Electron micrograph showing rod-like fibers within and adjacent to myofibrils. Reproduced with permissions from (Gonatas et al., 1966), Copyright Massachusetts Medical Society. (B,C) Electron micrographs of variable NM rod sizes and small rods and thin actin filament disorganization (highlighted by asterisks). Adapted from (Sewry et al., 2019). (D) Representative examples of various pathological features in NM by histology and immunohistochemistry. Adapted from (Laitila & Wallgren-Pettersson, 2021).

D. Treatment and clinical considerations

Currently, there is no cure for NM and, thus, treatment focuses on improving quality of life. As part of multidisciplinary care, monitoring respiratory function and musculoskeletal symptoms is imperative (Carina Wallgren-Pettersson et al., 2004; C. H. Wang et al., 2012). This will require a multifaceted approach by physical, occupational and speech therapists in addition to medical clinicians (Cervera-Mérida et al., 2020). Respiratory muscle training may be helpful in improving function (Smith et al., 2011). Respiratory function must also be monitored in any instances where anesthesia is administered (Oliveira et al., 2018; Tran & Smith, 2017; Tran & Chhibber, 2016). Using MRI may improve the selection of region to biopsy (Ennis et al., 2015; Quijano-Roy & Carlier, 2014). There is limited evidence that the pharmacologic agents L-tyrosine and acetylcholinesterase inhibitor pyridostigmine are helpful for NM patients; however, these benefits have not been recapitulated in zebrafish and mouse NM model (Messineo et al., 2018; Natera-de Benito et al., 2016; M.-A. T. Nguyen et al., 2011; Sahin et al., 2019; Sztal et al., 2018). Some have also suggested that pharmacologically targeting thin filament interactions and promoting muscle growth should be future directions of study in NM (Jungbluth et al., 2017). Further study into the mechanisms of disease for NM has the potential for inspiring novel NM treatments.

IV. ACTIN

Actin is a ubiquitous protein responsible for a myriad of roles throughout the cell: structural integrity, cell migration, force generation, trafficking, and gene

expression. Monomeric G-actin (also known as its globular form) has four subdomains that bind to ATP/ADP in the protein interior. F-actin, the filamentous polymer, is a helix of two strands of G-actin monomers (H. E. Huxley, 1963). The barbed end of the actin filament has ATP bound while the pointed end has ADP bound. Filament formation in physiologic conditions involves elongation from a seed of monomers (actin nucleus). Since the addition of ATP-bound actin is faster at the barbed end than the pointed end the filament tends to grow on its barbed end while monomers are depolymerized on the pointed end; this process is termed treadmilling. Polymerization can exert force, which is a strategy used by the cell for migration. There have been six actin isoforms identified in vertebrates (Figure 1.9), originally described by their expression pattern in skeletal muscle (α_{sk} and α_{ca}), smooth muscle (α_{sm} and γ_{sm}), or in the cell cytoplasm (β_{cyto} and γ_{cyto}; Vandekerckhove & Weber, 1978). Muscle actins incorporate into the sarcomere, but non-sarcomeric γ-actin networks are involved in other cell tasks, such as anchoring to the membrane, localization of organelles and structure of the Z-disc (Craig & Pardo, 1983; Nakata et al., 2001; Papponen et al., 2009; Rybakova et al., 2000). Beta-actin is the only isoform required for cell viability, according to studies in mouse cells (Bunnell et al., 2011). There is a transition in the muscle cell from smooth muscle to cardiac to skeletal muscle actin isoforms expression over time. Mutations in actin genes can cause nemaline myopathy (*ACTA1*), familial thoracic aortic aneurysms (*ACTA2*), hypertrophic and dilated forms of cardiomyopathy (*ACTC1*), Baraitser-Winter syndrome (*ACTB*, *ACTG1*), deafness (*ACTG1*), and megacystis microcolon-intestinal hyperperistalsis syndrome (*ACTG2*; Parker et al., 2020).

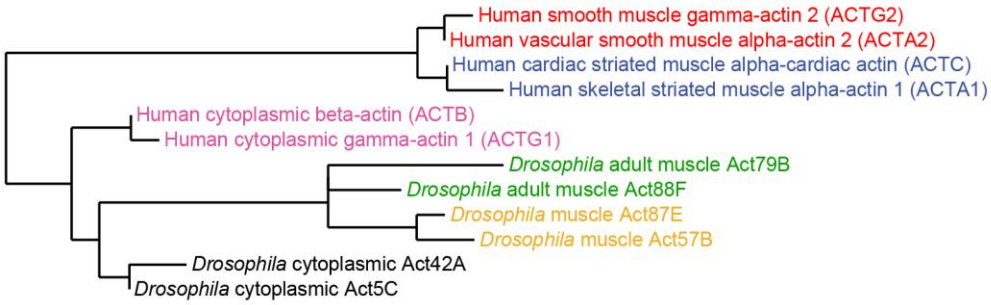

Figure 1.9: Actin isoforms. Phylogenetic tree of human and *Drosophila* actin isoforms and differences in their amino acid sequences.

Other organisms, such as *Drosophila*, also have multiple actin isoforms (Figure 1.9) considered to be cytoplasmic (Act 5C, Act42A), embryonic/larval muscle (Act57B, Act87E), and adult muscle (Act88F, Act79B; Röper et al., 2005; Wagner et al., 2002). However, there is evidence that these actins may be present in all cells but at varying levels, and that they all incorporate into structures, like the sarcomere to a certain extent (Röper et al., 2005). Additionally, there is some compensation between the various isoforms (Wagner et al., 2002).

Actin dynamics are regulated by post-translational modifications (PTMs) and complex interactions with actin-binding proteins (ABPs). Actin PTMs have effects on actin structure, interaction with ABPs and cell activity, including cell division, movement, and entry into nucleus [reviewed in (Varland et al., 2019)]. For example, arthrin—first discovered in insect flight muscle—is actin with ubiquitin modifications at regularly spaced intervals along the thin filament which is thought to be important for contraction (Bullard et al., 1985). Acetylation on actin has also been reported to be important for organization of the thin filament of the *Drosophila* indirect flight muscle (Viswanathan et al., 2015).

ABPs (Figure 1.10) interact with actin to complete a variety of functions: sequestering monomers, maintaining structural networks, nucleation, and growth of the filament, severing, transport and force [reviewed in (Pollard, 2016)]. Actin structures throughout the cell require capping proteins (e.g. Cap, tropomodulin), cross-linking proteins (e.g. fimbrin, filamin, actinin, spectrin), filament binding (e.g. tropomyosin), and anchors (e.g. dystrophin, talin, vinculin). Profilin binds to ATP-actin and prevents elongation at the pointed end. The Arp2/3 complex and proteins with WH2 domains nucleate and elongate the actin filament. Formins are also actin nucleators. The ADF/Cofilin (described further below) and gelsolin protein families are responsible for severing the filament, which is necessary for proper G-actin/F-actin dynamics. Lastly, myosin motors and polymerization of the filament contribute to force production and transport within the cell.

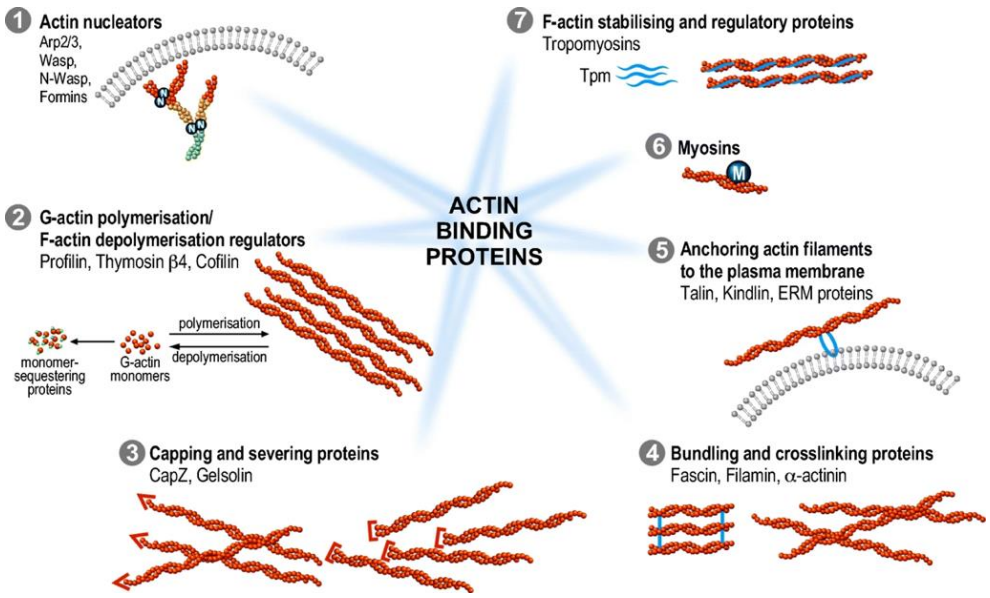

Figure 1.10: Actin binding proteins throughout the cell.
Adapted from (Ruggiero & Lalli, 2021).

V. COFILIN

A. Biochemistry

The cofilin/actin depolymerizing factor (ADF) family is responsible for various context-dependent actions in actin dynamics, including filament severing and stabilization (Figure 1.11A). Cofilin interacts with both actin monomers and filaments as it has binding sites for G/F-actin and F-actin (Figure 1.11B). When bound to a filament, cofilin induces a conformation change at two longitudinally adjacent subunits which enhances torque on the helix of the filament resulting in a break (McGough et al., 1997; Wioland et al., 2019). Recent work suggests that the severing happens at the most vulnerable point in between bare and cofilin-bound segments of the filament (Huehn et al., 2020). *In vitro* experiments with optical tweezers have shown that actin filament tension may slow down severing by cofilin (Hayakawa et al., 2011). Cofilin concentration relative to actin and other ABPs—which can vary throughout the cell—determines cofilin's function (Andrianantoandro & Pollard, 2006). At low cofilin concentrations, rapid filament severing by the protein is favored (Figure 1.11C). Remaining fragments can then be nucleated or participate in nucleotide exchange and recycling onto the filament. Meanwhile, at high concentrations, cofilin saturates sites along the filament. This, in turn, reversibly stabilizes portions and reduce the likelihood of severing because there is a less strained interface (Figure 1.11D). The stabilized portions can be removed from the filament and processed in one of three ways: fully depolymerized, grown from the barbed ends, or bundled into rods. These cofilin-actin rods are not the same as the nemaline rods or bodies seen in NM, which are composed of actin and sarcomeric proteins. Cofilin also

has a nuclear localization signal, as it also chaperones actin monomers into the nucleus (Dopie et al., 2015).

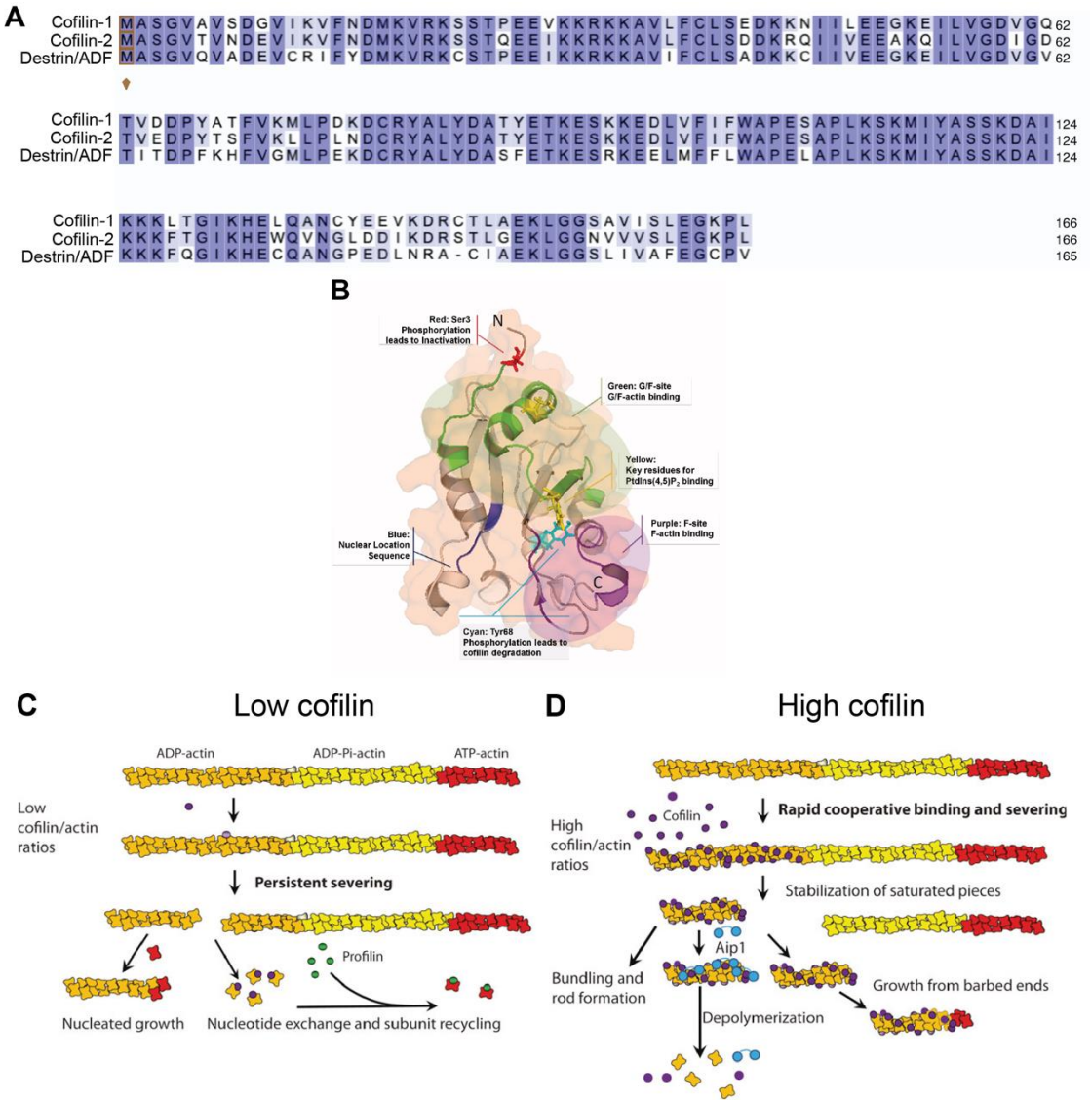

Figure 1.11: Human cofilin protein. (A) Amino acid sequence of human Cofilin-1, Cofilin-2, and Destrin/Actin-depolymerizing factor (ADF). (B) Protein structure of human Cofilin-2 showing domains. Adapted from (Zheng et al., 2016). (C,D) Cofilin's function depends on its concentration, where its main function at low concentrations (C) it persistently severs filaments while at high concentrations (D) it both stabilizes and severs the filament. Adapted from (Bamburg & Bernstein, 2010).

Cofilin is regulated by PTMs, PIP_2 binding, and presence of other ABPs [reviewed in (Ohashi, 2015; Van Troys et al., 2008)]. Phosphorylation at Ser3 by LIM kinase (LIMK) or Testicular Protein Kinase (TESK) inactivates cofilin (Scott & Olson, 2007; Toshima et al., 2001). Cofilin can be dephosphorylated—thus reactivated—by the phosphatases Slingshot (SSH) and chronophin (Gohla et al., 2005; Niwa et al., 2002; Ohta et al., 2003). Phosphorylation state may also influence the subcellular localization of cofilin (Nagaoka et al., 1996). ABPs like AIP and tropomyosin can enhance or block ADF/cofilin function, respectively (Bernstein & Bamburg, 1982; Shoichiro Ono, 2003). Binding of PIP_2 has also been proposed to inhibit the interaction of cofilin and actin because its binding site lies between the two cofilin actin-binding domains (Hosoda et al., 2007).

In vertebrates, the family comprises ADF/destrin, cofilin-1 (i.e. non-muscle cofilin or nm-cofilin), and cofilin-2 (i.e. muscle cofilin or m-cofilin; Nakashima et al., 2005). These proteins each have their own biochemical profile *in vitro*; they do not have a preference for a particular actin subtype but ADF is more efficient and cofilin-2 has a higher affinity for ATP-actin monomers (Vartiainen et al., 2002). Additionally, mouse cofilin-2 binds more readily to F-actin than cofilin-1 (Nakashima et al., 2005).

Cofilin expression in muscle shifts during development: cofilin-1 predominates until the postnatal period where cofilin-2 becomes the main isoform in mature skeletal muscle (Abe et al., 1989; K Mohri et al., 2000). However, there is evidence that cofilin-1 is involved in muscle because it assists in sarcomere integrity in the context of mutation in the LMNA gene that results in Emery-Dreifuss muscular dystrophy (Vignier et al., 2021). Cofilin-2 is important for

skeletal muscle development, maintenance, regeneration and maintaining thin filament length (Agrawal et al., 2012; Gurniak et al., 2014; Kremneva et al., 2014; S Ono et al., 1994; Thirion et al., 2001). Cofilin-2 expression is increased when muscle is damaged by injury or dystrophin-deficiency (i.e. model of Duchenne muscular dystrophy) presumably due to muscle regeneration in these models (Thirion et al., 2001).

B. Affecting cofilin-2 in humans and models

Unsurprisingly, affecting cofilin has great impact on muscle structure and function. Mutations in the *CFL2* gene lead to truncation, misfolding, and degradation of the protein, resulting in human NM. Patients experience the muscle weakness and other symptoms typical of NM, but at variable severity (summarized in Table 1.3). *CFL2* NM is discussed in more detail in Chapter 2.

Muscle tissue culture and animal models affecting cofilin exhibit similar muscle deterioration changes. Primary myoblasts can be cultured from *Cof2* null mice, suggesting that CFL2 is not necessary for myoblast fusion that leads to myotube formation (Gurniak et al., 2014). Suppression of cofilin by morpholino causes actin aggregate formation only during the formation of myotubes and not once myotubes have formed in cultured muscle cells (Miyauchi-Nomura et al., 2012). In C2C12 myoblasts, CFL2 is needed for myogenic differentiation into myotubes, and miR-141-3p regulates the amount of CFL2 impacting this process (M. T. Nguyen & Lee, 2022; M. T. Nguyen et al., 2020). CFL2 may also play a role in regulating the expression of the various myosin heavy chain isoforms during differentiation (Zhu et al., 2018).

Table 1.3: Summary of CFL2 patient case reports. From (Fattori et al., 2018)

TABLE 1 Clinical features of patients presented in this study in comparison to previously reported families with *CFL2* mutations

Reference	This study			Agrawal et al[8]		Ockeloen et al[17]		Ong et al[18]
CFL2 mutation	p.[(Asp86Asn)];[(Asp86Asn)]	p.[(Asp79Tyr)];[(Ser94LeufsX6)]		p.[(Ala35Thr)];[(Ala35Thr)]		p.[(Val7Met)];[(Val7Met)]		p.[(Lys34GlnfsX6)];[(Lys34GlnfsX6)]
Patient (age at examination)	Pt 1 (4 y)	Pt 2 (1 y)	Pt 3 (1 mo)	Pt 1 (16 y)	Pt 2 (2 y)	Pt 1 (21 y)	Pt 2 (5 y)	Pt 1 (1 mo)
Onset	Congenital	Congenital	Congenital	Congenital	Delayed motor milestone	Breech presentation at birth	Breech presentation at birth	Respiratory distress and apnea at 5 days requiring intubation
Floppy infant	Yes	Yes	Yes	Yes	No	No	No	Yes
Respiratory distress at birth	Yes (tracheostomy at 2 mo)	Yes (tracheostomy at 2 mo)	Yes	No	No	No	Yes	Yes
Nutritional support	Yes (gastrostomy at 2 mo)	Yes (gastrostomy at 3 mo)	NA	No	No	No	No	Yes
Motor development	None	None	None	Delayed	Delayed	Delayed walking	Normal until age 2 y and 7 mo	Compromised
Facial weakness	Yes	No	No	NA	NA	High-arched palate, low-pitched voice	No	NA
Contractures	Severe ankles, wrists and fingers	Initial at ankles	NA	NA	NA	Knees	No	NA
Scoliosis	Yes, thoracolumbar scoliosis	No	No	NA	NA	Yes, severe kyphoscoliosis	Increased lordosis	NA
Muscle mass	Hypertrophy	Wasting	Wasting	NA	NA	Wasting	Normal	NA
Distribution of weakness	Diffuse and symmetric	Diffuse and symmetric (no head control, absence of tendon reflexes)	Diffuse and symmetric	NA	NA	Axial and proximal	Neck flexors, axial muscles, hip abductor, and periscapular muscles	NA
Best motor achievement and outcome	None	None	None	Can walk short distances but uses a wheelchair outside	Walking cannot run	Wheelchair dependent since age 21 y	Waddling gait	24-h continuous ventilation support. Died at 12 mo
Peculiar features	Macroglossia	No	No	No	No	Head drop	No	No
Cardiac involvement	No	No	No	NA	NA	No	No	No
CK	1500	600	800	NA	NA	Normal	NA	Mild elevation

Abbreviations: mo, month; NA, not available; Y, year.

Cfl2 null mice are born with normal sarcomeres at birth but show sarcomeric aggregates similar to nemaline rods by P7; these mice die by P8 (Agrawal et al., 2012). This suggests that cofilin-2 is not necessary for initial myofibrillogenesis but rather for muscle maintenance. Cofilin-2 deficiency mice show transcriptomic changes that point to alterations in cell cycle regulation and proliferation (Morton et al., 2015). Muscle-specific knockout and post-natal excision of *Cfl2* resulted in small mouse pups with growth retardation with sarcomeric degeneration on muscle biopsy histological examination (Agrawal et al., 2012). Mice with a conditional knockout of *Cfl2* die between P10 and P12 and also have protein aggregates in muscle (Gurniak et al., 2014). These *Cfl2* conditional knockout mice also show alterations of Extrasarcomeric actin (Gurniak et al., 2014). Chimeric mice with both *Cfl2* knockout and wild type muscle fibers are born small and develop scoliosis (Kurato Mohri et al., 2019). The knockout fibers still degenerate by the second week of life despite being surrounded by normal fibers (Kurato Mohri et al., 2019). Introduction of the A35T mutation—known to be pathogenic in human NM—into mice also leads to myopathy, premature death at P9, and actin accumulation in muscle throughout the cell that was separate from rods near the sarcomere (Rosen et al., 2020).

Affecting the cofilin isoform UNC-60B in *C. elegans* triggers actin aggregate formation in body wall muscle, since it is required to incorporate actin into developing myofibrils (K. Ono et al., 2003; Shoichiro Ono et al., 1999). Mutants for *unc60* had muscle function defects that correlated with the severity of the actin disorganization phenotype (Shoichiro Ono et al., 1999). Additionally, our lab has previously characterized the muscle disruption seen in *Drosophila* model where levels of *twinstar* (*Drosophila* cofilin, *DmCFL*) are reduced using

RNA interference (RNAi). More details about this model are discussed in a subsequent section.

VI. *DROSOPHILA* MUSCULATURE

A. Embryonic and larval muscle development

There are four developmental periods in the *Drosophila* life cycle: embryogenesis, larval growth, metamorphosis, and adult (Figure 1.12A). At 25ºC, embryogenesis occurs during the first day after egg laying in 17 stereotyped stages. Larval development has three stages (instars). The first two instars (L1 and L2) each take one day, while the final instar (L3) takes two days. At the culmination of L3, the larva wanders to a site where it will form a pupa, within which it will metamorphose into an adult fly over the span of five days.

Drosophila and vertebrate skeletal muscle have similar organizations, although each muscle in *Drosophila* is equivalent to one cell rather than the additional layers of bundling seen in vertebrates. In both, each multinucleated muscle cell is composed of various myofibrils that are made up of concatenated sarcomeres. Human and adult *Drosophila* sarcomeres are also of similar length at about 3 μm and contain similar components (X. Chen et al., 2016; Reedy & Beall, 1993). Therefore, *Drosophila* is a useful model for studying general principles of muscle development. The below discussion focuses on embryonic and larval muscle development; more details about secondary myogenesis in adults is reviewed in (Laurichesse & Soler, 2020).

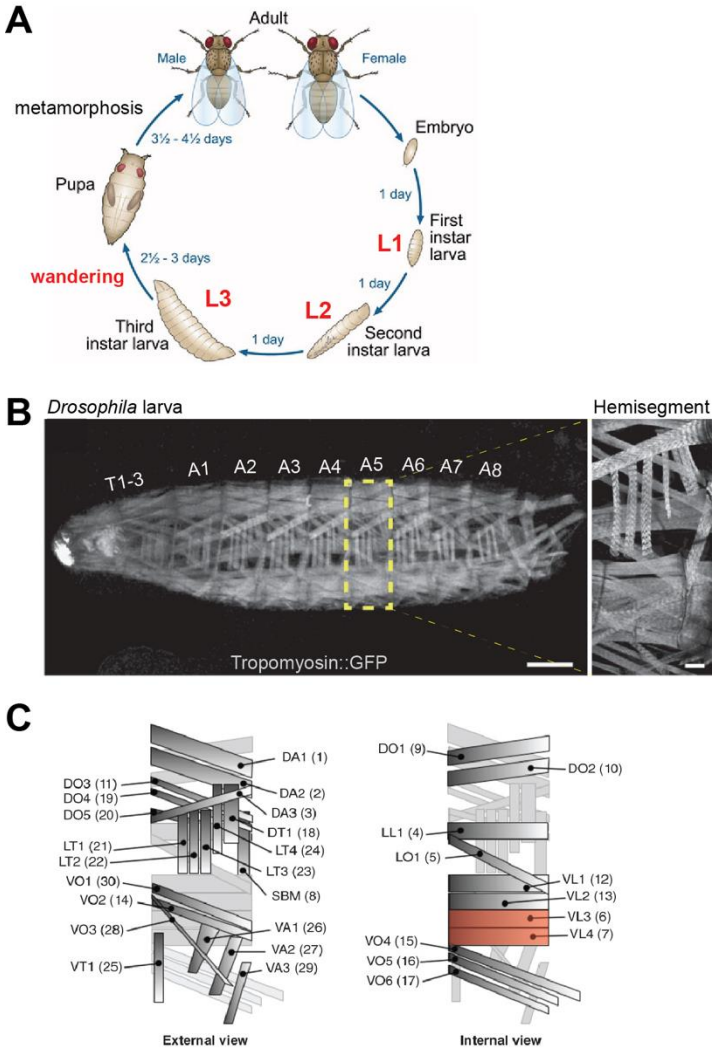

Figure 1.12: *Drosophila* life cycle and muscle. (A) Ten-day *Drosophila* life cycle at 25ºC. Larval instar stages are labeled in red. Adapted from (C. Ong et al., 2015). (B) *Drosophila* larva expressing protein trap tropomyosin::GFP to visualize muscles in thoracic (T1-3) and abdominal (A1-8) hemisegments, in addition to a magnification of a hemisegment viewed (Schulman et al., 2015) from the exterior. Adapted from (Schulman et al., 2015). (C) Diagram of abdominal hemisegment muscles from external (left) and internal (right) views. Muscle naming follows the following convention: dorsal muscles (DA), dorsolateral (DO/DT/LL), lateral (LT/LO/SBM), and ventral (VA/VL/VO/VT). Number in parentheses indicates the alternate numbering system for *Drosophila* muscle. VL3 and VL4 muscles (also known as muscles 6 and 7) which are used in this study are indicated in red. Adapted from (Schulman et al., 2015).

Muscle is established during embryogenesis and grows during larval instars ; it then has to be reformed post-histolysis for adult flies [steps of myogenesis and strategies for studying them are reviewed in (Dubey et al., 2020) and (Bothe & Baylies, 2016)]. On the left and right sides of the embryo, there are 12 repeating abdominal hemisegments containing about 30 muscles that are attached in various orientations to allow for different angles of contraction (Figure 1.12B-C; Bate, 1990). In this study, we focus on ventral longitudinal (VL) muscles 3 (i.e. VL3 or muscle 6) and 4 (i.e. VL4 or muscle 7). Embryonic myogenesis is similar to vertebrate muscle development where muscle progenitors need to be specified, post-mitotic myocytes fuse, and muscle cells mature.

Drosophila somatic muscle develops from mesoderm (Figure 1.13A), which is specified by expression of *twist*, which activates gene expression of the myogenic differentiation factor *Mef2*, and *lethal of scute* (*l'sc*), which activates founder cell transcription factors (Baylies & Bate, 1996; Carmena et al., 1995; Sandmann et al., 2007). Our lab identified proteins that interacted with Twist during early muscle development, including Twinstar (DmCFL; further discussed in a subsequent section; Balakrishnan, Howard, et al., 2021). Muscle progenitors with high *l'sc* expression are designated as cardiac and somatic muscle by external signaling pathways and the proper expression of combinations of muscle identity genes, including *even-skipped* (*eve*), *ladybird* (*lb*) and *msh*, amongst others (Baylies et al., 1995; Carmena et al., 1995; Jagla et al., 2002). *Twist* expression is subsequently maintained in progenitor cells that become latent adult muscle precursors (i.e. AMPs), while the remaining progenitors—known as founder cells—are further differentiated by the pattern of expressed transcription factors [reviewed in (Figeac et al., 2007; Junion &

Jagla, 2022)]. Meanwhile, fusion competent myoblasts (FCMs) have low *l'sc* expression (Carmena et al., 1995).

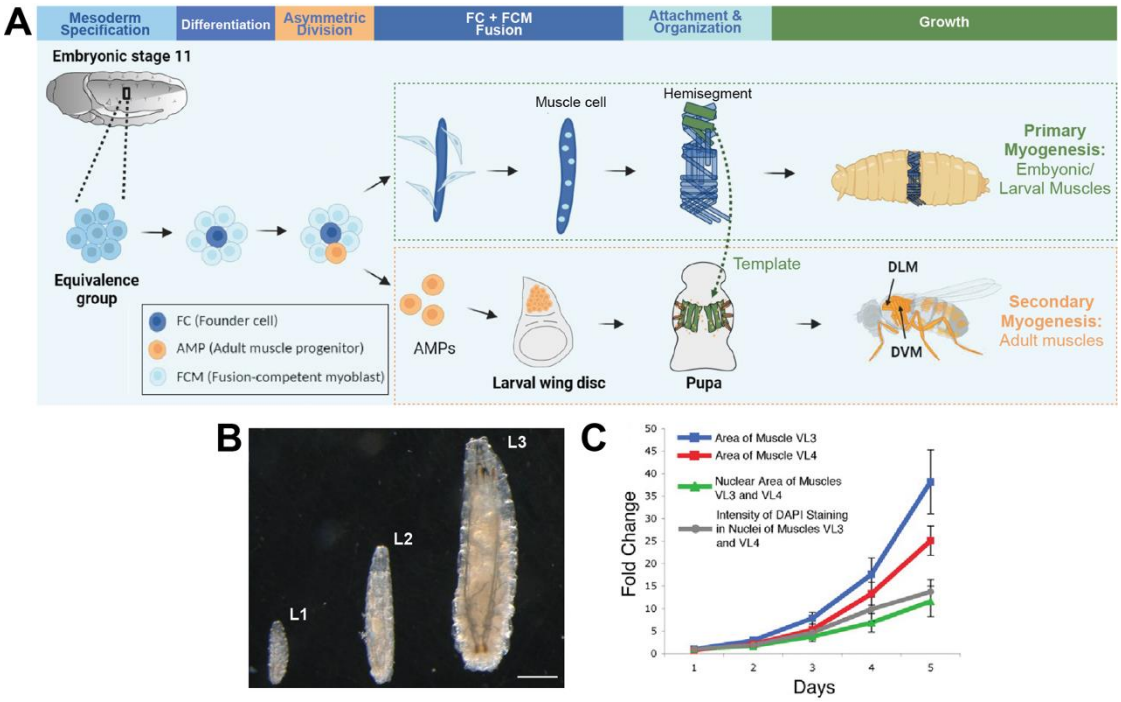

Figure 1.13: *Drosophila* myogenesis and muscle growth. (A) Schematic of embryonic/larval (primary) and adult (secondary) myogenesis in *Drosophila*. Adapted from (Poliacikova et al., 2021). (B) Representative images of larvae of different developmental instar stages. Adapted from (Zwart et al., 2013). (C) Graph quantifying the increased fold change in VL3/4 muscle area, nuclear area, and nuclear DNA content over the five days of larval development. Adapted from (Demontis & Perrimon, 2009).

Each founder cell is the starting cell for what will become a muscle fiber. During stages 12 and 15, myotubes form by the fusion of founder cells and FCMs [reviewed in (Deng et al., 2017)]. These cells are multinucleate and their gene expression becomes coordinated based on their muscle identity (Bataillé et al., 2017). The myotubes must then attach to the tendon cells which anchor them within the hemisegment organization pattern (Schweitzer et al., 2010; Soler et al., 2016). Innervation by the motor neuron happens post-fusion (described

more fully in next section). Multiple nuclei determine their positions via the activity of microtubules, microtubule motor proteins, and microtubule-associated proteins, while myofibrils must assemble in the muscle cytoplasm, although the mechanism of myofibrillogenesis remains elusive (Dlugosz et al., 1984; Folker et al., 2012; Holtzer et al., 1997; Lemke & Schnorrer, 2017; Schulman et al., 2014).

As the embryo hatches into the larva, muscle growth continues exponentially over five days (Figure 1.13B-C) to meet the increased functional and energetic demands at this stage (Demontis & Perrimon, 2009). Insulin/FOXO and dMyc are critical for muscle growth and the increase in DNA content (by endoreplication) necessary to supply the muscle with gene products (Demontis & Perrimon, 2009). Larvae are an ideal model for postnatal muscle development because each muscle is one cell and they are easily accessible and visualized both live and by dissection (Figure 1.14A; Balakrishnan, Sisso, et al., 2021; Brent et al., 2009; Ramachandran & Budnik, 2010). In particular, the ventral longitudinal (VL) muscles are a commonly studied muscle group given their position and orientation.

B. Neuromuscular junction

As described in the previous section on excitation-contraction coupling (section IIB), muscle contraction is triggered by signals from brain via the motor neuron. The first twitches in the embryo originate from the muscle as they are not innervated until much later in embryonic development (stages 13-15) and are not mature until end of embryonic and early larval development (Crisp et al.,

2008). Coordinated contractions are not seen until the end of embryonic development (Crisp et al., 2008). Just as the organization of the embryonic musculature is stereotyped, the 36 motor neurons (Figure 1.14B-D) also have expected body wall muscle partners that they innervate in a stereotypical manner (Landgraf et al., 1997).

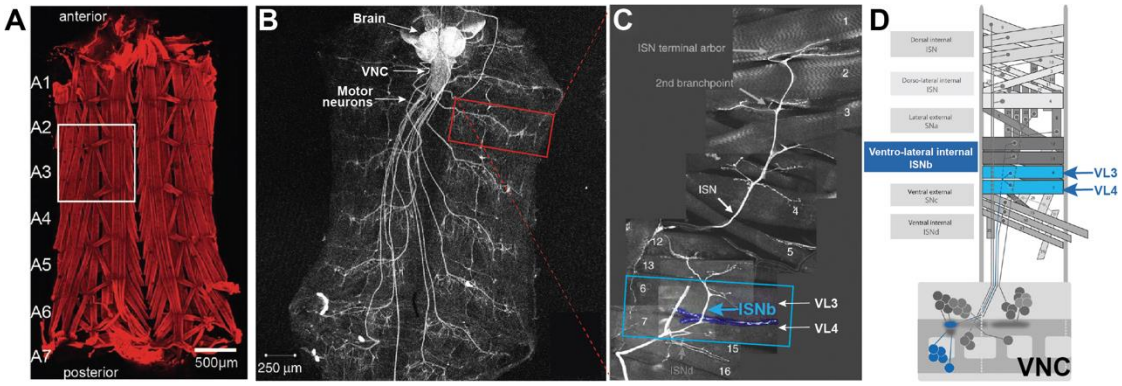

Figure 1.14: *Drosophila* larval motor system. (A) L3 larval fillet prep exposing internal body wall muscles, labeled with phalloidin (F-actin, red). Labels identify abdominal hemisegments and white box outlines an individual hemisegment. Adapted from (Sun et al., 2023). (B) L3 larval fillet prep with central nervous system expressing GFP (gray). Red box outlines an individual hemisegment. VNC = ventral nerve cord. Adapted from (Menon et al., 2013). (C) Magnification of muscles in a single hemisegment with motor neurons expression GFP (gray). Intersegmental nerve b (ISNb) outlined in blue. Blue box identifies VL3/4 muscles. Adapted from (Menon et al., 2013). (D) Diagram of connectivity and myotopic map. Highlighted in blue are the VNC nuclei and ISNb motor neuron that innervate VL3/4 muscles. Adapted from (Kohsaka et al., 2012).

Motor neurons leave the ventral nerve cord in two bundles, known as the segmental nerves (SN) and intersegmental nerves (ISN). These motor neurons require proper development of the mesoderm for their own continued development (Landgraf et al., 1999). There are attractive (e.g. Netrin B, Connectin, Capricious, FasII, FasIII) and repulsive (e.g. Sema-IIA, Toll) cues for

axon contact with the muscle (Nicholson & Keshishian, 2006). For example, the adhesion protein FasIII is expressed in a time-dependent manner as the growth cone of the motor neuron is extending and eventually contacting the muscle (Halpern et al., 1991). The growth cone becomes a motor neuron terminal onto the muscle after a transition point where pre-varicosities which contain early presynaptic components form (Yoshihara et al., 1997). The NMJ grows in coordination with the muscle during larval development [reviewed in (Atwood et al., 1993; Menon et al., 2013)].

Boutons are the individual contact points of the motor axon terminal onto the muscle (Figure 1.15A). Live imaging revealed that new boutons bud from existing boutons as muscle grows (Zito et al., 1999). There are different types of boutons with type I being described as more prominent (innervating ventral longitudinal muscles VL3 and 4) and type II and type III having smaller boutons (innervating VL1 and 2). Type I boutons are subdivided into Type Ib (big) and Type Is (small; Hoang & Chiba, 2001). Additionally, the postsynapse of Type II and III boutons does not have specialized muscle membrane at the NMJ and rely on the neurotransmitter octopamine (Prokop, 2006; Ruiz-Cañada & Budnik, 2006).

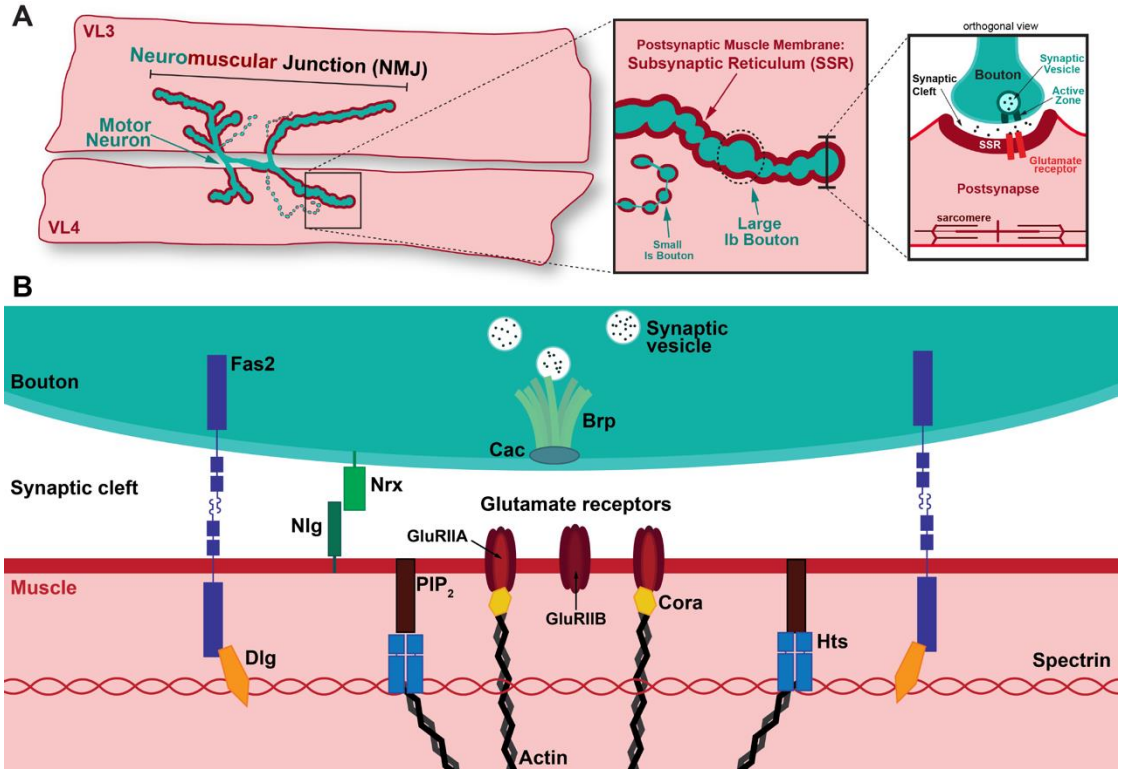

Figure 1.15: *Drosophila* larval NMJ synapse. (A) Diagram of (left) VL3 and VL4 muscle pair innervated by branches of the same motor neuron projection (cyan). Middle: magnification of individual boutons showing the size difference between type I large (Ib) and small (Is) boutons in addition to the postsynaptic muscle membrane (i.e. subsynaptic reticulum, SSR). Right: Magnification shows orthogonal view of the synapse between a single bouton and the postsynapse. (B) Schematic of the presynaptic and postsynaptic components of the NMJ synapse at a single bouton. Based on (Chou et al., 2020; Koper et al., 2012; S. J. H. Wang et al., 2014).

While the vertebrate NMJ is a cholinergic synapse, the *Drosophila* NMJ is a glutamatergic synapse which has been well studied (Johansen et al., 1989). Synapse components are diagramed in Figure 1.15B. The synapse is similar to that of the vertebrate where at the presynapse there is an active zone (often visualized using antibodies directed at the protein Bruchpilot, Brp) where synaptic vesicles bind and release neurotransmitter. The region of the muscle

side that contains all components is called the postsynaptic density (PSD), which in the case of the *Drosophila* NMJ is the muscle's postsynaptic membrane known as the subsynaptic reticulum (SSR). Several structural proteins are present at and maintain the SSR, including Discs-large (Dlg), Spectrin, Adducin/hu-li-tai shao (Hts), Neuroligin (Nlg), Fasciclin (Fas2; Banovic et al., 2010; K. Chen & Featherstone, 2005; Kohsaka et al., 2007; Pielage et al., 2006; S. J. H. Wang et al., 2014). Glutamate receptors (GluRs) on the postsynaptic side are heterotetramers composed of essential subunits GluRIIC, D, and E with either GluRIIA or B (David E Featherstone et al., 2005; Marrus et al., 2004; Petersen et al., 1997; Qin et al., 2005). GluRs are ionotropic receptors that allow calcium entry into the muscle and are similar to vertebrate non-NMDA GluRs (Schuster et al., 1991). GluRIIA-B subunit composition depends on postsynaptic density maturity and presynaptic glutamate release (Schmid et al., 2008).

Neurotransmission at the larval NMJ relies on levels of glutamate and activation of GluRs. NMJ activity recordings are taken using the two-electrode voltage clamping (TEVC) technique (Figure 1.16), where the motor neuron is stimulated by a suction electrode and the resulting excitatory current in the muscle is recorded (Zhang & Stewart, 2010). The excitatory junctional current (EJC) or potential (EJP) is the response in the muscle when the motor neuron is stimulated. The miniature extra-junctional potentials (mEJP) or currents (mEJC) are the activity of the muscle spontaneously. Meanwhile, the quantal content or size is the activity recorded in the muscle after spontaneous release and binding of the contents of a single vesicle. Studies of muscle activity have shown that EJC and mEJP amplitude are linked to quantal content (DiAntonio et al., 1999).

Levels of GluRIIA and B are thought to be proportional. Overexpression of *GluRIIA* leads to increased EJC while *GluRIIA* mutants have reduced EJC, suggesting that GluRIIA-containing glutamate receptors contribute most to the EJC activity at the NMJ (Sigrist et al., 2002).

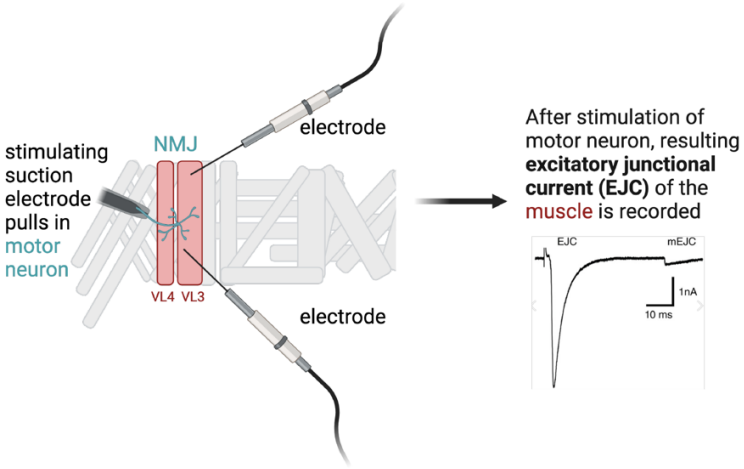

Figure 1.16: Two-electrode voltage clamping (TEVC). Diagram of technique for recording muscle electrophysiologic activity. Made using Biorender.

C. *Drosophila cofilin* (*DmCFL)* knockdown (KD) model

Our lab conducted a yeast-based double interaction screen to find Twist-interacting proteins, since Twist is expressed in the mesodermal and muscle progenitor lineage (Balakrishnan, Howard, et al., 2021). Through this screen, 37 genes were found to interact with Twist at the Dmef2 or tinman enhancers. DmCFL (i.e. twinstar) was identified in this screen as interacting with the C-terminus of Twist. DmCFL, a severing protein, was first identified as being involved in cytokinesis: it is required for both mitosis in the larval neuroblast and for meiosis in the larval testis (Gunsalus et al., 1995). DmCFL is homologous to *C. elegans* UNC-60A/B and vertebrate cofilins (Shukla et al., 2018). Disrupting

DmCFL results in cytoplasmic actin accumulation and impairs planar cell polarity (Blair et al., 2006; Gunsalus et al., 1995).

DmCFL homozygous mutants showed severely disrupted embryonic muscle development (Balakrishnan, Howard, et al., 2021). These *DmCFL* mutants are not viable, and thus our lab employed an RNAi strategy to knockdown *DmCFL* RNA levels specifically in body wall muscle (Balakrishnan et al., 2020). This model and observed phenotypes are discussed in a more detailed manner in the introduction to Chapter 2. Briefly, *DmCFL* knockdown (KD) larvae properly hatch and survive to the end of larval development when the RNAi construct is driven by the muscle *Mhc*-Gal4 promoter. By L3, many of the muscles have deteriorated significantly in a progressive manner with functional consequences on larval locomotion. Some muscles retain proper sarcomeric integrity (designated class 1). Actin accumulates are seen at the fiber ends in class 2 muscles, while actin aggregates are found throughout the cytoplasm of the muscle cell in class 3. Interestingly, both class 1 and 2 muscles have fewer and longer sarcomeres than control muscles. Affecting the proteasome or increased expression of *Drosophila* and human cofilin isoforms can improve the muscle deterioration phenotype (Balakrishnan et al., 2020).

VIII. SUMMARY

Drosophila melanogaster is a useful model for human muscle disease, as many questions remain about muscle development and maintenance. While NM is often described as a disease of the sarcomere, we wanted to know if there were non-sarcomeric effects of muscle *DmCFL* KD. To address this, I analyzed RNA

sequencing data and identified changes in NMJ-related genes. I hypothesized that actin would be disrupted at the postsynapse, and that this would affect postsynaptic integrity. I characterized DmCFL and actin at the NMJ (Chapter 2) and the structural and functional consequences in the context of *DmCFL* KD (Chapter 3). These findings have implications for understanding NM disease mechanisms and for devising new clinical care strategies for these patients.

CHAPTER 2:
COFILIN REGULATES ACTIN AT THE MUSCLE POSTSYNAPSE

I. INTRODUCTION

Nemaline myopathy (NM) is a skeletal muscle disorder that has been linked to 12 actin- and sarcomere-related genes (Christophers et al., 2022; Sewry et al., 2019). One such gene is *CFL2*, which encodes the actin-severing protein cofilin-2. Cofilin is a member of the actin depolymerizing factor (ADF)/cofilin family. These proteins are involved in severing actin filaments and preventing monomer exchange, in turn regulating actin filament length (Galkin et al., 2011; Hayden et al., 1993). Cofilin-2 is the predominant isoform in mature skeletal muscle, as the expression of cofilin-1 decreases in early postnatal muscle (K Mohri et al., 2000). Previous work has established the role of cofilin-2 in skeletal muscle development, maintenance, and regeneration (Agrawal et al., 2012; Gurniak et al., 2014; Kremneva et al., 2014; S Ono et al., 1994; Thirion et al., 2001).

NM patients with *CFL2* mutations share the hallmark features of the disease: muscle weakness and nemaline bodies (also known as nemaline rods) seen in muscle biopsies. Such nemaline bodies can be appreciated by histological staining (such as Gömöri Trichrome, Figure 2.1A) and electron microscopy (Figure 2.1B). In addition to nemaline bodies emanating from the sarcomere, electron micrographs of *CFL2* patient tissue show disorganization of cytoplasmic actin (Figure 2.1B). *CFL2* mutations cause variable disease severity at birth. Some patients present with delayed motor milestones—such as walking—that then further progresses to a decline in muscle function in the

teenage years (Agrawal et al., 2007; Ockeloen et al., 2012). Other patients require immediate respiratory ventilatory assistance during the neonatal period due to apnea (Fattori et al., 2018; R. W. Ong et al., 2014). In its most severe form, *CFL2* NM can lead to premature death within the first year of life (Fattori et al., 2018; R. W. Ong et al., 2014).

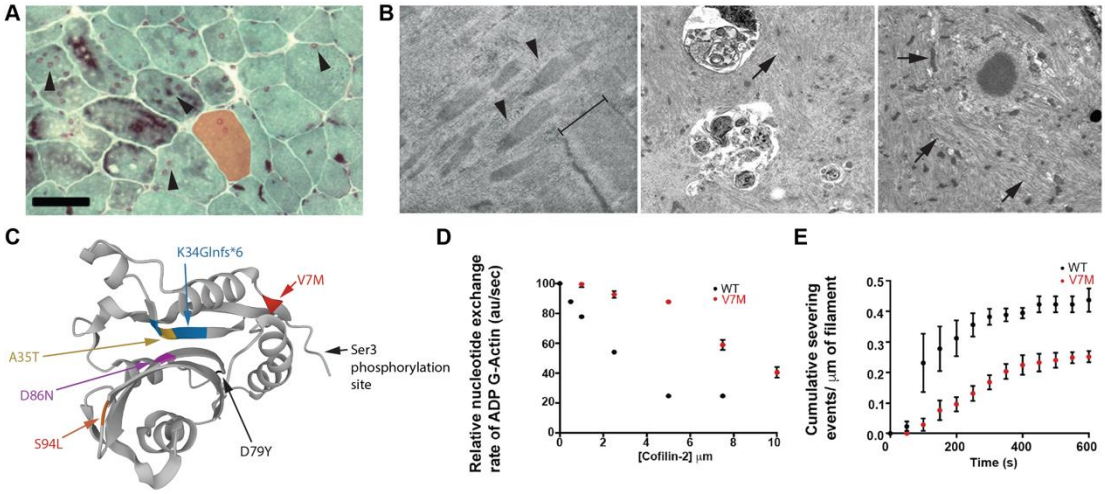

Figure 2.1: Human CFL2 nemaline myopathy genetics and histopathology. (A) Gomori Trichrome staining of muscle biopsy from *CFL2* NM patient. Red shading shows the area of a single myofiber. Arrowheads point to nemaline bodies within muscle fibers. Scale bar = 50 μm. Adapted from (Ockeloen et al., 2012). (B) Electron micrographs of muscle biopsy from *CFL2* NM patient. Arrowheads indicate areas of sarcomeric dissolution, bracket shows the span of one sarcomere, and arrows point to areas of cytoplasmic actin thin filament disorganization. Adapted from (Fattori et al., 2018). (C) Three-dimensional protein structure of human cofilin-2 with amino acids affected by NM mutations labeled. Generated using AlphaFold. (D) *In vitro* ADP-actin monomer nucleotide exchange rate of human *CFL2*^{WT} and CFL2^{V7M} at various increasing concentrations. Adapted from (Balakrishnan et al., 2020). (E) Actin filament severing activity of human CFL2WT and CFL2V7M in vitro over time. Adapted from (Balakrishnan et al., 2020).

Several *CFL2* mutations have been identified in NM patients (illustrated in Figure 2.1C). The first mutation (A35T) was identified near the protein's nuclear

localization signal, and it is thought to affect protein misfolding or tertiary structure destabilization (Agrawal et al., 2007). A four base pair deletion in this region (Lys34Glnfs*6) has also been found and is thought to lead to more severe disease because it is a null mutation (R. W. Ong et al., 2014). The V7M mutation is located near the phosphorylation site at Ser3, and the authors of the study hypothesize that the mutation could lead to a truncation of the amino acids at the N-terminus (Ockeloen et al., 2012). Cofilin harboring the V7M mutation produces a protein that is inefficient in nucleotide exchange and filament severing (Figure 2.1D,E; Balakrishnan et al., 2020). Most recently, mutations have been identified D86N, D79Y, and S94L; the latter two were present in a case of compound heterozygosity (Fattori et al., 2018).

In *Drosophila*, Twinstar (also known as DmCFL) is the only cofilin isoform with 37% sequence homology to the vertebrate cofilin-2 protein (Figure 2.2A). Previous work in our lab has shown that Twinstar is expressed throughout muscle development and that homozygotes of hypomorph or null mutations lead to missing or improperly attached muscles in the embryo (Figure 2.2B,C).

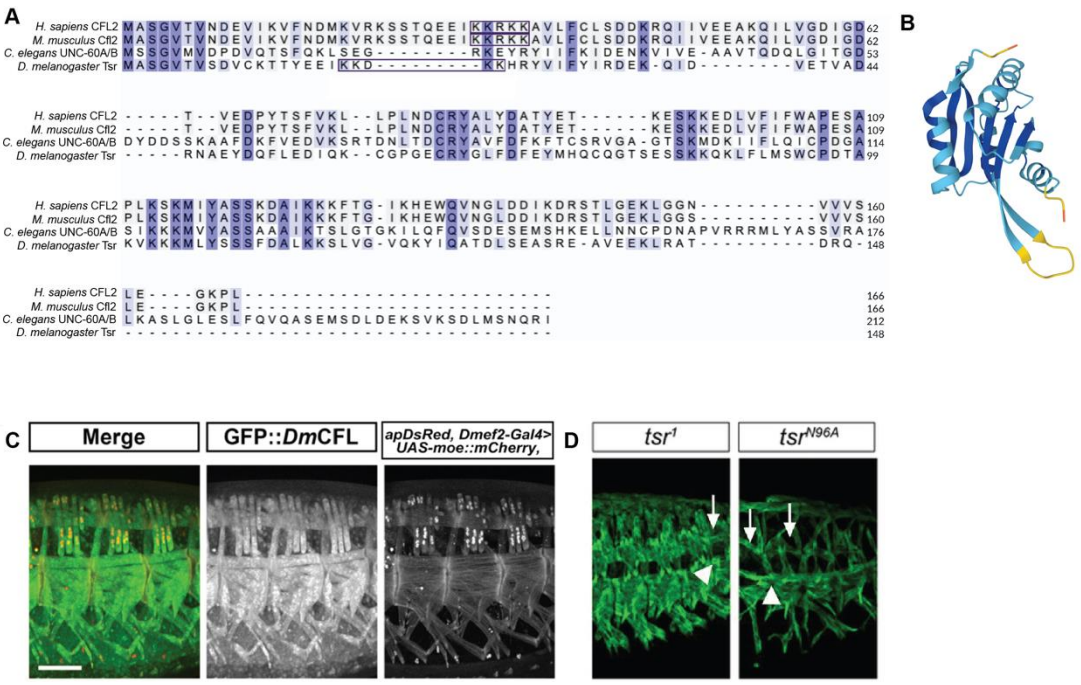

Figure 2.2: *Drosophila* cofilin (DmCFL) and its orthologues. (A) Protein alignment for cofilin-2 orthologues. Highlight indicates amino acid residue similarity. (B) DmCFL protein structure generated using AlphaFold. (C) Live imaging of stage 16 embryo with body wall muscle labeled by moesin::mCherry and endogenous DmCFL::GFP. Scale bar = 50 µm. Adapted from (Balakrishnan et al., 2020). (D) Fixed tissue imaging of stage 16 *tsr* mutant embryos stained with anti-Myosin heavy chain to show body wall muscles, some of which were missing (arrows) or misattached (arrowheads). Scale bar = 50 µm. Adapted from (Balakrishnan et al., 2020).

Given that these mutations when homozygous are not viable, our lab has used an RNA interference (RNAi) strategy to reduce levels of *DmCFL* (*DmCFL* knockdown) in muscle by using the Gal4/UAS system, specifically the muscle-specific promoter (*Mhc*-Gal4) to drive an RNAi (UAS-*tsr* RNAi) construct targeting a 21 base pair region of the *twinstar* gene (Figure 2.3A; Balakrishnan et al., 2020; Brand & Perrimon, 1993). *DmCFL* KD larvae show progressive muscle deterioration with three clear phenotypes that can be classified (Figure 2.3B). Class 1 muscles sarcomeric organization is intact. Class 2 muscles show an accumulation of F-actin at the cell poles, although there sarcomeric structure

is retained throughout the cell, suggesting it is a transition stage. Class 3 muscles have lost structural integrity and contain accumulations of actin throughout the cytoplasm in addition to the cell poles. By late third instar stage, all three classes are present, although the majority are class 3 (53.1%; Figure 2.3C). A similar progressive deterioration and actin accumulation was seen in *C. elegans* mutant for *UNC60B*, the cofilin homolog (K. Ono et al., 2003; Shoichiro Ono et al., 1999). The deterioration phenotype could be mostly rescued by introducing wild type DmCFL or the human versions of cofilin-1 and cofilin-2; however, expression of the mutant DmCFL^{V7M} or human CFL2^{V7M} version provided only partial rescue (Figure 2.3D). The accumulations seen throughout the muscle cell in class 3 are ubiquitinated, suggesting that the ubiquitin-proteasome system is not efficiently clearing these debris. In fact, increasing activity of the proteasome improves the phenotype (Figure 2.3E).

Here, I used transcriptomic analysis to expand the avenues of inquiry into the *DmCFL* KD model, which led us to look at the neuromuscular junction (NMJ). The NMJ is the specialized synapse between the presynaptic motor neuron and postsynaptic muscle that is critical for communication about muscle contraction. I found that cofilin is present at the postsynapse and that KD reduces its levels in this region. In tandem, disorganization of actin is seen at postsynapse as the overall muscle deteriorates. These findings suggest that cofilin plays an important role in maintenance of postsynaptic actin structure.

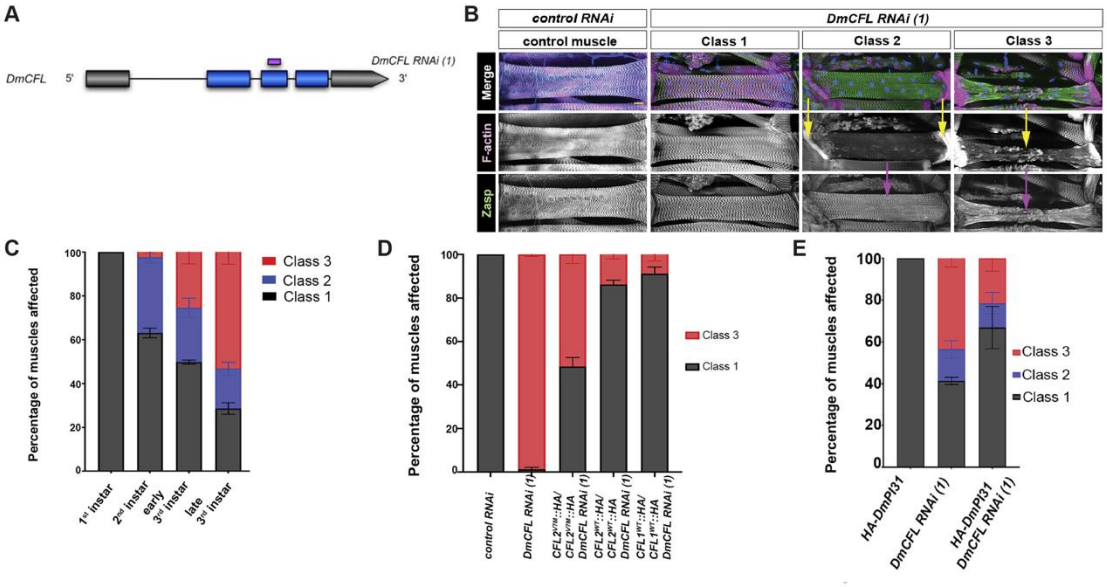

Figure 2.3: Characterization of DmCFL KD model. (A) Schematic depicting *DmCFL* gene locus and indicating site targeted by the UAS-*tsr* RNAi construct (purple bar). (B) Representative images of VL3 muscle in control and *DmCFL* KD larvae labeled with anti-Zasp (Z disc) and phalloidin (F-actin). Examples of the three phenotypic classes present in *DmCFL* KD are shown. Scale bar = 25 µm. (C) Quantification of muscle class proportions seen in *DmCFL* KD larvae of each larval stage. (D) Quantification of muscle class proportions seen in third instar control and *DmCFL* KD larvae compared to larvae expressing human cofilin protein ($CFL1^{WT}$, $CFL2^{WT}$, or mutant $CFL2^{V7M}$) in combination with the *DmCFL* RNAi. (E) Quantification of muscle class proportions seen in third instar control and *DmCFL* KD larvae compared to larvae with increased proteasomal activity due to overexpression of DmPI31. Figure adapted from (Balakrishnan et al., 2020).

II. RESULTS

A. Muscle deterioration phenotype is variable in DmCFL KD larval muscles

Since the *DmCFL* KD phenotype is progressive, in this study, I wanted to examine larvae at mature larval muscle. I considered wandering larvae, which are at the latest stage of their development at five days post-egg laying and

preparing for pupation. I confirmed that at the wandering stage *DmCFL* KD larvae had decreased *DmCFL* RNA (27.9% of control level) by qPCR and reduced DmCFL protein (38.2% of control level) and inactive p-DmCFL protein (33.2% of control level) by western blot (Figure 2.4A-C, experiment done in collaboration with David Soffar, Baylies lab). For these experiments, I used antibodies against DmCFL and p-DmCFL from the Tadashi Uemura lab, which had not previously been used to study muscle. The reduction seen by western blot is comparable to the DmCFL protein reduction seen in previous studies probing for a fluorescently-tagged DmCFL (Balakrishnan et al., 2020).

Figure 2.4: Cofilin is expressed in sarcomeres and reduced in DmCFL KD. (A) Relative level of *DmCFL* RNA in muscle-enriched preparations of wandering *DmCFL* KD larvae relative to control by quantitative PCR (0.279 ± 0.142; N = 3 replicates, *n* = 5-10 larvae). (B) DmCFL and p-DmCFL protein levels in control and *DmCFL* KD wandering larvae by western blot (N = 3 replicates, *n* = 5-10 larvae). Experiment done in collaboration with David Soffar. (C) Quantification of DmCFL (*DmCFL* KD mean 0.382 ± 0.197) and p-DmCFL (*DmCFL* KD 0.3321 ± 0.128) protein normalized to glyceraldehyde 3-phosphate dehydrogenase (GAPDH) as a loading control in control and *DmCFL* KD larvae. (D) Sum slices projection of VL3-VL4 muscle pair in live larva expressing GFP-tagged DmCFL. Scale bar = 50 μm. (E) Magnified confocal image showing DmCFL::GFP expression at live larval muscle sarcomere. Scale bar = 25 μm. (F) Magnified confocal image showing DmCFL::GFP expression at live larval muscle sarcomere. Scale bar = 25 μm. (G) Structured illumination microscopy (SIM) images of sarcomeres in control and *DmCFL* KD larval muscles stained with phalloidin (red) and anti-DmCFL (cyan, lower panel in gray) by Scale bar = 5 μm. (H) Representative confocal images of VL3-VL4 muscle pairs of wandering control and *DmCFL* KD larvae labeled with phalloidin (red) and anti-Dlg (cyan). *DmCFL* KD images illustrate how VL3 and VL4 in same pair can be of different classes. Scale bar = 100 μm. (I) Quantification of VL3-VL4 muscle pair classes in *DmCFL* KD larvae grouped by combination of classes (*n* = 45 larvae, 270 muscle pairs).

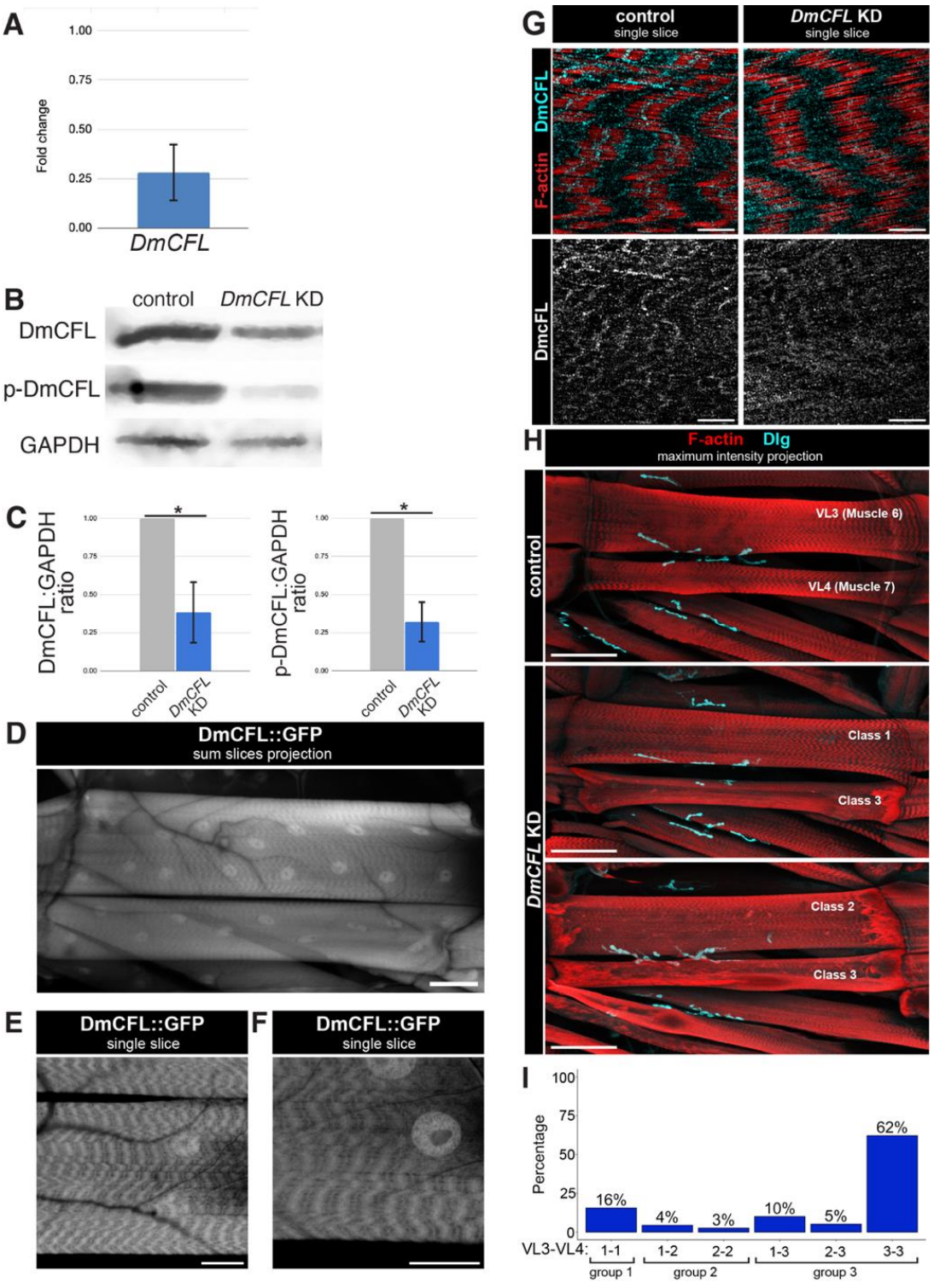
A
Fold change
1.00
0.75
0.50
0.25
0.00
DmCFL
B
control
DmCFL KD
DmCFL
p-DmCFL
GAPDH
C
DmCFL:GAPDH ratio
p-DmCFL:GAPDH ratio
control
DmCFL KD
D
DmCFL::GFP
sum slices projection
E
DmCFL::GFP
single slice
F
DmCFL::GFP
single slice
G
control
single slice
DmCFL KD
single slice
F-actin
DmCFL
DmcFL
H
F-actin Dlg
maximum intensity projection
control
VL3 (Muscle 6)
VL4 (Muscle 7)
DmCFL KD
Class 1
Class 3
Class 2
Class 3
I
Percentage
100
75
50
25
0
16%
4%
3%
10%
5%
62%
VL3-VL4:
1-1
1-2
2-2
1-3
2-3
3-3
group 1
group 2
group 3

Using live imaging of control larvae expressing the DmCFL::GFP protein trap, I confirmed that DmCFL localizes to the Z disc and H zone (Figure 2.4D-F). A similar sarcomeric localization pattern for DmCFL can be appreciated using structured illumination microscopy (SIM) of fixed control and *DmCFL* KD larval muscles using antibodies directed to DmCFL (Figure 2.4G). Some DmCFL still localizes to the sarcomere in *DmCFL* KD muscles (Figure 2.4G).

Ventral longitudinal muscles 3 and 4 (VL3 and VL4) are often used in *Drosophila* larval muscle studies. These muscles are easily accessible upon flat-prep dissection, run parallel to each other, and are innervated by the same motor neuron branch. Interestingly, since all muscle classes are present in late *DmCFL* KD larvae, I found that muscles VL3 and VL4 can be of different classes (Figure 2.4H,I). This suggests that muscles in *DmCFL* KD larvae do not deteriorate at the same rate. For all experiments, I considered both VL3 and VL4 in one hemisegment as a pair, which required grouping the various class combinations of these muscles. For example, group 1 pairs were those in which both VL3 and VL4 were class 1. Meanwhile, group 3 pairs had at least one class 3 muscle, which could be VL3, VL4 or both. The majority (77%) of the muscle pairs in wandering *DmCFL* KD larvae were categorized as group 3, with predominantly pairs where both muscles were class 3 (62%, Figure 2.4I). Only 16% of pairs fit into group 1 at this timepoint.

B. RNA sequencing (RNAseq) reveals transcriptional changes related to the neuromuscular junction

Transcriptomic comparison of control and *DmCFL* KD larvae was done to open new avenues of inquiry about the *DmCFL* KD model. Third-instar larvae were dissected to produce muscle-enriched preparations; the RNA extracted from these larval fillets was submitted for bulk sequencing (Figure 2.5A). I used the DESeq2 pipeline to do differential expression analysis on genes with a minimum two-fold change difference.

This analysis identified 1417 differentially-expressed genes in *DmCFL* KD larvae compared to control (Figure 2.5B-F). The heat map illustrating the Z score (i.e. number of standard deviations that a data point is from the mean expression) of each gene shows a clear clustering of up- and down-regulated genes with little dispersion (Figure 2.5F). Decreased expression was found for 558 genes, including *DmCFL* (Figure 2.5D). MA plot visualization shows how *DmCFL* is highly expressed in muscle and is decreased by $\log_2$ fold change of 2.3 in *DmCFL* KD samples (Figure 2.5E).

Figure 2.5: Transcriptomic analysis identifies changes at the neuromuscular junction (NMJ) in DmCFL KD muscles.

(A) Bulk RNA sequencing (RNAseq) was performed on muscle-enriched preparations from third-instar control and *DmCFL* KD larvae (N = 3 replicates, each with *n* = 7-10 larvae per genotype. Diagram made using Biorender). Procedure was conducted by Mridula Balakrishnan. (B) Volcano plot representing the significantly (FDR 0.05) differentially-expressed genes by their fold change in *DmCFL* KD compared to control larvae (red = increased, blue = decreased). *DmCFL* is highlighted on the graph. (C) Principle component analysis (PCA) plot showing the samples by two dimensions of the differentially-expressed genes. (D) Plot showing expression of *DmCFL* (*twinstar*) in control and *DmCFL* KD samples by RNAseq. (E) MA plot visually representing the log fold change versus average expression of differentially-expressed genes (blue = downregulated, red = upregulated) between control and *DmCFL* KD larvae. (F) Heat map displaying the Z-score of each gene (green = downregulated, magenta = upregulated) to show differential gene expression between control and *DmCFL* KD larvae. (G) Top significantly downregulated pathways identified as decreased by two-fold change (FDR = 0.05) using gene ontology (GO) biological processes (BP) gene sets. (H) Top significantly upregulated pathways identified as increased by two-fold change (FDR = 0.05) using gene ontology (GO) biological processes (BP) gene sets. (I) Gene expression fold change of selected genes related to the neuromuscular junction.

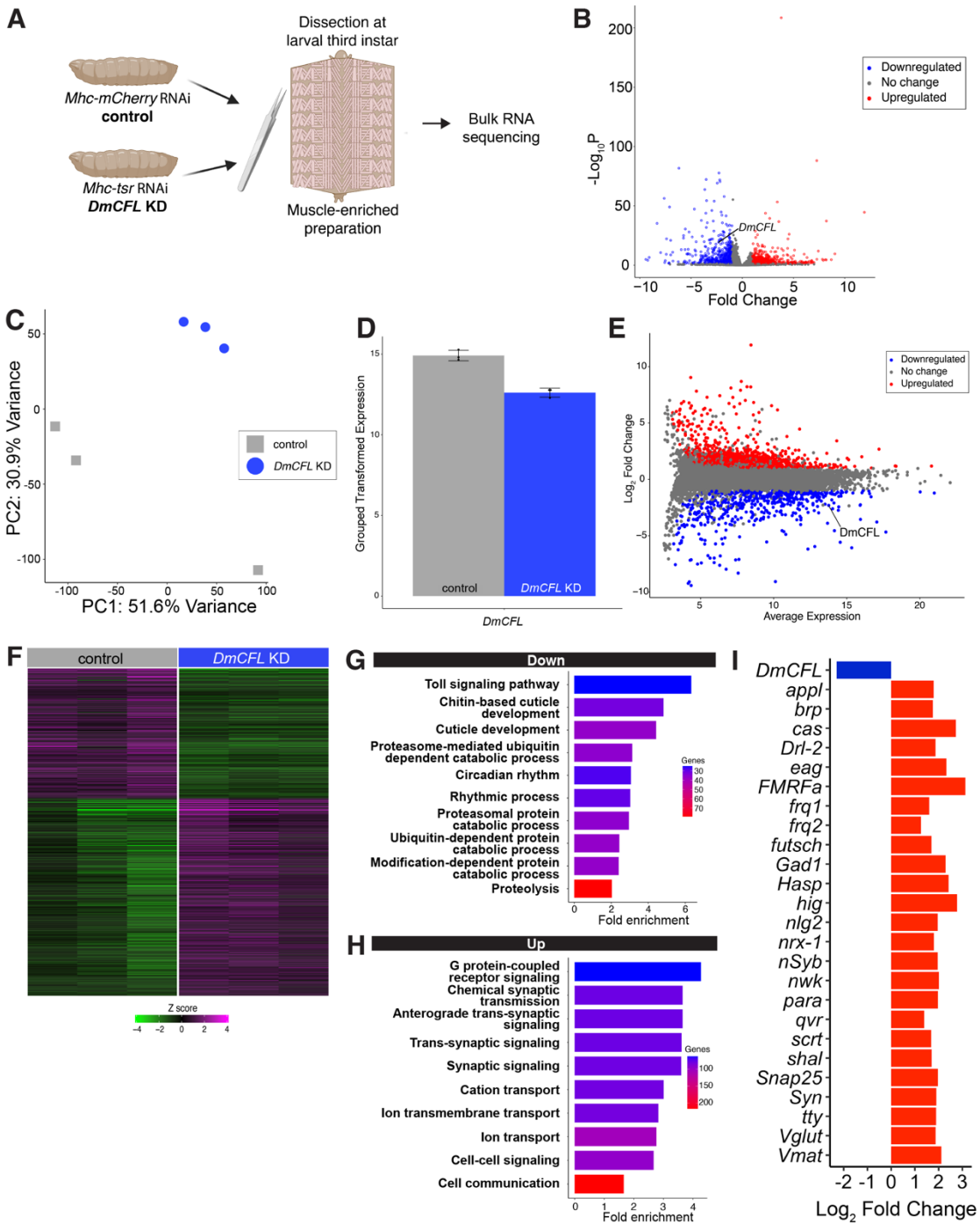
A
Dissection at larval third instar
Mhc-mCherry RNAi control
Mhc-tsr RNAi DmCFL KD
Bulk RNA sequencing
Muscle-enriched preparation
B
Downregulated
No change
Upregulated
-Log10 P
Fold Change
DmCFL
C
PC2: 30.9% Variance
PC1: 51.6% Variance
control
DmCFL KD
D
Grouped Transformed Expression
control
DmCFL KD
DmCFL
E
Downregulated
No change
Upregulated
Log2 Fold Change
Average Expression
DmCFL
F
control
DmCFL KD
Z score
G
Down
Toll signaling pathway
Chitin-based cuticle development
Cuticle development
Proteasome-mediated ubiquitin dependent catabolic process
Circadian rhythm
Rhythmic process
Proteasomal protein catabolic process
Ubiquitin-dependent protein catabolic process
Modification-dependent protein catabolic process
Proteolysis
Genes
Fold enrichment
H
Up
G protein-coupled receptor signaling
Chemical synaptic transmission
Anterograde trans-synaptic signaling
Trans-synaptic signaling
Synaptic signaling
Cation transport
Ion transmembrane transport
Ion transport
Cell-cell signaling
Cell communication
Genes
Fold enrichment
I
DmCFL
appl
brp
cas
Drl-2
eag
FMRFa
frq1
frq2
futsch
Gad1
Hasp
hig
nlg2
nrx-1
nSyb
nwk
para
qvr
scrt
shal
Snap25
Syn
tty
Vglut
Vmat
Log2 Fold Change

Gene set enrichment analysis (GSEA) using gene ontology (GO) biological processes (BP) gene sets revealed changes in the proteasomal degradation pathway, which was also seen in overrepresentation analysis (ORA) using the same gene set (Table 2.1, Figure 2.5G). These findings are aligned with the improvement seen in previous work where proteasomal activation improved the deterioration phenotype in *DmCFL* KD larvae (Balakrishnan et al., 2020).

Differential expression analysis identified 850 genes with increased expression in *DmCFL* KD. GSEA and ORA highlighted synaptic signaling pathways, such as excitatory postsynaptic potential (Table 2.1, Figure 2.5H). The muscle forms a synapse with the motor neuron known as the neuromuscular junction (NMJ), where stimulus from the motor neuron leads to a cascade resulting in muscle contraction. The motor neuron is the presynaptic side that releases neurotransmitter, while the muscle subsynaptic reticulum membrane is the postsynaptic side that receives the neurotransmitter stimulus. Various genes associated with the NMJ showed increased expression by RNAseq (Figure 2.5I). These findings motivated me to further examine the NMJ in *DmCFL* KD larvae to investigate if there were any neuromuscular structural and/or functional alterations in this model.

C. Measuring levels of postsynaptic components

To visualize the NMJ, horseradish peroxidase (HRP) and Discs-large (Dlg) are typically used as markers (Figure 2.6A): anti-HRP labels the motor neuron presynaptic membrane (Jan & Jan, 1982) and anti-Dlg labels the structural protein at the muscle postsynaptic membrane (Lahey et al., 1994).

Table 2.1. Top affected pathways by DESeq2.
NES = normalized enrichment score.

Direction	Gene Ontology: Biological Processes	NES	Genes	Adj *P* value
Down	Puparial adhesion	-0.975	7	9.20E-05
	Multicellular organism adhesion	-0.975	7	9.20E-05
	Multicellular organism adhesion to substrate	-0.975	7	9.20E-05
	Proteasomal ubiquitin-independent protein catabolic process	-0.825	22	9.50E-04
	Chitin-based cuticle development	-0.625	131	3.40E-08
Up	G protein-coupled receptor signaling pathway coupled to cyclic nucleotide second messenger	0.9134	9	3.70E-03
	Serotonin receptor signaling pathway	0.9134	9	3.70E-03
	G protein-coupled serotonin receptor signaling pathway	0.9134	9	3.70E-03
	Excitatory postsynaptic potential	0.8107	17	1.70E-02
	Chemical synaptic transmission postsynaptic	0.8107	17	1.70E-02
	Neuropeptide signaling pathway	0.7769	71	2.90E-10
	Response to monoamine	0.7477	22	4.00E-02
	Cellular response to monoamine stimulus	0.7477	22	4.00E-02
	Response to catecholamine	0.7477	22	4.00E-02
	Cellular response to catecholamine stimulus	0.7477	22	4.00E-02
	Response to dopamine	0.7477	22	4.00E-02
	Cellular response to dopamine	0.7477	22	4.00E-02
	Regulation of neurotransmitter secretion	0.7252	28	2.20E-02
	Regulation of neurotransmitter transport	0.7252	28	2.20E-02
	Regulation of postsynaptic membrane potential	0.7221	26	4.30E-02
	Regulation of membrane potential	0.7073	79	3.30E-07
	Organic hydroxy compound transport	0.674	34	4.60E-02
	Adenylate cyclase-activating G protein-coupled receptor signaling pathway	0.662	41	2.20E-02
	Adenylate cyclase-modulating G protein-coupled receptor signaling pathway	0.6544	61	2.10E-03
	G protein-coupled receptor signaling pathway	0.6469	203	4.60E-12
	Larval behavior	0.6427	52	9.50E-03
	Courtship behavior	0.6243	64	5.60E-03
	Male courtship behavior	0.6219	52	2.60E-02
	Learning	0.6112	63	1.20E-02
	Male mating behavior	0.6061	59	2.20E-02

For this study, I was interested in examining changes in the postsynaptic compartment of *DmCFL* KD muscles. Given the three-dimensional alterations in class 3 *DmCFL* KD muscles (Figure 2.6B), limiting the quantification of protein intensities in the muscle postsynaptic compartment without including signal from the sarcomere is challenging. Therefore, I used a three-dimensional analysis approach to restrict the volume in which fluorescence intensity of the stained proteins of interest were be measured. After measuring the intensities of the HRP- and F-actin signals in the Z dimension using an orthogonal view (Figure 2.6C), I found that setting a conservative threshold of 0.5 μm away from the HRP signal would exclude the brightest F-actin signal (assumed to be sarcomeric actin). Therefore, I defined the postsynaptic volume as being within 0.5 μm of HRP.

I leveraged Imaris software for subsequent analyses of the postsynaptic region, as it allows for the creation of a three-dimensional volume created from the fluorescent signal in an image. First, I created a volume of the HRP-positive signal (i.e. motor neuron) shared between a VL3 and VL4 muscle pair (Figure 2.6D). Then, I created a second volume that started at the surface edge of the HRP volume and then was expanded by 0.5 μm away from the surface (Figure 2.6E,F); the postsynaptic region was defined as this expanded volume. Fluorescence intensities were then measured within the postsynaptic region and normalized to the expanded volume.

Figure 2.6: Measuring levels of postsynaptic proteins in three-dimensions. (A) Left: Confocal images of NMJ labeled by postsynaptic membrane anti-Dlg (red) and presynaptic membrane labeled by anti-HRP (cyan). Right: Dlg channel alone (grayscale). Scale bar = 10 μm. (B) Three-dimensional representation of a muscle pair where VL3 is Class 3 and VL4 is Class 1 labeled by phalloidin (red) and anti-HRP (cyan). Generated using Imaris software. Scale bar = 10 μm. (C) Confocal image of an individual bouton from control muscle labeled with HRP (cyan) and the underlying muscle actin labeled with phalloidin (red), resliced to show XZ dimensions. Plot of mean intensity for HRP and actin signal across individual boutons in the Z dimension. Cutoff of 0.5 μm from the HRP signal was used for all intensity measurements of the postsynaptic region. Plot shows the average of 15 individual boutons in Mhc-mCherry RNAi larva. (D) Three-dimensional representation of a confocal Z stack of a control muscle pair labeled with phalloidin (red) and a surface generated from HRP-positive signal (cyan). Generation of surfaces and quantification of intensity was done using Imaris version 10.0.0. Scale bar = 10 μm. (E) Three-dimensional expanded surface (red outline) generated a distance of 0.5 μm from the HRP surface (cyan). Postsynaptic intensity of proteins was measured within this expanded volume. Mean intensity was defined as the sum of the sum intensity within the expanded surface then divided by the volume of the expanded surface. Scale bar = 10 μm. (F) Magnification of area shown in C. Arrow indicates postsynaptic domain. Scale bar = 2 μm. (G) Three-dimensional representation of a confocal Z stack of muscle pair labeled with cofilin (yellow) and expanded surface generated in prior steps (red). (H) Magnification of area shown in E. Arrow indicates postsynaptic domain. Scale bar = 2 μm.

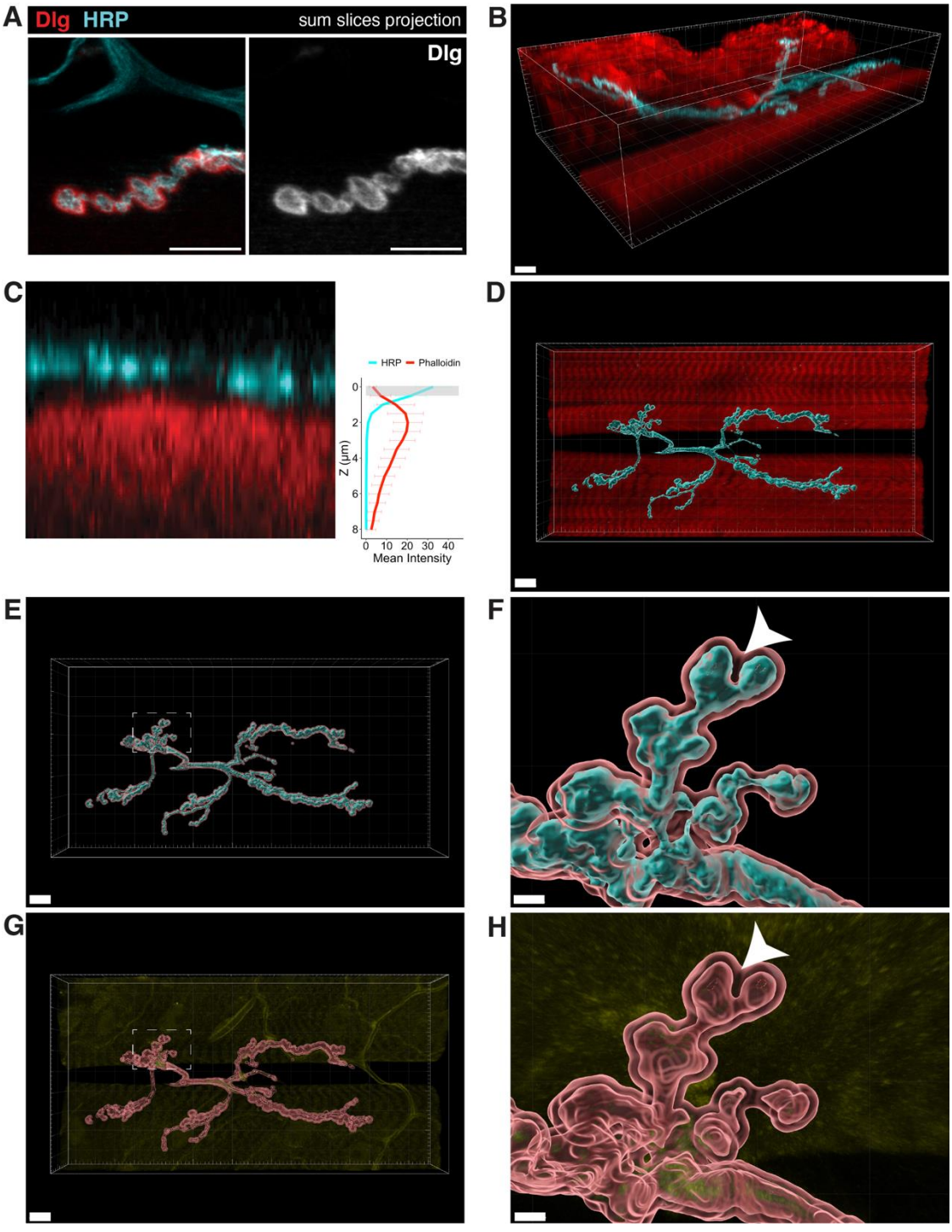
A
Dlg HRP
sum slices projection
Dlg
B
C
HRP Phalloidin
Z (µm)
0
2
4
6
8
0 10 20 30 40
Mean Intensity
D
E
F
G
H

D. Cofilin localizes to the postsynapse and is reduced in *DmCFL* KD

I sought to visualize cofilin at the postsynaptic region, for which I imaged both live and fixed samples. Using the DmCFL::GFP protein trap, I found that cofilin localizes to the postsynaptic region in live muscle preparations in addition to the staining seen at the sarcomere (Figure 2.7A). Bright rings of fluorescently-tagged cofilin protein organize in a similar pattern to Dlg. In fixed tissue cofilin is present throughout the muscle, including at the postsynapse and the levels are reduced in *DmCFL* KD muscles (Figure 2.7B). The postsynaptic localization of DmCFL in fixed tissue was better visualized using SIM (Figure 2.7C).

To measure the levels of DmCFL at the postsynapse, I employed the previously described method using Imaris. This analysis revealed that postsynaptic DmCFL is significantly reduced by 30.8% in KD muscles compared to control (Figure 2.7D). Similarly, in the KD, the levels of the inactive phosphorylated form of DmCFL (p-DmCFL) are reduced postsynaptically by 51.6% (Figure 2.7E-F).

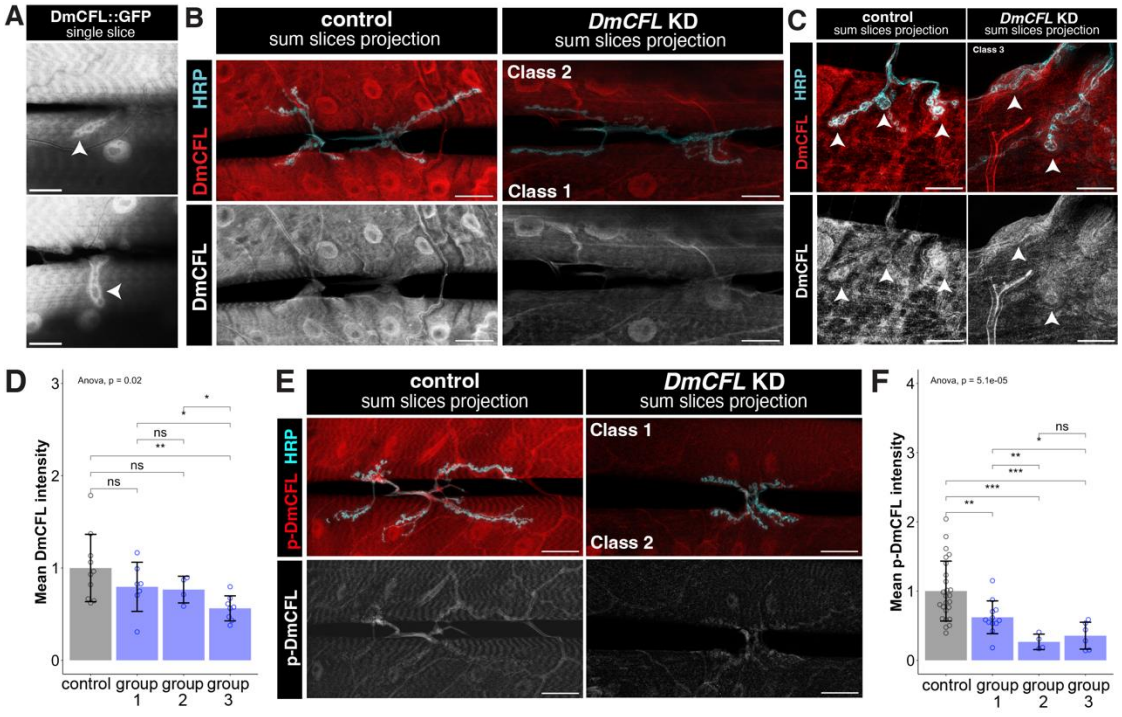

Figure 2.7: DmCFL localizes to the postsynapse and is reduced in KD. (A) Two representative confocal images of DmCFL protein at the postsynapse of the NMJ in live larvae expressing the protein trap DmCFL::GFP. Arrowheads indicate DmCFL at postsynaptic surrounding individual boutons. Scale bar = 20 μm. (B) Confocal images (top) of larval NMJ in control (left) and *DmCFL* KD (right) muscles labeled with anti-DmCFL (red) and anti-HRP (cyan). Bottom: DmCFL channel alone (grayscale). Scale bar = 25 μm. (C) SIM images (top) of NMJ boutons at the larval NMJ in control (left) and *DmCFL* KD (right) muscles labeled with anti-DmCFL (red) and anti-HRP (cyan). Bottom: DmCFL single channel (grayscale). Arrows indicate DmCFL at postsynaptic surrounding individual boutons. Scale bar = 10 μm. (D) Quantification of mean postsynaptic DmCFL intensity normalized to control (control 1 ± 0.365, *n* = 11 NMJs; overall *DmCFL* KD 0.692 ± 0.217, *n* = 19 NMJs). (E) Confocal images (top) of larval NMJ in control (left) and *DmCFL* KD (right) muscles labeled with p-DmCFL (red) and anti-HRP (cyan). Specific *DmCFL* KD classes noted. Bottom: p-DmCFL channel alone (grayscale). Scale bar = 25 μm. (F) Quantification of mean postsynaptic p-DmCFL intensity at postsynapse normalized to control (control 1 ± 0.433, *n* = 24 NMJs; overall *DmCFL* KD 0.484 ± 0.245, *n* = 22 NMJs). Quantifications show mean ± SD and statistics calculated by ANOVA (* $p < 0.05$, ** $p < 0.01$, **** $p \leq 0.0001$).

E. Actin and actin-binding proteins are disorganized at the postsynapse in the context of *DmCFL* KD

Since filamentous actin associated with the sarcomeres becomes disorganized as *DmCFL* KD muscles deteriorate, I was interested in examining actin in the postsynaptic domain. In class 3 muscles there was clear actin disorganization at the entire NMJ, while only some boutons in class 2 muscles were surrounded by actin accumulations, suggesting progressive deterioration of postsynaptic actin organization (Figure 2.8A, arrowheads). The actin enveloping the boutons was especially obvious when looking at individual slices. The actin accumulations in this region were only seen in the more affected muscles, regardless of the class of the adjacent muscle in the pair. For example, a class 3 VL3 muscle had actin accumulations throughout the NMJ even if the paired VL4 muscle in that hemisegment was class 1. Additionally, in class 3 muscles, postsynaptic actin tended to be pulled away toward the motor neuron (Figure 2.8B). Using the three-dimensional quantification method, I found that actin intensity was increased at the postsynapse in all three *DmCFL* KD muscle classes compared to control, but increasingly so in class 2 and 3 muscles (Figure 2.8C).

Figure 2.8: Actin are disorganized at the postsynapse in DmCFL KD Class 2 and 3 muscles. (A) Confocal images (top) of larval NMJ in control (left) and *DmCFL* KD (right) muscles labeled with phalloidin (F-actin, red) and anti-HRP (cyan). Bottom: F-Actin single channel (grayscale). Arrowheads indicate accumulation of actin surrounding the boutons in *DmCFL* KD which is absent in control. Scale bar = 20 μm. Magnification of boxed area. Scale bar = 10 μm. (B) SIM images (top) of larval NMJ in control (left) and *DmCFL* KD (right) muscles labeled with phalloidin (red) and anti-HRP (cyan). Specific muscle classes noted in *DmCFL* KD. Scale bar = 25 μm. (C) SIM images (top) of larval NMJ in control (left) and *DmCFL* KD (right) muscles of different classes labeled with anti-Tmod (red) and anti-HRP (cyan). Bottom: Tmod single channel (grayscale). Scale bar = 20 μm. Magnification shown below with scale bar = 5 μm. Quantifications show mean ± SD and statistics calculated by ANOVA (* $p < 0.05$, ** $p < 0.01$, **** $p \leq 0.0001$).

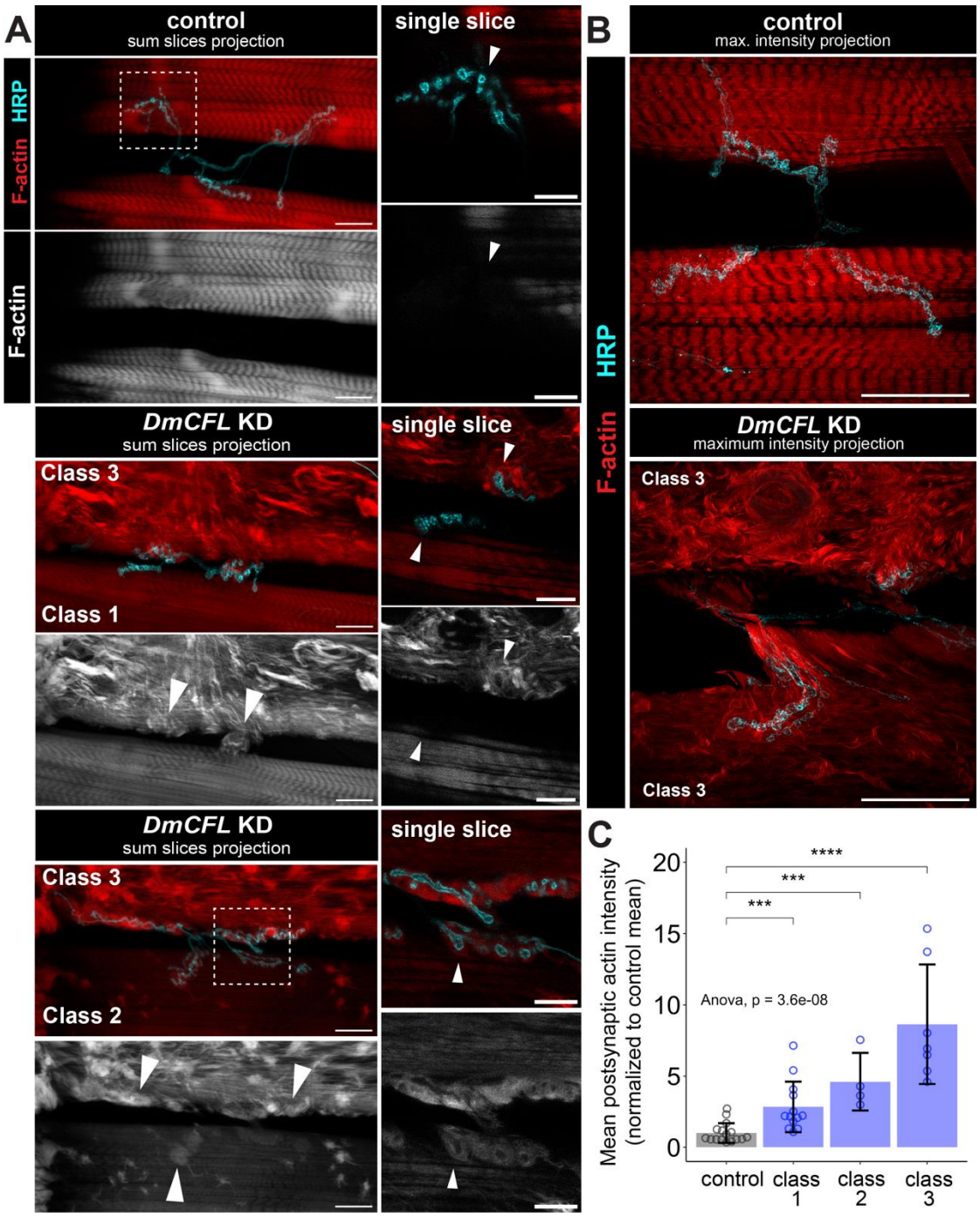
A
control
sum slices projection
single slice
F-actin HRP
F-actin
DmCFL KD
sum slices projection
Class 3
Class 1
Class 2
B
control
max. intensity projection
F-actin HRP
DmCFL KD
maximum intensity projection
C
Mean postsynaptic actin intensity (normalized to control mean)
Anova, p = 3.6e-08
control
class 1
class 2
class 3

To visualize actin near the postsynapse using transmission electron microscopy (TEM), I developed a novel strategy to visualize this by TEM (done in collaboration with Victoria von Saucken, Baylies lab). Typically, the subsynaptic reticulum (SSR), the specialized postsynaptic membrane, is visualized by dissecting the muscle at a plane parallel to the muscle surface (coronal or frontal plane). This approach reveals the SSR folds that surround the boutons. However, this perspective does not adequately show the postsynaptic domain below the SSR within the muscle. Therefore, we devised a protocol to (1) trim the flat larval fillet to the edge of the ventral longitudinal muscles and then (2) orient the blade in a longitudinal direction in order to dissect the larva in a sagittal direction, resulting in the sagittal surface would be exposed (diagram in Figure 2.9A). We sectioned the samples until we reached muscles that were oriented in a parallel direction to the body length (Figure 2.9B). At individual boutons, we could visualize the underlying muscle, and I found that the synaptic cleft—the space between the bouton and the SSR—was collapsed in *DmCFL* KD muscles (Figure 2.9C). At the control NMJ, the actin filaments were organized parallel to each other. In contrast, the actin was disorganized at the postsynapse and throughout the muscle in *DmCFL* KD organisms.

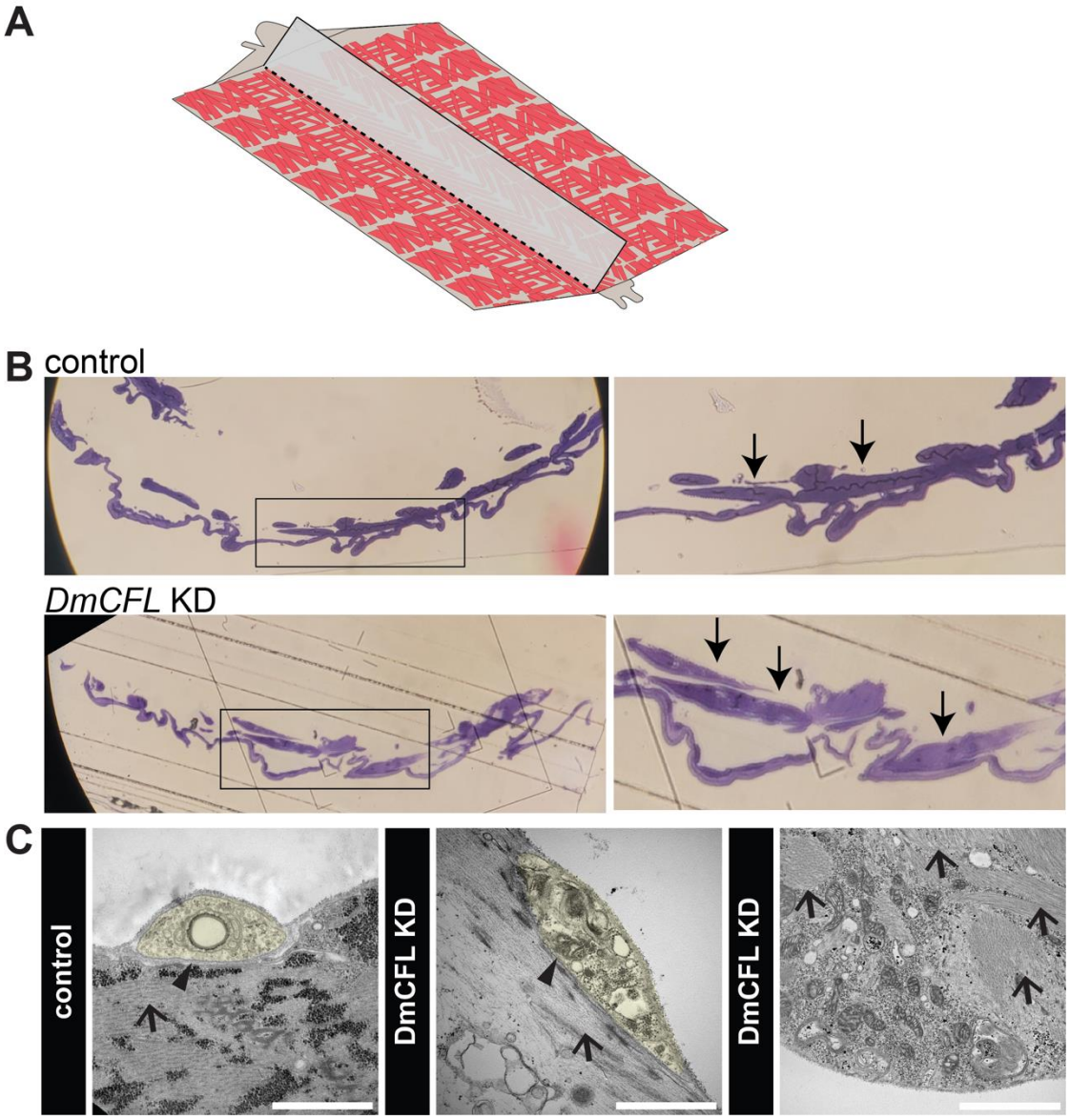

Figure 2.9: Ultrastucture at NMJ shows disorganized actin in DmCFL KD. (A) Diagram of electron microscopy strategy where larvae were dissected in a sagittal direction. (B) Representative sections stained with Toluidine Blue. Arrows indicate ventral longitudinal muscles. (C) NMJ electron micrographs (sagittal sections) in control (left) and *DmCFL* KD (middle). Presynaptic boutons (pseudocolor in yellow) with muscle interface (arrowheads) and actin filaments (arrows). Right: disorganized actin filaments (arrows) throughout cytoplasm in *DmCFL* KD muscle. Scale bar = 1 μm. Experiment was done in collaboration with Victoria von Saucken.

To better understand how the filamentous actin was affected at the postsynapse, I examined localization of two actin-binding proteins: tropomodulin (Tmod) and alpha-Spectrin in this region. Tmod is known to cap actin filaments and, in the *DmCFL* KD model, it has been reported that its levels are reduced at the sarcomere but increased at the cell poles in deteriorated muscles (Balakrishnan et al., 2020). I found that Tmod is highly expressed at the postsynapse (Figure 2.10A). The postsynaptic levels of Tmod are greatly reduced, qualitatively, in *DmCFL* KD muscles of all classes (Figure 2.10A). Alpha-spectrin is also present at the postsynapse and plays a role in the membrane's integrity (Pielage et al., 2006). Similar to Tmod, levels of alpha-Spectrin are visibly reduced surrounding the boutons in *DmCFL* KD compared to control (Figure 2.10B).

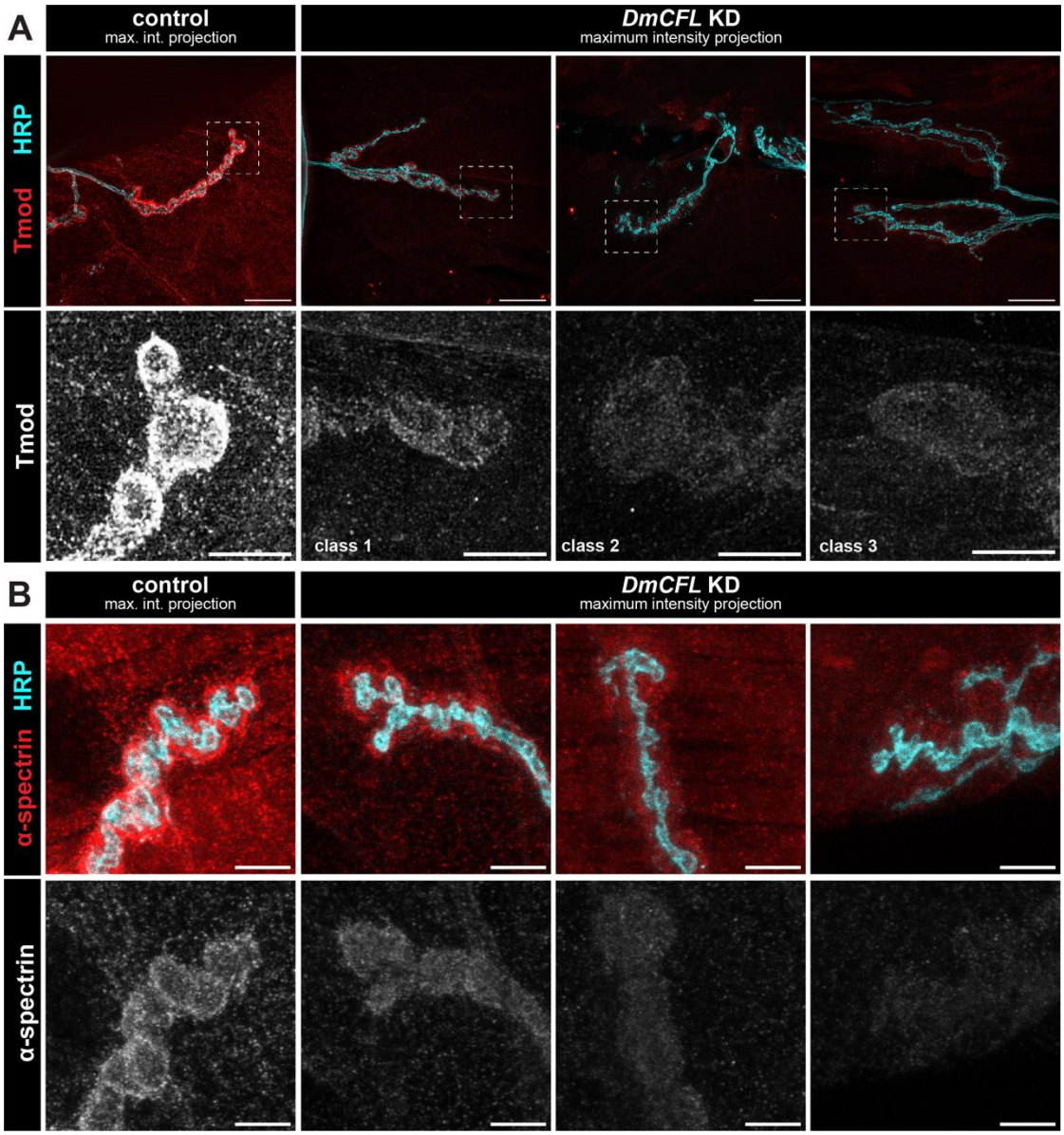

Figure 2.10: Postsynaptic localization of actin-binding proteins Tmod and alpha-spectrin is disrupted in DmCFL KD. (A) SIM images (top) of larval NMJ in control (left) and *DmCFL* KD (right) muscles of different classes labeled with anti-Tmod (red) and anti-HRP (cyan). Bottom: Tmod single channel (grayscale). Scale bar = 20 μm. Magnification shown below with scale bar = 5 μm. (B) Confocal images (top) of larval NMJ in control (left) and *DmCFL* KD (right) muscles of different classes labeled with anti-alpha-spectrin (red) and anti-HRP (cyan). Bottom: Alpha-spectrin single channel (grayscale). Scale bar = 10 μm.

III. DISCUSSION

A. Transcriptional changes as a result of *DmCFL* KD

Previous work from our lab showed that DmCFL is critical for sarcomeric addition and maintenance in larval muscle. In this work, we used RNA sequencing to further understand the consequences of altering muscle DmCFL levels. The transcriptional profile of the *DmCFL* KD larvae confirmed a reduction in pathways related to proteolysis and revealed that there may be an additional role of DmCFL at the NMJ. This was a novel finding considering studies of transcriptional changes by microarray in *Cfl2* deficient mice describe significant changes in cell cycle and growth pathways (Morton et al., 2015). Many of the transcriptional changes were genes involved in NMJ signaling found on both the pre- and postsynaptic sides. This finding prompted me to examine the NMJ, and, indeed, I detected defects at the postsynapse.

The first group of genes identified as differentially-expressed are involved in the structure of the NMJ and maintenance of the synaptic cleft. Neuroligins and neurexins are cell adhesion partners present on each side of the synaptic membrane and are important for synapse assembly, and the organization of the active zone and glutamate receptors (Banerjee et al., 2017; K. Chen et al., 2010; Li et al., 2007). DNlg1 has a known association with the WAVE regulatory complex (WRC), while DNlg2 has been proposed to be involved in the cycle of inactive to active cofilin states in muscle; both mechanisms affect postsynaptic actin organization (Sun et al., 2023; Xing et al., 2018). In the *Drosophila* brain, the secreted proteins Hig-anchoring scaffold protein (Hasp) and hikaru genki

(Hig) are located within the cholinergic synaptic cleft but their distribution is segregated (Nakayama et al., 2014, 2016). Hig is necessary for proper distribution of nicotinic acetylcholine receptors in neurons (Nakayama et al., 2014).

Other genes with increased expression in *DmCFL* KD encode proteins reported to affect motor axon and bouton development. Appropriate levels of the transmembrane glycoprotein APPL, the *Drosophila* homolog to β-amyloid precursor protein (APP), are important for determining bouton number (Torroja et al., 1999). Castor is a transcription factor involved in the cascade that patterns neural progenitors (Doe, 2017; Kambadur et al., 1998). At the NMJ, the timing of Cas expression is critical for bouton number (Meng et al., 2020). Derailed receptor is activated by WNT signaling for proper bouton number (Liebl et al., 2008). Futsch is part of the bouton division process by forming loops with microtubules presynaptically (Roos et al., 2000). Nervous wreck (Nwk) is involved in growth of the NMJ, and its loss leads to motor neuron overgrowth (Coyle et al., 2004). Scratch (Scrt) mutants form motor neuron axons but do not make proper contact with the muscle to form an NMJ; mutants also have altered levels of glutamate receptor mRNA throughout embryogenesis (Ganesan et al., 2011).

Finally, some of the genes are related to neurotransmitter release and neuromodulation of the electrical activity at the NMJ. Brp is involved in the docking and release of the vesicle; however, despite the significant upregulation of this gene, the protein levels at the NMJ is not increased in *DmCFL* KD (Wagh et al., 2006). A subset of the genes relate to exocytosis of the vesicle, such as

the SNARE protein synaptobrevin and SNAP-25, (Broadie et al., 1995; Megighian et al., 2010). Vglut and Vmat are related to the packaging of glutamate neurotransmitter into secretory vesicles (Daniels et al., 2004; Simon et al., 2009). NMJ activity is modulated by the FMRFamide peptide and glutamic acid decarboxylase (Gad; D E Featherstone et al., 2000; Hewes et al., 1998). Expression of several ion channel genes were altered which affect vesicle release or excitatory response of the muscle: potassium (i.e. *eag*, *qvr*, *shal*), calcium (*frq*), sodium (*para*), and chloride (*tty*; Bergquist et al., 2010; Ganetzky & Wu, 1983; Ganetzky, 1984; Humphreys et al., 1996; Kaplan & Trout, 1969; Romero-Pozuelo et al., 2007; Suzuki, 2006).

The broad range of NMJ-related genes increased in the context of *DmCFL* KD suggests that maintenance of the postsynapse is critical for proper function. Some of the genes encode proteins thought to localize to the presynapse, which opens the question about whether the motor neuron is attempting to compensate for the defects at the postsynapse; we were unable to further examine this possibility since these larvae were at the latest stage of development before pupation. Future studies can consider further characterizing the presence of this proteins presumed to be at the presynapse to determine whether the changes in gene expression correspond to increase in protein levels or not, such as was the case with Brp.

B. Cofilin is present at various locations in larval muscle

In this work, I show that, in addition to being present at the sarcomere, DmCFL localizes at the postsynapse of the NMJ in live and fixed samples. This NMJ

pattern is similar to the NMJ localization described of other actin-binding proteins, including α-Spectrin, Twinfilin, and Coracle (K. Chen et al., 2005; Pielage et al., 2006; Song et al., 2022; D. Wang et al., 2010).

To measure protein levels at the postsynapse, I developed an innovative approach to quantify intensity in three-dimensions. This approach can be adapted to examine other postsynaptic proteins in future studies. I found that the levels of DmCFL are significantly reduced at the postsynapse in *DmCFL* KD muscles. Similarly, there is less inactive p-DmCFL protein at the *DmCFL* KD postsynapse, which could suggest that there is an attempt to have as much DmCFL in its active state as possible in this region even if total DmCFL is reduced. A muscle biopsy of an NM patient harboring a *CFL2* mutation also showed that phosphorylated cofilin-2 is absent (Agrawal et al., 2007).

One study implicates Nlg2 as one of the players influencing the levels of active and inactive postsynaptic cofilin pools; however, it is unclear whether another pathway also modulates the proportion of active cofilin, as overexpression of either active and inactive cofilin in *dnlg2* mutants causes an increase in actin at the NMJ (Sun et al., 2023). Future studies can examine the activity of LIM kinase (LIMK) and the phosphatase Slingshot (Ssh) which are responsible for cofilin phosphorylation dynamics to better understand if and how these proteins work postsynaptically. Additionally, the mechanism for targeting DmCFL to the postsynapse remains to be elucidated.

C. Postsynaptic actin organization and functions

The *DmCFL* KD model shows a progressive, yet uncoordinated, muscle deterioration phenotype. *DmCFL* KD VL3 and VL4 muscles in a hemisegment do not deteriorate at the same rate despite being innervated by the same motor neuron and having similar body function, producing the various groups described in this work. These findings are consistent with the progressive decline in structure and function found in *CFL2* NM patients and other mutant cofilin animal models. Interestingly, even in chimeric mice where only some muscle fibers harbor *Cfl2* mutations, the mutant fibers deteriorate, indicating that health of surrounding cells does not impact muscle disease progression (Kurato Mohri et al., 2019). In the fly model, I found that the state of one ventral longitudinal muscle in the pair is independent of the extent of deterioration of the neighboring muscles, although by the wandering stage most pairs are group 3. While technically challenging, live imaging of *DmCFL* KD muscles would provide key insight into the points of transition and timing of deterioration in a single muscle. A better understanding of class 1 muscles would provide information as to how normal these muscles are throughout development and how to develop interventions to retain organization.

Six actin isoforms with myriad roles have been identified in vertebrates and *Drosophila*. In flies, the different isoforms are expressed during particular developmental stages and in specific tissues (Fyrberg et al., 1981, 1983; Röper et al., 2005; Wagner et al., 2002). While the actins are typically categorized as cytoplasmic or muscle actins, there is evidence that all of the various isoforms are present at the sarcomere in larval muscles (Röper et al., 2005). Röper and

colleagues speculate that the formation and localization of particular actin structures within the cell may be driven by actin-binding proteins with different affinities (Röper et al., 2005). Vertebrate non-sarcomeric γ-actin present in skeletal muscle is responsible for muscle maintenance and for anchoring myofibrils and organelles in addition to being a component of the Z-disc (Belyantseva et al., 2009; Craig & Pardo, 1983; Gokhin & Fowler, 2011; Nakata et al., 2001; Papponen et al., 2009; Pardo et al., 1983; Rybakova et al., 2000; Sonnemann et al., 2006). Gamma-actin (γ_{cyto}) is only needed for proper maintenance of the cytoskeleton in muscle but not its development; its absence however, does lead to myopathy (Belyantseva et al., 2009; Sonnemann et al., 2006). Interestingly, human cofilin has a higher Hill coefficient for binding βγ-actin filaments than muscle actin *in vitro*, suggesting greater positive cooperativity in the binding of cofilin to cytoplasmic actin (De La Cruz, 2005). The authors of the prior study hypothesize that cofilin's binding may trigger different conformational changes in the actin filament depending on the isoform comprised (De La Cruz, 2005). Additionally, actin is present at the vertebrate neuromuscular junction, starting in early development before formation of the junctional folds (Hall et al., 1981). In adult muscle, there is an organized subsarcolemmal network of cytoplasmic actin (Berthier & Blaineau, 1997). One study showed that the actin-binding proteins vinculin, alpha-actinin, and filamin are present at the NMJ in rat, mouse, chick, and *Xenopus* muscle samples (Bloch & Hall, 1983). Additionally, in vertebrates, actin podosomes are critical for shaping the complex organization of postsynaptic proteins (reviewed in Bernadzki et al., 2014).

At the postsynaptic region, I showed that actin becomes disorganized in an uncoordinated fashion in *DmCFL* KD over time, which consistent with a decrease in DmCFL severing activity due to reduced DmCFL at this site. The actin accumulated in halos or swirls surrounding the boutons at the NMJ. The phenotype is similar to the filamentous actin structures reported in mutants for the Act57B actin isoform and for the actin-binding protein Twinfilin, which also surround portions of the NMJ (Blunk et al., 2014; D. Wang et al., 2010). Work in the *Cfl2* knockout mouse model has shown that there is a greater increase in F-actin than G-actin seen in knockout muscles (Agrawal et al., 2012). More detailed study of the actin isoforms using fluorescently-tagged proteins may provide more insight into whether the actin accumulations—both throughout the muscle and at the NMJ—seen in *DmCFL* KD are preferentially comprised of one or more of the isoforms.

One study shows that larvae heterozygous for a null cofilin allele have an increase in postsynaptic G-actin (Sun et al., 2023). While cofilin is an actin-severing protein, it also inhibits nucleotide exchange and inhibits actin polymerization (Brieher, 2013). These functions are influenced by the structural conformation of the protein (Tanaka et al., 2018). In addition, work examining the various mouse ADF/cofilins showed that muscle cofilin-2 has weaker F-actin severing efficiency and higher affinity for monomers than ADF and cofilin-1 *in vitro* (Vartiainen et al., 2002). In *Drosophila*, DmCFL has high affinity for ADP-G-actin and weak inhibitor of actin polymerization (Shukla et al., 2018). Thus, its reduction in *DmCFL* KD muscles may allow for more available G-actin monomers and more actin polymerization. Additionally, cofilin severing can lead to shorter actin filaments (not just monomers), so it is possible that the

accumulated filaments observed the postsynapse are of shorter length than typical at this locale. The increase in actin filaments in the postsynaptic region may also make access more difficult for the limited cofilin protein present. The presence of other actin-severing proteins (such as gelsolin) and proteins responsible for cofilin's activation (Slingshot, chronophin) and inactivation (LIMK) at the postsynapse should also be explored.

The postsynaptic actin disorganization seen in *DmCFL* KD is greatest in class 3 muscles where the actin filaments become distorted around the boutons. Actin at the postsynapse in class 2 muscles is disorganized only at certain boutons of individual branches of the NMJ. The actin swirls seen in class 2 preceded the sarcomeric defects, which suggests that actin in this region does not come from nor is exclusively from the sarcomere. Additionally, the levels of other actin-interacting proteins—Tmod and α-Spectrin—are reduced at the postsynapse. Our lab's previous work illustrated that Tmod is sequestered away to the growing poles of the *DmCFL* KD muscle cell as it deteriorates, which may explain reduced Tmod in other parts of the cell such as the NMJ (Balakrishnan et al., 2020). However, the level of Tmod is reduced even in class 1 muscles where there is no Tmod accumulation at the muscle ends, suggesting that sequestration is likely not the only reason. Another possibility is that the accumulated filaments have altered structural organization, making access for these actin-binding proteins more difficult. It is possible that these accumulations are similar to nemaline bodies seen in human NM; our lab has previously shown that the actin accumulations in the cytoplasm also contain sarcomeric proteins like alpha-actinin and kettin (Balakrishnan et al., 2020).

Lastly, the findings of this study have several implications for understanding NM. Muscle biopsies from *CFL2* NM patients have shown cytoplasmic disorganization of actin filaments, but these have not been deeply studied (Fattori et al., 2018; Sewry et al., 2019). I found by TEM that there are disorganized filaments near the postsynapse in *DmCFL* KD, although they are not as dense as those seen emanating from the sarcomere. One possibility is that they do not contain sarcomeric alpha-actinin like pathognomonic NM bodies emanating from the Z-disc, though this requires direct testing. The collapse of the synaptic cleft seen by electron microcopy should motivate future studies into how the disrupted actin may affect structural proteins between the pre- and postsynapse.

Altogether, the data described in this chapter identify the localization of DmCFL at the postsynapse and progressive deterioration of postsynaptic actin organization in *DmCFL* KD muscles. Next, I sought to look at composition and function of the NMJ synapse.

CHAPTER 3:
DmCFL IS IMPORTANT FOR POSTSYNAPTIC MEMBRANE MAINTENANCE AND COMPOSITION

I. INTRODUCTION

Few reports about NM discuss the neuromuscular junction. Some early case reports about NM patients show the NMJ in electron micrographs of muscle biopsies (Figure 3.1). However, the disease causative mutations for these patients are unknown. Heffernan *et al.* describe focal dilatations of some of the synaptic clefts (Heffernan et al., 1968). There is also evidence from one case that the motor end plates are disrupted by nearby fibrous tissue in NM; however, there was no correlation between the distance from the motor end plate and the number of nemaline rods counted (Fukuhara et al., 1978). One recent paper about *ACTA1* NM patients described reduced postsynaptic folds in two biopsies examined (Labasse et al., 2022). Functionally, it is unclear whether there is a superimposed NMJ transmission defect in addition to the typical myopathic pattern seen on electromyogram (EMG) in NM. A longitudinal study showed that after age nine some NM patients had neuropathic findings when their distal muscles were tested by EMG, possibly indicating that there is motor unit degeneration or reinnervation by neighboring units (C Wallgren-Pettersson et al., 1989).

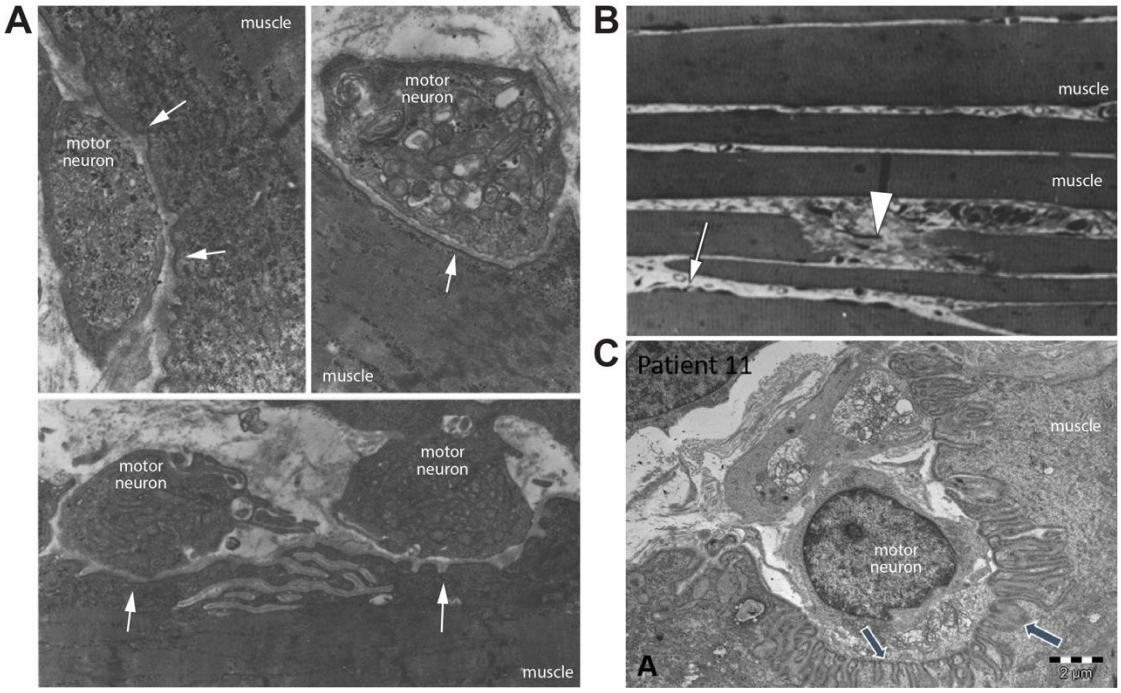

Figure 3.1: NM patient neuromuscular junction histology and ultrastructure. (A) Electron micrograph of NMJ with poorly developed, shortened or absent synaptic clefts (arrows) in NM muscle biopsy. Adapted from Fukuhara *et al*., 1978. (B) NM muscle sample stained with Toluidine blue showing fibrous tissue (arrow) near motor end-plate (arrowhead). Adapted from Fukuhara *et al*., 1978. (C) Reduced postsynaptic folds (arrows) seen in electron micrograph of *ACTA1* NM muscle biopsy. Adapted from Labasse *et al*., 2022.

The *Drosophila* larval NMJ is a useful model for understanding whether there are structural and functional changes as a result of NM mutations. Signals to contract originate in the larva's brain, travel through the ventral nerve cord, and propagate along the motor neuron axon that synapses onto the muscle. The postsynaptic side of the muscle membrane (i.e. subsynaptic reticulum, SSR) is specialized as it contains the components necessary to maintain the synapse and carry out the various steps of excitation-contraction coupling.

Table 3.1. NMJ effects of actin and actin-related protein manipulations.

		Postsynapse			Presynapse		
Protein	**Manipulation**	**Postsyn-aptic actin**	**Subsynaptic Reticulum (SSR)**	**Glutamate receptor (GluR)**	**Bouton number**	**Active zones**	**Electro-physiology**
Act57B (Blunk et al., 2014)	Mutant	Swirls	Diffuse, less complex	Large, less punctate		Some absent, expanded, or unapposed	↓ EJC
α-, β-spectrin (Pielage et al., 2006)	RNAi		Disrupted Dlg, less complex	Larger clusters, disrupted GluRIIA	↓	Altered spacing, larger size	↑ EPSP amplitude, ↑ mEPSP
Coracle (K. Chen et al., 2005)	Mutant			↓ GluRIIA cluster size, no change GluRIIB			↓ EJC amplitude
Twinfilin (D. Wang et al., 2010)	Mutant	↑ intensity		↓ GluRIIA, no change GluRIIB			↓ EJP only with extended stimulation
Neurexin-Neuroligin 1 (Xing et al., 2018)	Mutant	↓	Dlg unaffected, spectrin expanded	Some boutons with no GluR, GluRIIA and B unchanged	↓	More unapposed	Nlg1 mutant ↓ EJC
Filamin (G. Lee & Schwarz, 2016)	RNAi, mutants		↓ width and Dlg intensity	↓ GluRIIA			
Dynamin (S.-S. Lin et al., 2020)	Mutant		thicker SSR, disorganized spectrin				↑ mEJP
Dystrophin (van der Plas et al., 2006)	Mutant					↑ AZ with T-bars	↑ EJP

Postsynaptic actin and some of its binding partners have been shown to be important for proper development of the larval NMJ (Table 3.1). Loss or gain of filamentous actin in these fly models can have detrimental effects on NMJ structure and function. Myopodia are actin-rich structures extending from the muscle membrane that assist in synaptic establishment by making contact with the motor axon growth cone and stabilizing the new points of contact (Ritzenthaler & Chiba, 2003). Bouton number was decreased when *α-spectrin* or *nrx/nlg* were knocked down or mutated (Pielage et al., 2006; Xing et al., 2018). *Act57B* and *twinfilin* mutants showed altered organization or increased levels of postsynaptic actin, respectively (Blunk et al., 2014; D. Wang et al., 2010). On the other hand, reducing Neurexin/Nlg1 or Nlg2 led to decreased postsynaptic actin (Sun et al., 2023; Xing et al., 2018). In some actin-binding protein manipulations, the number or spacing of active zones were increased (Blunk et al., 2014; G. Lee & Schwarz, 2016; Pielage et al., 2006; Xing et al., 2018). Affecting Act57B, α-Spectrin, Neurexin/Nlg1, Filamin, or Dynamin altered the complexity of the SSR membrane (Blunk et al., 2014; G. Lee & Schwarz, 2016; S.-S. Lin et al., 2020; Pielage et al., 2006; Xing et al., 2018). The levels of GluRIIA were decreased or the fields of GluRIIA-containing receptors were expanded in *α-spectrin*, *coracle*, *twinfilin*, *filamin* mutant or knockdown models (Blunk et al., 2014; K. Chen et al., 2005; G. Lee & Schwarz, 2016; D. Wang et al., 2010).

In vertebrates, postsynaptic actin within podosomes is important for expanding the postsynaptic density into a more complex shape (reviewed in Bernadzki et al., 2014). The vertebrate postsynapse is often visualized by staining for acetylcholine receptors (AchR; Figure 3.2A-B), and the organization of the

receptor fields takes on a 'pretzel' shape later in development (Proszynski et al., 2009). An *in vitro* study using the *Xenopus* NMJ showed that the balance of active and inactive cofilin (Figure 3.2C) combined with a dynamic actin network were important in the proper addition of AChR to the membrane (C. W. Lee et al., 2009).

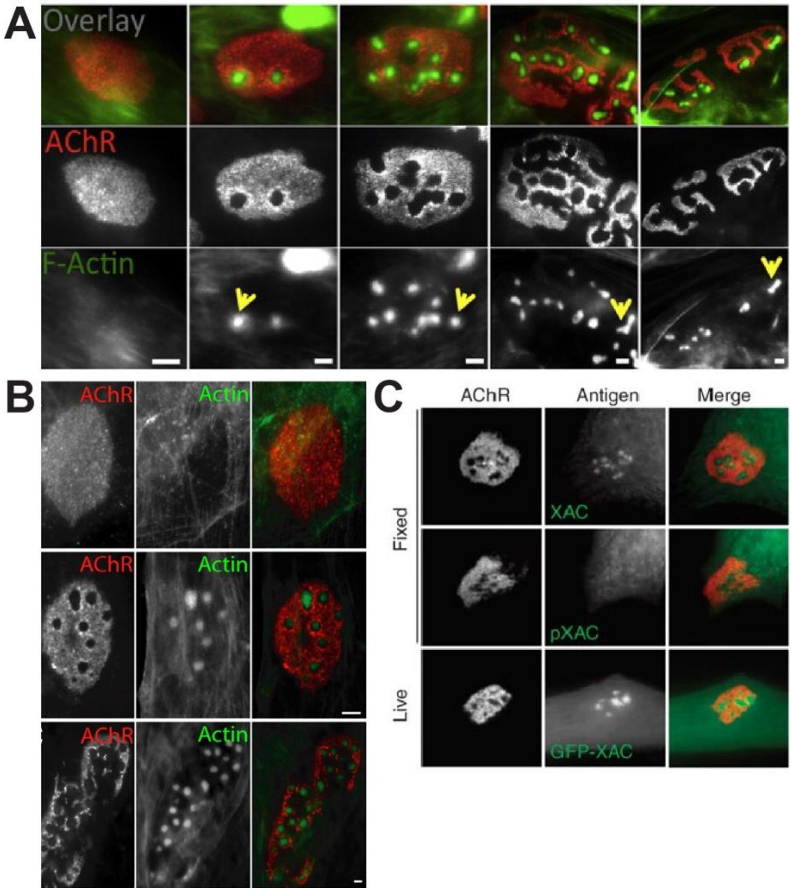

Figure 3.2: Actin podosomes in acetylcholine receptor (AchR) clustering. (A) Podosomes containing F-actin (green) are involved in the maturation of AchR (red) clusters in C2C12 myotubes over time. Scale bar = 5 μm. Adapted from (Bernadzki et al., 2014). (B) AchR plaques (top, 3 days post-fusion) are perforated by actin-rich podosomes over time (middle panel shows 4 days post-fusion, bottom panel shows 5 days post-fusion). Scale bar = 5 μm. Adapted from (Proszynski et al., 2009). (C) ADF/Cofilin (green) localizes within AchR clusters (red) that assemble spontaneously as seen in both fixed and live *Xenopus* aneural muscle cell culture. Adapted from (C. W. Lee et al., 2009).

To further examine the effects of reduced postsynaptic cofilin and altered postsynaptic actin organization in *DmCFL* KD muscles, I examined the morphology and composition of the pre- and postsynapse. While presynaptic development is unaffected, postsynaptic organization progressively deteriorates at the KD NMJ. Additionally, the active zone protein Brp and corresponding postsynaptic glutamate receptors (GluR) are appropriately present at the *DmCFL* KD presynapse and postsynapse, respectively. Finally, *DmCFL* KD results in the reduced presence of the GluRIIA subunit, which led to a functional decrease on neurotransmission. These data indicate that proper cofilin localization and actin organization at the postsynapse are required for appropriate postsynaptic structure, GluRIIA presence, and neurotransmission.

II. RESULTS

A. General presynaptic morphology is not affected by muscle *DmCFL* KD

First, I sought to visualize the NMJ in both control and *DmCFL* KD larvae via immunofluorescence. Muscles in all segments in the *DmCFL* KD larvae were properly innervated by motor neurons (labeled with anti-HRP) regardless of their deterioration class (Figure 3.3A). VL3-VL4 muscle pairs of all groups were appropriately innervated by the shared branch of ISNb, suggesting that axonogenesis and motor neuron pathfinding to the muscle are unaffected, despite the reduced expression of *DmCFL* in the muscle throughout the entire developmental period (Figure 3.3B). The complexity of the motor axons is also unaffected: there are multiple branches that synapse onto VL3 and VL4. Additionally, the motor neuron branches cover the same span along the length

of the muscle pair in *DmCFL* KD as control regardless of VL3-VL4 group or segment (Figure 3.3C). Given that affecting some actin-binding proteins in larval muscle leads to a decrease in boutons, I counted the number of boutons synapsing onto each muscle pair. I found that there is no difference in the number of boutons between *DmCFL* KD and control muscles (Figure 3.3D). There were no ghost (immature boutons lacking a corresponding SSR), footprint (presynaptic retractions that have SSR but no HRP+ bouton), or satellite boutons (small boutons that bud from a parent bouton on a terminal arbor).

B. Reduction of *DmCFL* in muscle leads to deterioration of the SSR

Since the *DmCFL* KD model is a muscle-specific manipulation, I sought to examine the SSR more closely in these muscles. All *DmCFL* KD muscles had the structural protein Dlg at the SSR, and Dlg signal was found at the contact point of the boutons (Figure 3.4A). To quantify the SSR area, I measured the Dlg-positive area relative to the combined muscle cell area. This measurement could only be done for group 1 and group 2 pairs because the muscle area cannot be reliably measured in class 3 muscles due to their distorted shape that is not rectangular on a Z projection. The SSR area was unchanged in group 1 and 2 pairs compared to control, indicating that the minimal disorganization in class 2 muscles was not enough to alter the mean SSR coverage overall (Figure 3.4B). However, there were changes in SSR morphology in class 2 and 3 muscles.

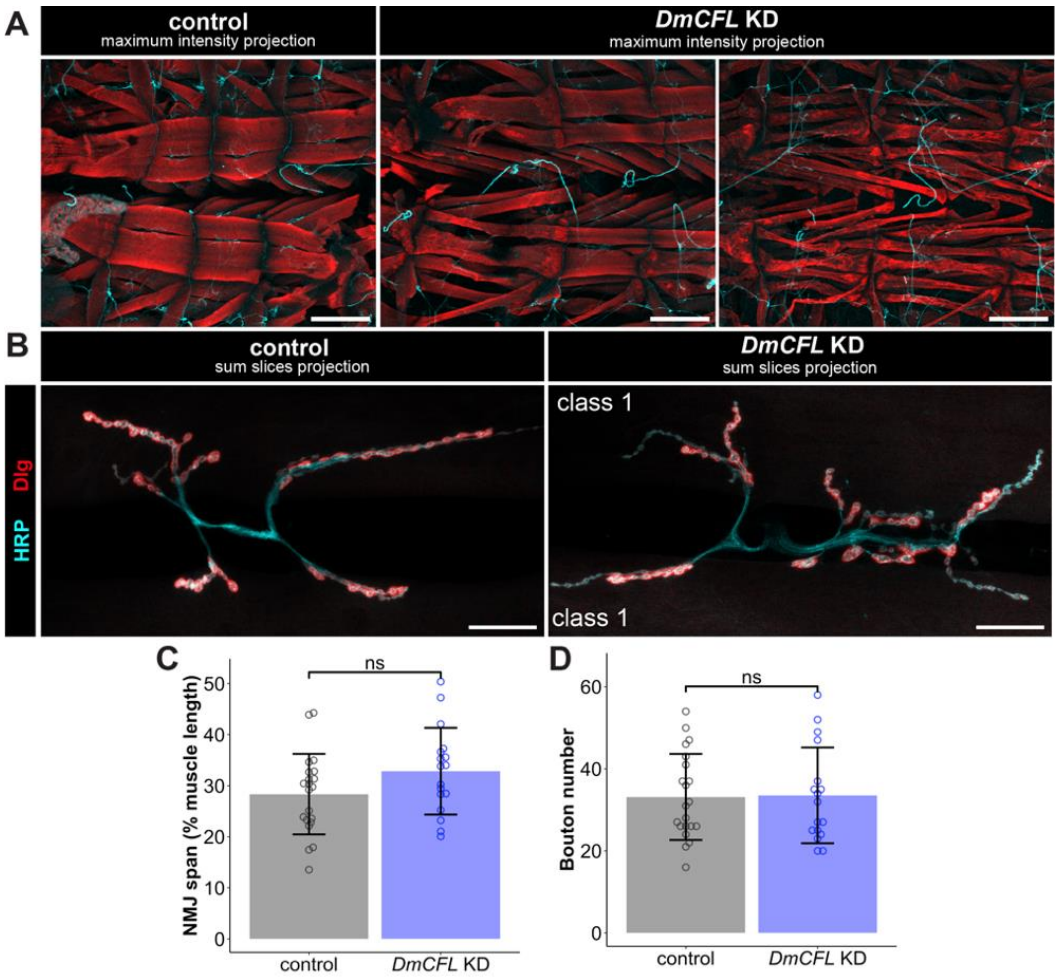

Figure 3.3: Motor neuron properly innervates DmCFL KD muscles. (A) Confocal images of larval muscles in control and *DmCFL* KD muscles labeled with phalloidin (red) and anti-HRP (cyan). Scale bar = 200 μm. (B) Confocal images of larval NMJ in control and *DmCFL* KD muscles labeled with anti-Dlg (red) and anti-HRP (cyan). Scale bar = 25 μm. (C) Quantification of NMJ span (NMJ length normalized to cell length) reported as percent of muscle length (control 28.35 ± 7.87%, *n* = 21 NMJs; *DmCFL* KD 32.84 ± 8.51%, *n* = 17 NMJs). (D) Quantification of total Ib (large) bouton number (control 33 ± 11, *n* = 21 NMJs; *DmCFL* KD 34 ± 12, *n* = 17 NMJs). Quantifications show mean ± SD and student's *t* test result (ns = $p > 0.05$).

Firstly, as seen in the control NMJ, class 1 muscles had Dlg signal closely surrounding the boutons. However, in class 2 muscles, the Dlg pattern was more diffuse yet still surrounding the boutons. Meanwhile, in class 3 muscles, Dlg was

even more expanded away from the boutons. The change in the Dlg pattern in class 2 and 3 compared to control and class 1 muscles suggests a progressive deterioration in postsynaptic structure. I quantified this change by drawing line scans across the diameter of single boutons to record the intensity of Dlg compared HRP signal at each position. This analysis showed that there were two intense Dlg peaks on either side of the HRP peak in control and DmCFL KD class 1, which is consistent with Dlg surrounding the bouton (Figure 3.4C). In class 3 boutons, the Dlg intensity plateaued along the diameter irrespective of the HRP peak. The range of disruption in Dlg organization over the three classes shows that postsynaptic structural integrity deteriorates progressively, much like defects seen in postsynaptic F-actin and the sarcomeres in the *DmCFL* KD model.

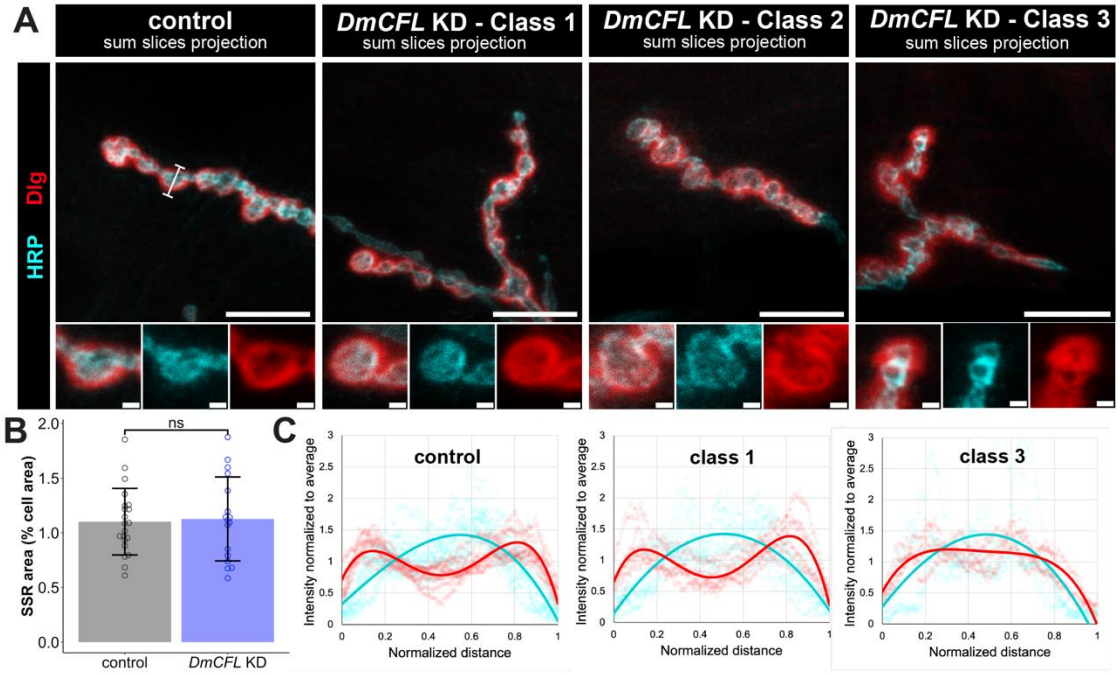

Figure 3.4: The organization of the SSR progressively deteriorates at DmCFL KD NMJ. (A) Confocal images of larval boutons in control and *DmCFL* KD (class 1, class 2 and class 3 muscles labeled with anti-Dlg (red) and anti-HRP (cyan). Scale bar = 10 µm. Bottom panels show individual boutons (merge and individual channels). Scale bar = 1 µm. (B) Quantification of subsynaptic reticulum (SSR) area, defined as Dlg-positive area normalized to cell area (control 1.10 ± 0.30, *n* = 21 NMJs; *DmCFL* KD 1.13 ± 0.38, *n* = 17 NMJs). Quantifications show mean ± SD with significance calculated by student's *t* test (ns = not significant, $p > 0.05$). (C) Line graph of Dlg (red) and HRP (cyan) intensity across the span across a single bouton (example span shown by white bar in part A) in control and *DmCFL* KD class 1 and 3 NMJs. Intensity was normalized to the average intensity of signal.

C. Cofilin is not necessary for presynaptic Brp and postsynaptic GluRIIC at the NMJ

Signaling at the NMJ relies on neurotransmitter release from the presynapse and its binding to receptors on the postsynapse. To better understand whether there were consequences at the active zone due to muscle *DmCFL* KD, I

examined the levels of the structural protein Brp (Figure 3.5A). *Brp* RNA expression was increased by over three-fold in *DmCFL* KD compared to control, according to RNA sequencing differential gene expression analysis (Figure 2.5I). Visually, arrangement of Brp protein at the presynapse in *DmCFL* KD is not expanded and retains the typical punctate pattern. Intensity of Brp protein was unchanged with *DmCFL* KD regardless of muscle pair group (Figure 3.5B).

The RNAseq analysis also identified terms related to postsynaptic potential, which motivated an analysis of GluRs on the muscle membrane. I focused first on GluRIIC since this subunit is present in all GluRs. Similar to Brp, GluRIIC pattern was punctate and not expanded in KD muscles (Figure 3.5A). There was no change in the levels of GluRIIC at the postsynapse in *DmCFL* KD compared to control (Figure 3.5C). The overlap between Brp and GluRIIC was appropriate, and there were no obvious areas of unapposed active zones (i.e. Brp puncta with no GluRIIC overlap and vice versa).

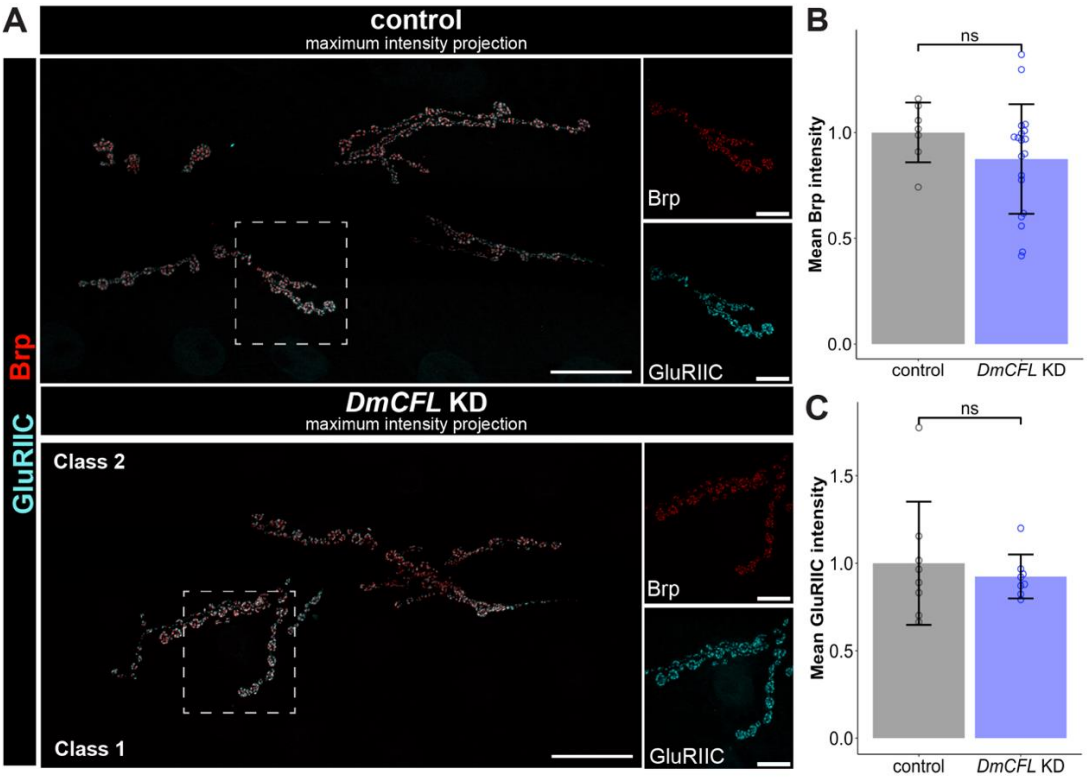

Figure 3.5: Presynaptic Brp and postsynaptic GluRIIC unchanged with DmCFL KD. (A) Confocal images of control and *DmCFL* KD labeled with presynaptic anti-Brp (red) and postsynaptic anti-GluRIIC (cyan). Right has magnification of boxed areas, with each stain shown separately. Scale bar = 25 µm, magnification scale bar = 10 µm. (B) Quantification of mean Brp intensity normalized to control (control 1 ± 0.14, *n* = 8 NMJs; *DmCFL* KD 0.87 ± 0.26, *n* = 19 NMJs of all groups). (C) Quantification of mean GluRIIC intensity normalized to control (control 1 ± 0.35, *n* = 9 NMJs; *DmCFL* KD 0.92 ± 0.13, *n* = 8 NMJs of all groups). Quantifications show mean ± SD with significance calculated by student's *t* test (ns = not significant, $p > 0.05$).

D. GluRIIA subunit presence at the postsynapse depends on cofilin

Although the levels of total GluR are unaffected in *DmCFL* KD, there was the possibility that there was a change in the other subunits of the GluR tetramer which are more variable. I examined the GluRIIA subunit since the disruption of some other actin-binding proteins (e.g. Spectrin, Coracle, Twinfilin, Filamin) is

associated with a disruption or decrease of this subunit (K. Chen et al., 2005; G. Lee & Schwarz, 2016; Pielage et al., 2006; Song et al., 2022; D. Wang et al., 2010). Additionally, one screen identified that various cytoskeleton-related genes specifically affect GluRIIA subunit levels detected by immunofluorescence (Liebl & Featherstone, 2005). To test the hypothesis that reducing DmCFL would affect GluRIIA at the postsynapse, I quantified GluRIIA fluorescence intensity and found that GluRIIA intensity was reduced in KD muscles compared to control (Figure 3.6A-B). This reduction was only seen in group 2 and 3 muscle pairs (Figure 3.6B). In other words, VL3-VL4 pairs where both muscles were class 1 had comparable GluRIIA levels as control while pairs with at least one class 2 or 3 muscle had decreased levels.

Interestingly, SIM imaging showed that, in Class 2 or 3 muscles, there are GluRIIA-containing receptors that are no longer tightly associated with the SSR surrounding the boutons (Figure 3.6C). However, this was not seen in every bouton of class 2 and 3 muscles. GluRIIA is thought to be anchored to the actin cytoskeleton by the 4.1 protein Coracle (K. Chen et al., 2005; Gardiol & St Johnston, 2014; Song et al., 2022). Consistent with the Coracle regulatory mechanism, there is reduced Coracle at the postsynapse in class 2 and 3 muscles but not class 1 *DmCFL* KD muscles (Figure 3.6D).

Figure 3.6: DmCFL KD reduced NMJ GluRIIA levels and neurotransmission. (A) Confocal images of control and *DmCFL* KD NMJs labeled with anti-GluRIIA (red) and anti-HRP (cyan). Scale bar = 25 μm. Right shows magnification of boxed areas of GluRIIA channel alone (grayscale). Scale bar = 10 μm. (B) Quantification of mean GluRIIA intensity normalized to control by *DmCFL* KD muscle group (control 1 ± 0.36, n = 10 NMJs; *DmCFL* KD 0.66 ± 0.45, n = 19 NMJs). (C) SIM images of boutons labeled with anti-GluRIIA (red) and HRP (cyan). Arrowheads indicate GluRIIA fields that do not overlap with HRP. Scale bar = 5 μm. (D) SIM images labeled with anti-Coracle (red) and anti-HRP (cyan) in control (left) and *DmCFL* KD (right) muscle classes. Coracle single channel (grayscale) is shown below. Scale bar = 5 μm. (E) Example evoked excitatory junctional current (EJC) traces showing ten consecutive evoked traces at 0.2 Hz. Experiment was done by Shannon Leahy, Vanderbilt University. (F) Quantification of EJC amplitude from individual NMJs (control 184.4 ± 55.52 nA, n = 11 NMJs; *DmCFL* KD 104.4 ± 034.37 nA, n = 13 NMJs). Quantifications show mean ± SD and statistics calculated by ANOVA (* $p < 0.05$, ** $p < 0.01$).

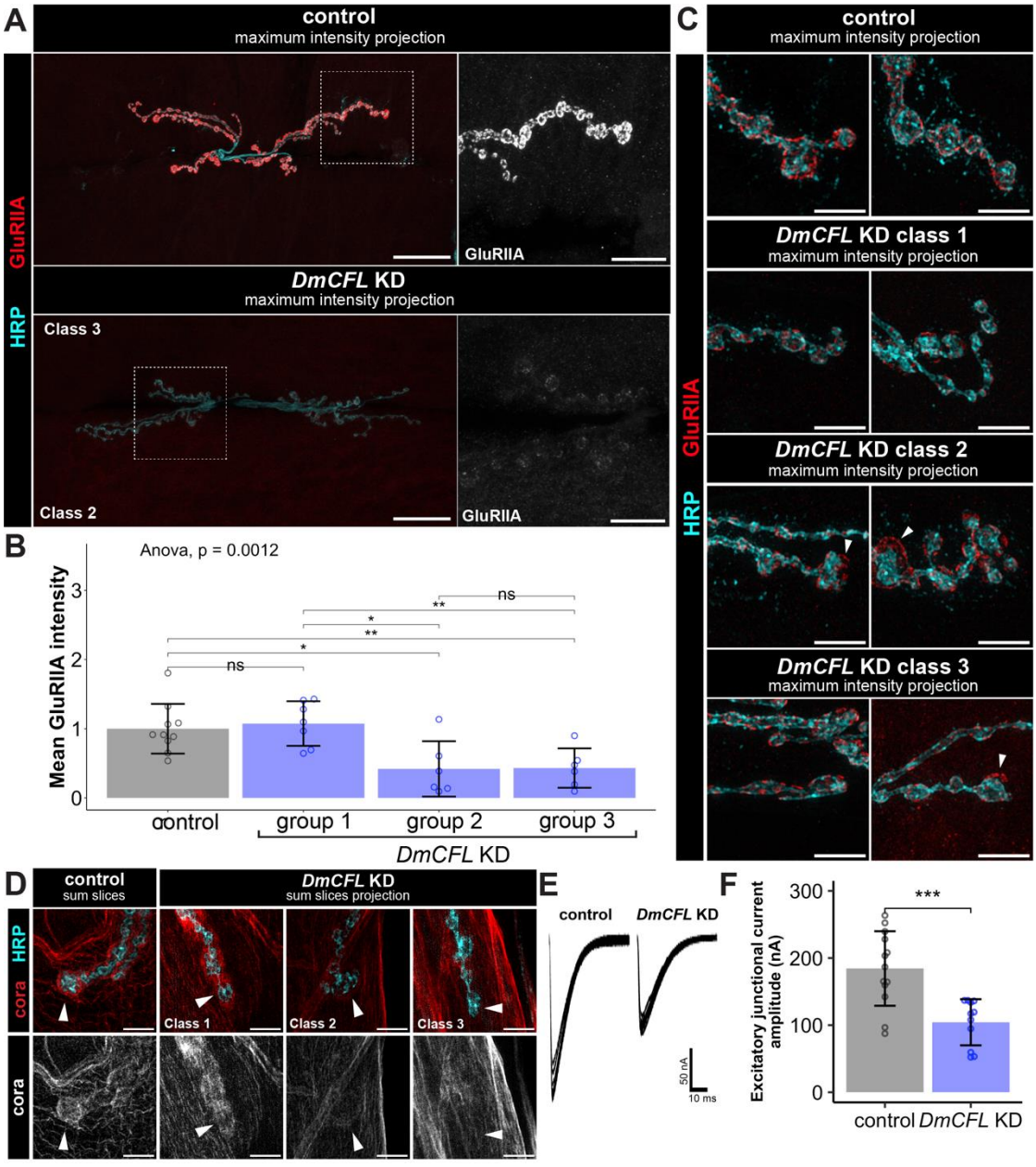
A
control
maximum intensity projection
GluRIIA
HRP
GluRIIA
DmCFL KD
maximum intensity projection
Class 3
Class 2
GluRIIA
B
Anova, p = 0.0012
Mean GluRIIA intensity
0
1
2
3
ns
**
*
**
*
ns
control
group 1
group 2
group 3
DmCFL KD
C
control
maximum intensity projection
DmCFL KD class 1
maximum intensity projection
DmCFL KD class 2
maximum intensity projection
DmCFL KD class 3
maximum intensity projection
GluRIIA
HRP
D
control
sum slices
DmCFL KD
sum slices projection
HRP
cora
Class 1
Class 2
Class 3
cora
E
control
DmCFL KD
50 nA
10 ms
F
Excitatory junctional current amplitude (nA)
0
100
200
300
***
8
8
control
DmCFL KD

E. Neurotransmission is affected by muscle cofilin reduction

Postsynaptic neurotransmission strength is linked to the levels of GluRIIA-containing receptors; NMJs with reduced GluRIIA have decreased excitatory junctional currents in response to stimulation (DiAntonio et al., 1999; Petersen et al., 1997). Our collaborators at Vanderbilt University (Shannon Leahy and Kendal Broadie, PhD) conducted a two-electrode voltage-clamp (TEVC) experiment to record glutamate release and GluR activation (Leahy et al., 2023). As illustrated in Figure 1.16, TEVC is done by stimulating the motor neuron with a suction electrode at voltages that are suprathreshold (0.2 Hz). The resulting evoked excitatory junction current (EJC) in the VL3 muscle is recorded and averaged to give the mean neurotransmission strength. For this experiment, a mix of the VL3-VL4 pair groups were tested in a blinded configuration. In *DmCFL* KD muscles, the EJC amplitude is reduced compared to control (Figure 3.6E-F). This reduction indicates decreased neurotransmission in the context of *DmCFL* KD.

III. DISCUSSION

Given the results of the RNA sequencing results pointing to changes at the NMJ, I characterized NMJ morphology and function in the *DmCFL* KD model. To do this, I examined structure and signaling components on both the presynaptic and the postsynaptic sides of the NMJ.

A. Disrupting postsynaptic DmCFL does not alter presynaptic development

The motor neuron properly innervates *DmCFL* KD muscles over a consistent span by the end of larval development. In *Drosophila* embryos, myopodia containing actin filaments are involved in stabilizing initial contact between the motor neuron and the postsynaptic membrane (Ritzenthaler & Chiba, 2003). The fact that the motor neuron appropriately contacts *DmCFL* KD muscles supports that there is proper development of the NMJ in embryogenesis and early larval development. A major benefit of studying the *Drosophila* NMJ is that all contacts between the motor neuron and muscle can be visualized. In vertebrates, the motor neuron penetrates into the muscle and contacts each myofiber at a different motor end plate, making it challenging to view depending on the location sampled in the muscle.

Actin-binding *spectrin* knockdown or *nrx/nlg* mutants have fewer boutons (Pielage et al., 2006; Xing et al., 2018). Meanwhile, bouton number is unchanged in other *Drosophila* models where actin or actin-binding proteins, including Act57B, Coracle, Twinfilin, Filamin, Dynamin and Dystrophin are affected (Blunk et al., 2014; K. Chen et al., 2005; G. Lee & Schwarz, 2016; S.-S. Lin et al., 2020; van der Plas et al., 2006; D. Wang et al., 2010). *DmCFL* KD muscles have the same number of boutons as control; additionally, all are true boutons as I found no satellite, footprint, or ghost boutons. This finding, combined with the results of the other actin-binding protein models, suggests that in some instances the motor neuron grows properly and establishes new boutons, regardless of postsynaptic actin disorganization. One possibility is that

affecting actin-binding proteins that are involved in actin dynamics more generally—rather than Spectrin and Nrx/Nlg which are NMJ structural proteins—would cause less disruption to the initial bouton formation process. It is also interesting that despite the decreased levels of Spectrin in *DmCFL* KD (Figure 2.10) there is not a similar phenotype to what has been reported in *spectrin* KD. Another possibility is that the use of mutants in these other studies may affect more than the muscle or cause a more severe phenotype than knocking down via RNAi.

The RNA sequencing analysis identified various differentially-expressed genes that encode for proteins reported to localize to the motor neuron. However, reducing DmCFL in muscle did not affect the amount of presynaptic active zones, despite an increase in Brp RNA expression suggested by sequencing. Other affected genes are associated with ion channels responsible for the neuron's own membrane potential which is critical for propagation of its action potential (e.g. *eag*, *frq1/2*, *para*, *shal*) and neurotransmitter release (e.g. *vglut*). The change in *vglut* might suggest an attempt to have more vesicles to package more glutamate for eventual release. It is possible that the alterations detected by RNA sequencing indicate that the motor neuron is starting the process of compensating for the defects seen in class 3 muscles by the wandering stage, but there is not enough time prior to pupation to lead to changes at the protein level or in their function. Proteomics would be informative to address this question.

B. Muscle postsynaptic membrane components become progressively disorganized in *DmCFL* KD

As shown in Chapter 2, levels of the SSR actin-binding protein alpha-Spectrin levels are reduced at the *DmCFL* KD NMJ in all muscle classes, despite actin being increased at the postsynapse in class 2 and 3 muscles. Postsynaptic structural protein Dlg is present in *DmCFL* KD. However, Dlg becomes progressively disorganized over the various muscle classes, meaning there is enough DmCFL for initial formation and organization of the SSR but not for its maintenance over larval development. While Dlg does not bind to actin, it does form a complex with the actin-binding proteins Adducin/Hts and Spectrin (S. J. H. Wang et al., 2014). Thus, Dlg disorganization in class 3 muscles is likely due to an effect on this complex, rather than a direct effect of postsynaptic actin accumulation on Dlg. There are examples from the other actin-binding protein models where Spectrin and Dlg are affected in different ways or not at all. In *Act57B* mutants, *spectrin* KD, *nrx/nlg* mutants, and *filamin* mutants Dlg is diffuse and less complex (Blunk et al., 2014; G. Lee & Schwarz, 2016; Pielage et al., 2006; Xing et al., 2018). Spectrin organization is affected in *nrx/nlg* mutants and *dynamin* mutants (S.-S. Lin et al., 2020; Xing et al., 2018).

There have been no reports of obvious NMJ structural defects in mouse cofilin models (Agrawal et al., 2012; Gurniak et al., 2014). Oftentimes the vertebrate postsynapse is visualized by staining for AchR and no other membrane components. It is possible that subtle changes membrane structure may not be appreciated by AchR staining. TEM images from NM patient biopsies have shown alterations at the postsynapse, including collapsed or dilated primary and

secondary synaptic clefts (Fukuhara et al., 1978; Heffernan et al., 1968; Karpati et al., 1971). Similarly, we found examples of collapsed synaptic clefts by TEM at the *DmCFL* KD NMJ (Figure 2.9). Collectively, the presented data imply that the preservation of a specific quantity and/or dynamic condition of postsynaptic actin is significant in upholding SSR structural integrity. Consequently, the increased postsynaptic actin resulting from reduced cofilin induces a gradual disorganization.

C. Neurotransmission reduction in *DmCFL* KD is linked to reduced GluRIIA levels

In this study, I found that total active zone and GluR levels are unchanged in *DmCFL* KD compared to control. The unaltered GluR levels in *DmCFL* KD is consistent with the fact that no gross changes in AchR have been reported in mouse models. At the *DmCFL* KD NMJ, the intensity of one particular subunit, GluRIIA, was reduced only in group 2 and 3 muscle pairs; there was decreased neurotransmission in *DmCFL* KD muscles consistent with GluRIIA reduction. The fact that group 1 muscles do not have decreased GluRIIA levels suggests that this is another progressive phenotype in *DmCFL* KD. GluRIIA-containing receptor levels are sensitive to actin manipulations or mutations: in several actin and actin-binding protein manipulations GluRIIA levels or cluster sizes are reduced even if there is no change in GluRIIB (K. Chen et al., 2005; G. Lee & Schwarz, 2016; Pielage et al., 2006; D. Wang et al., 2010). Thus, actin plays an important role in maintaining GluRIIA levels at the postsynapse.

One explanation for why GluRIIA levels are reduced in more deteriorated KD muscles is that actin dynamics are critical for addition of receptors to the surface and for their recycling. AMPA receptors (AMPARs) are the ionotropic glutamate receptors found in the vertebrate central nervous system. There is evidence in vertebrate that long-term potentiation may contribute to alternating ADF/cofilin phosphorylation states, where cofilin activation led to AMPAR addition (Gu et al., 2010). Treatment with latrunculin A leads to decreased GluRIIA cluster size in *Drosophila* and causes GluR1 addition in hippocampal neurons (K. Chen et al., 2005; Gu et al., 2010). Meanwhile, treatment with jasplakinolide to inhibit depolymerization also blocks addition of GluR1 in hippocampal neurons (Gu et al., 2010). Additionally, actin is important for endocytosis of AMPARs (Zhou et al., 2001). Together, these findings indicate that proper GluR addition relies on being able to polymerize and depolymerize actin dynamically. The buildup of actin at the postsynapse in *DmCFL* KD, thus, may be affecting appropriate addition of GluRIIA receptors to the postsynapse, which may also explain why some GluRIIA was not perfectly apposed to the bouton. Live imaging has shown that turnover of GluRIIA-containing receptors is generally slow, taking hours when other postsynaptic proteins turnover in minutes (Rasse et al., 2005). GluRIIA-containing receptors are brought from across the membrane, not just near the NMJ, which means that transport of these receptors from the any part of the surrounding membrane to the postsynapse may be inhibited in *DmCFL* KD; one hypothesis is that the buildup of actin in this region physically prevents transport of these extra-synaptic receptors to the postsynapse (Rasse et al., 2005). However, extra-synaptic receptors may not be easily visualized since they are not clustered. Live imaging as done in (Rasse et al., 2005) will be a useful tool for future experiments to visualize the entry and exit of GluRIIA-

containing receptors at the *DmCFL* KD postsynapse as the muscle deteriorates. Additionally, the disruption of Coracle in class 2 and 3 muscles suggests that either there is less Coracle due to decreased GluRIIA-containing receptors at the NMJ or that anchoring of GluRIIA receptors to the actin cytoskeleton via coracle is affected. It is unclear, however, why the altered localization of GluRIIA-containing receptors is progressive (seen in class 2 and class 3) when Coracle levels appear to also be reduced in class 1 muscles relative to control. Driving localization of DmCFL to the postsynapse in the context of *DmCFL* KD would be especially informative to understand whether this would rescue the actin, structural, and neurotransmission defects. This could be done by creating a construct that adds a localization sequence from a protein known to localize to the postsynapse (e.g. Shaker ion channel or Fasciclin II cell adhesion molecule); however, it is possible that this may interfere with cofilin's functional sites or its ability to closely associate with the actin filament or monomers although the sequences are short at six amino acids (Zito et al., 1997).

My findings discussed in this chapter identify a role for cofilin and its regulation of actin in maintaining postsynaptic structure and composition. These experiments provide evidence that there are functional changes at the muscle postsynapse in *DmCFL* KD muscles that result from decrease and disorganization of components such as GluRIIA and Coracle.

CHAPTER 4:
CONCLUSIONS

The findings in this study suggest that alterations at the NMJ, particularly in the postsynaptic region, are part of the degradation that results from reducing muscle cofilin levels by RNAi KD. Perturbing non-sarcomeric actin dynamics may impact other muscle functions and, in turn, contribute to the advancement of muscular deterioration observed in neuromuscular disorders, such as NM. My work opens novel avenues for understanding the mechanism of disease and potentially new treatment possibilities while also opening questions about other roles of cofilin in the muscle.

I. FUTURE STUDY DIRECTIONS FOR THE *DMCFL* KD MODEL

A. Actin and cofilin at the NMJ

In previous and the current work, we identify that there are effects at the sarcomere and postsynapse when *DmCFL* is reduced in the muscle. However, the direct mechanism by which cofilin regulates postsynaptic composition and neurotransmission must be further examined. Rescue experiments would provide insight as to whether the NMJ deterioration phenotypes can be improved simply by increasing *DmCFL* levels in the muscle as was found with the sarcomeric alterations. In addition, we do not know what recruits cofilin to the postsynapse. It is possible that simply increasing the amount of DmCFL in the cytoplasm would not be enough to localize more protein at the postsynapse and ameliorate the defects seen at the KD NMJ. Further examining LIMK and Ssh—known regulators of cofilin's activation state—at the postsynapse would

be informative as the postsynaptic defects may be overcome by having more DmCFL in its active form. Transcriptional analysis of *Cfl2* null mouse muscle found that there is increased expression of *Ssh2*, suggesting that this slingshot phosphatase is upregulated in muscle to activate the reduced cofilin present in the muscle (Morton et al., 2015). Answers to these questions will be critical for understanding why the postsynaptic actin organization at this region is sensitive to levels of cofilin.

Another open question is whether the reduced levels of structural proteins, ABPs, and GluRIIA-containing receptors in *DmCFL* KD is due to improper trafficking as a result of affecting the cytoplasmic actin network. It is unknown if F-actin—which would then need to be properly severed by cofilin—is needed for transport of postsynaptic membrane components (e.g. GluRs, structural proteins) to the *Drosophila* larval postsynapse. Cofilin has been linked to trafficking proteins to the vertebrate muscle membrane in other contexts. For example, work in rat cultured myoblasts found that proper cofilin severing is critical for trafficking of the GLUT4 glucose transporter to the membrane along actin microfilaments (Chiu et al., 2010). Additionally, it remains to be seen whether the levels of G-actin at the postsynapse are impacted by *DmCFL* KD, given that DmCFL also interacts with monomeric actin. Lastly, it is unknown whether other actin-interacting proteins with severing activity like Twinfilin and Flightless I (FliI) could compensate for the *DmCFL* KD defects. Overexpression of these proteins would be informative because if they ameliorate the phenotype, as it would provide further evidence that it is the severing function of cofilin that is critical for maintaining the postsynapse.

B. Extra-sarcomeric actin at other muscle subcellular compartments

Actin plays many roles throughout the muscle cell, including at the sarcomere, costamere, T-tubule, nucleus, and, as shown in this work, at the postsynapse (Kee et al., 2009).

Cortical actin and membrane integrity

Given that we find disruption of postsynaptic structure in *DmCFL* KD, future studies should focus on whether destabilizing actin in this model also causes defects in overall muscle membrane integrity (i.e. sarcolemma, T-tubules), anchoring of the Z-discs to the membrane (i.e. costamere), and structure of the sarcoplasmic reticulum. It is possible that disturbing the organization of the overall muscle membrane would contribute to some of the structural defects seen at the postsynaptic membrane. Investigating proteins that link the cytoplasmic actin network with the extracellular matrix (e.g. integrins, dystrophin-glycoprotein complex) would be informative.

Nuclear actin

Actin is present not only in the cytoplasm along the inner surface of the cell membrane (cortical actin) but also surrounding and inside of the nucleus. Perinuclear actin secures the nucleus in a cage-like structure comprised of transmembrane actin-associated nuclear lines (Luxton et al., 2011). The nuclei in certain types of NM and NM models have been noted to be mispositioned,

are rounded and have altered envelopes (Berger et al., 2014; Ross et al., 2019). Additionally, nuclei in NM are sometimes internalized with rods encircling them when visualized by electron microscopy (Tan et al., 1999; Yin et al., 2021). Previous work in our lab has shown that reducing levels of the actin-capping protein Tmod by RNAi has striking effects on nuclear shape and positioning (Zapater I Morales et al., 2023).

First discovered in *Drosophila*, actin can travel into the nucleus via a specific import pathway (through importin 9), but only when bound to cofilin (Dopie et al., 2012). The intranuclear cytoskeleton plays several roles in response to external stimuli like cell stretching, mitotic exit, and infection, in addition to being involved in transcriptional regulation and DNA repair by various mechanisms (Caridi et al., 2019; Chuang et al., 2006; Dundr et al., 2007). Mechanosignaling from the cytoplasmic cytoskeleton provides cues for nuclear rigidity and chromosome organization within the nucleus (Mazumder et al., 2008). Work in our lab has found cofilin expressed in the nuclei of embryonic fly muscles (Balakrishnan, Howard, et al., 2021). An RNAi screen in *Drosophila* cells found several cofilin regulators in the nucleus (Dopie et al., 2015). Muscle biopsy in two NM patients showed a dense nucleolus yet dispersed chromatin (Karpati et al., 1971). The cell cycle was dysregulated in the muscles of a *Cfl2* mouse model where the negative regulator p21 was overexpressed (Morton et al., 2015). These data suggest that a proper intranuclear cytoskeletal network is needed to preserve chromatin organization in addition to DNA replication, which in the mammal is necessary for muscle regeneration, but may manifest as endoreplication in *Drosophila*. Our lab previously has described different nuclear parameters that could be evaluated in the *DmCFL* KD larval muscles,

including shape, ploidy, and cell cycle properties (Windner et al., 2019). Assay for transposase-accessible chromatin with sequencing (ATAC-Seq) analysis would also open avenues of inquiry into chromatin and gene expression changes.

C. Testing the effect of growth and exercise using the fly model

One mouse NM study show that exercise does not exacerbate nemaline rod formation and anecdotes suggest that human patients benefit from low-intensity exercise (Ilkovski et al., 2001; Nair-Shalliker et al., 2004). Speech exercises in NM patients can increase tongue strength and speech intelligibility, while respiratory exercises post-surgery can improve function (Cervera-Mérida et al., 2020; Smith et al., 2011). A question remains about what the appropriate balance of activity is for maintaining or building strength without exacerbating NM disease via potentially stressful hypertrophy.

DmCFL KD larvae to have significantly reduced crawling velocity after L2 that is linked to proportion of muscle classes. Larvae use their body wall muscles to crawl and burrow into their food. Exercise in *Drosophila* larva increases muscle excitation (Sigrist et al., 2003). One strategy to promote exercise in larvae is to place them into food of varying stiffness. A preliminary protocol (designed by Brooke Bergeron in our lab) for preparing fly food of various stiffnesses involves altering the proportion of agar included (Table 4.1). Downstream analyses could include functional assays (e.g. crawling assay) or live imaging. Preliminary results on wildtype larvae show that wandering larvae reared in less stiff food

for four days show a decreased time to roll over yet spend more time at rest when placed on an apple juice plate.

Table 4.1: Fly food recipes for varying stiffnesses (makes 200 mL)

Ingredient	Less stiff	Standard	More stiff
Water	0.17 L	0.17 L	0.17 L
Cornmeal	9.9 g	9.9 g	9.9 g
Molasses	10.6 mL	10.6 mL	10.6 mL
Yeast	4.16 g	4.16 g	4.16 g
Tegacept	3.84	3.84	3.84
Propionic acid	1.28	1.28	1.28
Agar	0.4	1.5	2.4

Another consideration for pediatric muscle degenerative disease is growth rate. Height and weight growth varies across childhood and adolescence, where it is high over the first few months of life then decelerates until the child reaches puberty where it increases again. *Drosophila* larvae experience an exponential growth rate with some muscles growing 40-fold over a five day period (Demontis & Perrimon, 2009). Hence, this model provides an interesting opportunity to systematically examine the impact of increased growth. Additionally, further pushing the system by upregulating growth through manipulation of the insulin pathway may reveal whether increased demand to grow exacerbates the deterioration phenotype (Demontis & Perrimon, 2009).

D. Adult DmCFL model

Further study of DmCFL's role in adult muscle would provide additional information about muscle formation during pupation, sarcomere development and muscle maintenance. A study from our lab found that the actin-severing protein Flightless I (FliI), a gelsolin family member, is critical in the early days of adulthood to regulate sarcomere size (Deng et al., 2021). Additionally, an adult

model affecting DmCFL would provide a new context in which to understand progression of disease as the flies age, since the study would not be restricted to five days of larval development. Several muscle function assays could be employed when studying the different muscle groups, including climbing (leg muscles), flight (direct and indirect flight muscles), and jump (jump muscles) assays. Logistically, one would need to use an inducible system to avoid the death seen in *DmCFL* KD RNAi prior to pupation. The temperature-sensitive Tubulin-Gal80 system could be used to repress Gal4 expression of the RNAi until the rearing temperature is increased (T. Lee & Luo, 1999). However, temperature change affects developmental rate and aging, which may confound the effects on muscle. Other more recent techniques—such as the optogenetic Shine-Gal4 tool—could also be used to activate the UAS without affecting temperature (di Pietro et al., 2021). Further studies of the NMJ could also be done in adult flies, as there are various innervation patterns for each of the adult muscle groups (Fernandes & Keshishian, 1999).

II. IMPLICATIONS FOR NEMALINE MYOPATHY

A. NMJ studies in other NM models

Occasional case reports from NM patient biopsies mention altered NMJ structural phenotypes (Fukuhara et al., 1978; Heffernan et al., 1968). However, the NMJ has not been reported to be deeply studied in NM animal models. There is mention of normal innervation seen in one *Cfl2* null mouse model when visualizing the presence of neurofilament in the motor neuron and acetylcholine receptor (Agrawal et al., 2012). The findings from my work should encourage further inquiry into alterations, both structural and functional, at the postsynapse

in NM. This could include examining postsynaptic proteins at the NMJ and acetylcholine receptor subunit composition since those bear the most similarity to the changes at the postsynapse seen in my work. One complication, however, is that the *Cfl2* mouse models have a short lifespan, dying at around postnatal day 9. Additionally, additional neuromuscular functional studies would be helpful to understand the electrophysiological profile more deeply in these models. The same inquiries could be made of NM animal models with mutations in other genes.

B. NM diagnosis and disease monitoring

It remains an open question whether the findings in this study are more generalizable to other NM causative mutations. The increased accessibility of sequencing as a part of diagnostics will make it possible to link the phenotypic changes observed in NM patients to causative mutations. The likelihood that diagnostic biopsies would include the NMJ are low.

More detailed neuromuscular studies—including nerve conduction studies and EMG studies—of NM patients would be helpful in determining functional changes, especially over time. NM patients typically have a myopathic pattern with low amplitudes on EMG studies. This finding seems to change over time: one longitudinal study found that after age nine, EMG of distal muscles began to show neuropathic changes in addition to myopathic changes (C Wallgren-Pettersson et al., 1989). This could be explained by the addition of degenerative changes to the motor units on top of the original myopathic changes reported. One case report speculated that the formation of rods in the

extrafusal muscle fibers was linked to improper innervation (Karpati et al., 1971). Therefore, it would be informative to have serial neuromuscular functional studies done over the lifespan of NM patients (especially in childhood) to try to correlate function test results with symptoms reported.

Modulating NMJ activity may be a treatment option in NM. Pyridostigmine, an acetylcholinesterase inhibitor, was reported in one case to improve ventilation, amount of spontaneous movement, and motor development over a period of two years (Natera-de Benito et al., 2016). The increased presence of acetylcholine in the synaptic cleft may have increased the probability of receptor binding and thus better neurotransmission. However, the patient in this case report had mutations in a gene not associated with NM in addition to the KLHL40 NM-related mutation, so it is unclear whether this strategy would help NM patients with mutations in other genes. Although the fly NMJ is a glutamatergic synapse rather than cholinergic, it still provides a convenient model for testing whether targeting certain parts of the ECC pathway would improve disease.

The findings of this study on the *DmCFL* KD model should encourage further study into the role of the NMJ in NM. *Drosophila* studies can continue to be helpful in pursuing the many open avenues of study related to NM disease progression and potential therapeutics.

CHAPTER 5:
METHODS

I. *Drosophila* husbandry, stocks, and crosses

All stocks and crosses were raised on standard cornmeal at 25°C on a 12-hour light/12-hour dark light cycle under humidity control. All experiments were done in wandering L3 larvae of both sexes reared at 25°C. *DmCFL* was knocked down specifically in muscle, as done in our previous study (Balakrishnan et al., 2020), by leveraging the Gal4-UAS system (Brand & Perrimon, 1993). The muscle-specific driver *Mhc*-Gal4 (BDSC #67044) was used to drive UAS-*mCherry* RNAi (for control, BDSC #35785) or UAS-*tsr* TRiP RNAi (for *DmCFL* knockdown, BDSC #65055) generated by the Transgenic RNAi Project (TRiP; Perkins et al., 2015). Live imaging experiments were done with larvae expressing tsr::GFP (ZCL2393, Kyoto Stock Center DGRC #110875) generated by the FlyTrap: GFP Protein Trap Database (Morin et al., 2001).

II. RNA-sequencing analysis

RNA-sequencing of control and *DmCFL* KD larvae as described previously (Zapater I Morales et al., 2023). Eight to ten late third instar larvae of each genotype were dissected in triplicate.

Read counts data were assessed and plotted with the integrated Differential Expression and Pathway analysis (iDEP) web application (versions 0.96 and 1.1; Ge et al., 2018). DESeq2 analysis was performed with the following parameters: false discovery rate of 0.05 and minimum two-fold change (Love et

al., 2014). Overrepresentation analysis was done using the Gene Set Enrichment Analysis (GSEA) method to identify the top 20 enriched pathways defined by Gene Ontology (GO) Biological Processes (BP) gene sets when considering the top 2000 genes at a false discovery rate of 0.05.

III. Western blot

Five to ten wandering late third-instar larvae were dissected in HL3.1 buffer as has been previously described in (Brent et al., 2009) to produce muscle-enriched preparations, which were then lysed in larval lysis buffer (50 mM HEPES [pH 7.5], 150 mM NaCl, 0.5% NP40, 0.1% SDS) supplemented with cOmplete mini protease inhibitor cocktail (Roche, #11836153001) and PhosSTOP phosphatase inhibitor cocktail (Roche, #4906837001). Ten micrograms from control and *DmCFL* KD lysates were run on a 12.5% polyacrylamide gel, then transferred to a nitrocellulose membrane (Thermo Fisher Scientific, PI88018). Blocking was done in 5% milk or 5% bovine serum albumin (BSA) in TBST (Tris-buffered saline + 0.1% Tween) for 1 hour at room temperature. Primary antibody staining was performed in Stamina Antibody Dilution Buffer (KindleBiosciences, R2004) overnight at room temperature using 1:1000 for rabbit anti-Twinstar (DmCFL, gift from Tadashi Uemura); 1:1000 for rabbit anti-phospho-Twinstar (p-DmCFL, gift from Tadashi Uemura); and 1:1000 for mouse anti-GAPDH (Abcam, #ab9484). Secondary antibody incubation was performed in 5% milk for 1 hour at room temperature using 1:5000 for anti-rabbit-HRP (Jackson Immunoresearch, 711-035-152) or anti-mouse-HRP (Jackson Immunoresearch, 715-035-151). Blot was imaged using the KwikQuant Imager (Kindle Biosciences, D1001) using 1-Shot Digital-ECL

(Kindle Biosciences, R1003) and intensities were quantified using FIJI Gel Analyzer tool (NIH). Protein expression was normalized to GAPDH loading control within each sample and repeated in triplicate.

IV. Quantitative polymerase chain reaction (q-PCR)

Total RNA was extracted from ten late third-instar wandering larvae muscle-enriched preparations (dissected as described in western blot methods) using TRIzol reagent (ThermoFisher #15596026) and was subsequently cleaned using the TURBO DNA-free Kit (Ambion, AM1907). Reverse transcription was done to synthesize cDNA using the SuperScript III First-Strand Synthesis System for RT-PCR (Invitrogen #18080-051) kit. PCR reactions were run on the CFX Opus 96 Real-Time PCR System using SYBR Select Master Mix for CFX (Applied Biosystems #4472937) in biological and technical triplicate. Primers used for tsr: (forward) GCTCTCAAGAAGTCGCTCGT; (reverse) GCAATGCACAGTGCTCGTAC. The delta-delta Ct method was used to calculate fold changes with Rpl32 as the normalization control. Reported values represent the $\log_2$ fold change of the gene in *DmCFL* KD compared to expression in control samples.

V. Dissection and immunostaining

Third-instar larvae at the wandering stage were dissected as previously described in (Azevedo et al., 2016; Brent et al., 2009) to expose the body wall muscles. Fixation was done using 4% paraformaldehyde in HL3.1 buffer for 15 minutes at room temperature for all antibodies except GluRIIA for which Bouin's fixative was used for 5 min at room temperature. Samples were blocked in BSA-

PBT (PBS supplemented with 0.1% BSA and 0.3% Triton X-100) for 30 minutes at room temperature, then incubated with primary antibody overnight at 4°C and subsequently washed in BSA-PBT. Samples were then incubated with Alexa Fluor-conjugated secondary antibodies, phalloidin and goat Alexa-647 conjugated horseradish peroxidase (HRP; Jackson Immunoresearch cat no. 123-605-021) at a concentration of 1:400. Alexa Fluor 555 conjugates secondary antibodies were used for all intensity quantifications. Final washes were done in PBT prior to mounting in Prolong Gold (Invitrogen, P36930). All slides were cured for at least 24 hours at room temperature prior to imaging.

Primary antibodies used in this study include rabbit anti-tsr (DmCFL, concentration 1:500, gift from Tadashi Uemura (Niwa et al., 2002) against C-terminal peptide CREAVEEKLRATDRQ; rabbit anti-p-Cofilin (concentration 1:500, gift from Tadashi Uemura) against N-terminal peptide (acetyl-A(pS) GVTVSDC ; mouse anti-Discs large (concentration 1:100, DSHB 4F3); mouse anti-Bruchpilot (concentration 1:250, DSHB nc82); rabbit anti-GluRIIC (concentration 1:1000, gift from Aaron DiAntonio); mouse anti-GluRIIA (concentration 1:100, DSHB 8B4D2, MH2B); rat anti-Tmod (concentration 1:200, gift from Velia Fowler); guinea pig anti-Coracle (concentration: 1:1500, gift from Richard Fehon); and mouse anti-alpha-spectrin (concentration: 1:50, DSHB 3A9).

VI. Confocal imaging

All samples for comparison were imaged with the same settings between genotypes. Pairs of ventral longitudinal muscles 3 and 4 (muscles 6 and 7) from

abdominal hemisegments 2-4 were imaged for all experiments. For *DmCFL* KD, muscle pairs were only imaged if one muscle was class 1 or 2. Z stack images were acquired using an upright Leica Stellaris 5 laser-scanning confocal microscope with dry HC PL Apo 20X/0.75 CS2, oil HC PL Apo 63X/1.40 CS2, or oil HC PL Apo 100X/1.40 CS2 objectives and HyD S detector (Leica Microsystems). Images were acquired sequentially by stack scanning bidirectionally at 400 Hz, with a pixel size of 283.95 nm x 283.95 nm and an area size of 2048 x 1024 pixels in Leica LASX software and saved as LIF files. For all images the pinhole size was 92.53 µm, calculated at 1 A.U. for 561 nm emission. Images were acquired with step sizes of 1 µm (for 20X) or 0.5 µm (for 63X or 100X). For all images for postsynaptic intensity, Z-stack was determined using the HRP channel with the start before and the end 1 µm below the last appreciable HRP signal. FIJI was used to create sum slices or maximum intensity Z projections (NIH).

VII. Live sample imaging

Live samples were imaged using a Leica Stellaris 5 laser-scanning confocal microscope with a water HC FLUOTAR L VISIR 25X/0.95 objective and HyD S detector (Leica Microsystems). Larvae were dissected and pinned to expose ventral muscles and imaged live in ambient temperature while the larvae were maintained in ice-cold HL3.1 buffer. Images were acquired sequentially by stack scanning bidirectionally at 400 Hz, with a pixel size of 283.95 nm x 283.95 nm and an area size of 2048 x 1024 pixels in Leica LASX software and saved as LIF files. For all images the pinhole size was 92.53 µm, calculated at 1 A.U. for

561 nm emission. Z-stacks were taken using a 1 µm step size and sum slices Z projections were created using FIJI (NIH).

VIII. Structured illumination microscopy (SIM) imaging

All samples were imaged with the same settings on a Zeiss Elyra 7 with Lattice SIM^2 confocal microscope with a Plan-Apochromat 63X/1.4 Oil DIC M27 objective. Images were acquired sequentially by stack with a pixel size of 0.06 µm x 0.06 µm and an area size of 80.1 µm by 80.1 µm in ZEN Black software and saved as CZI files. Images were taken with 13 phases and reconstructed using ZEN Black software at the "strong" sharpness setting (Zeiss). The Z stacks were acquired at a step size of 0.329 µm and sum slices Z-projections were made using FIJI (NIH).

IX. Three-dimensional NMJ intensity analyses

Postsynaptic intensity measurements were done using Imaris 10.0 (Bitplane). A three-dimensional surface for the HRP source channel was generated for each Z stack image with a surface detail grain level of 0.18 µm, smoothing enabled, and auto-thresholding (Figure 2.6). Small surfaces that were not part of the NMJ were removed. For Brp quantification, the sum of the sum intensity of the Brp channel was normalized to the total HRP volume and compared between genotypes. For DmCFL, p-DmCFL, GluRIIC, GluRIIA intensity measurements, an expanded volume was used. A mask was created from the HRP surface using the Distance Transform setting. A second surface was made using the distance transform mask, with a surface detail level of 0.18 and a manual threshold of 0 to 0.5 to limit the surface to a shell extending from the edge of the

HRP surface to 0.5 μm away. The sum of the sum intensity within this expanded surface was normalized to the expanded volume.

X. NMJ morphology measurements

The Dlg channel was used to quantify NMJ morphology in FIJI (NIH). The number of boutons in a Z-stack image was manually counted using the Cell Counter plugin. NMJ span was measured by drawing a line parallel to the length of the NMJ and normalizing to the length of muscle VL3 (6) or VL4 (7) based on whichever was longer. Cell length was determined by drawing a polygon around the phalloidin-positive shape of each muscle cell and then using the “length” measurement. SSR area was defined as Dlg-positive area normalized to total summed cell areas of muscle 6 and 7. Dlg-positive area was measured by creating a binary mask of the Dlg channel using the Yen thresholding method and recording the area. Cell area was determined by drawing a polygon around the phalloidin-positive shape of each muscle cell and then using the “length” measurement.

Dlg/HRP intensity surrounding individual boutons was done by (1) drawing a line along the diameter of a bouton; (2) recording the Dlg and HRP intensities along the length of the line; (3) normalizing length values to the total length; and (4) normalizing the Dlg and HRP intensities to the average intensities of that marker in that bouton.

XI. Electron microscopy

Wandering L3 larvae were dissected as described above and fixed overnight in 2.5% glutaraldehyde at 4°C. Larval filets were trimmed to remove the head and tail and to retain the ventral body wall muscles on both sides. Samples were washed three times in 0.1M sodium cacodylate buffer and then post-fixed in 1% osmium tetroxide for 1 hour at room temperature on a rotator. Next, samples were washed three times in 0.1M sodium cacodylate buffer for 10 minutes each wash at room temperature. A dehydration series in ethanol was conducted for 10 minutes at room temperature in each of the following: 30, 50, 70, 85, 95, 100, and 100% ethanol. Infiltration was done in four steps: first in a solution of 1:1 acetonitrile and 100% ethanol for 10 minutes at room temperature followed by infiltration in only acetonitrile for 10 minutes at room temperature. Samples were incubated in a 1:1 mixture of acetonitrile and Embed-812 resin for 30 minutes at room temperature, and then incubated in only Embed-812 resin overnight. In a semi-hardened resin block, larvae were oriented so that the longitudinal edge was along the cutting face of the block. The block was polymerized for 48 hours at 60°C. Thick sagittal sections of 5-10 µm were taken and stained with Toluidine Blue until muscles that were oriented in a longitudinal direction were identified (Figure 2.9). A Leica Ultracut UCT ultramicrotome with diamond knife was used to take 70 nm ultrathin sections which were then collected on 3 mm diameter mesh copper grids. Images of individual boutons and the underlying muscle were taken on a JEOL JEM-1400 transmission electron microscope at 100 kV.

XII. Two-electrode voltage-clamp (TEVC) electrophysiology

TEVC recordings were done on dissected wandering third instars as previously reported (Leahy et al., 2023). Briefly, all recording were done at 18^{o}C in physiological saline (in mM): 128 NaCl, 2 KCl, 4 MgCl2, 1.0 CaCl2, 70 sucrose, and 5 HEPES (pH 7.2). Longitudinally dissected larvae had internal organs removed and peripheral motor nerves cut at the ventral nerve cord (VNC) base. The body walls were glued down (Vetbond, 3M). The preparation was imaged with a 40X water-immersion objective on a Zeiss Axioskop microscope. Ventral longitudinal muscle 6 in abdominal segments 3 or 4 was impaled with two intracellular electrodes (1 mm outer diameter borosilicate capillaries; World Precision Instruments, 1B100F-4) of ~15 MΩ resistance (3M KCl). The muscle was voltage clamped at −60 mV using an Axoclamp-2B amplifier (Axon Instruments), and the motor nerve stimulated with a fire-polished glass suction electrode using 0.5 ms suprathreshold voltage stimuli at 0.2 Hz from a Grass S88 stimulator. Nerve stimulation–evoked excitatory junction current (EJC) recordings were filtered at 2 kHz. To quantify EJC amplitude, 10 consecutive traces were averaged, and the average peak value recorded. Clampex 9.0 was used for all data acquisition, and Clampfit 10.7 was used for all data analyses (Axon Instruments).

XIII. Statistical analysis

Pairwise comparisons between groups were performed using a two-tailed student's *t* test with an alpha of 0.05 using R statistical software (R Core Team, 2021). Plots were generated using the ggplot2 R package (Wickham, 2009, 2016). Figures report the mean ± standard deviation in addition to sample size

REFERENCES

Abe, H., Ohshima, S., & Obinata, T. (1989). A cofilin-like protein is involved in the regulation of actin assembly in developing skeletal muscle. *Journal of Biochemistry*, *106*(4), 696–702. https://doi.org/10.1093/oxfordjournals.jbchem.a122919

Agrawal, P. B., Greenleaf, R. S., Tomczak, K. K., Lehtokari, V.-L., Wallgren-Pettersson, C., Wallefeld, W., Laing, N. G., Darras, B. T., Maciver, S. K., Dormitzer, P. R., & Beggs, A. H. (2007). Nemaline myopathy with minicores caused by mutation of the CFL2 gene encoding the skeletal muscle actin-binding protein, cofilin-2. *American Journal of Human Genetics*, *80*(1), 162–167. https://doi.org/10.1086/510402

Agrawal, P. B., Joshi, M., Savic, T., Chen, Z., & Beggs, A. H. (2012). Normal myofibrillar development followed by progressive sarcomeric disruption with actin accumulations in a mouse Cfl2 knockout demonstrates requirement of cofilin-2 for muscle maintenance. *Human Molecular Genetics*, *21*(10), 2341–2356. https://doi.org/10.1093/hmg/dds053

Ahmed, S. T., Craven, L., Russell, O. M., Turnbull, D. M., & Vincent, A. E. (2018). Diagnosis and treatment of mitochondrial myopathies. *Neurotherapeutics*, *15*(4), 943–953. https://doi.org/10.1007/s13311-018-00674-4

Andrianantoandro, E., & Pollard, T. D. (2006). Mechanism of actin filament turnover by severing and nucleation at different concentrations of ADF/cofilin. *Molecular Cell*, *24*(1), 13–23. https://doi.org/10.1016/j.molcel.2006.08.006

Andrikou, C., & Arnone, M. I. (2015). Too many ways to make a muscle: Evolution of GRNs governing myogenesis. *Zoologischer Anzeiger - A Journal of Comparative Zoology*, *256*, 2–13. https://doi.org/10.1016/j.jcz.2015.03.005

Atwood, H. L., Govind, C. K., & Wu, C. F. (1993). Differential ultrastructure of synaptic terminals on ventral longitudinal abdominal muscles in Drosophila larvae. *Journal of Neurobiology*, *24*(8), 1008–1024. https://doi.org/10.1002/neu.480240803

Aulehla, A., & Pourquié, O. (2006). On periodicity and directionality of somitogenesis. *Anatomy and Embryology*, *211 Suppl 1*, 3–8. https://doi.org/10.1007/s00429-006-0124-y

Azevedo, M., Schulman, V. K., Folker, E., Balakrishnan, M., & Baylies, M. (2016). Imaging approaches to investigate myonuclear positioning in drosophila. *Methods in Molecular Biology*, *1411*, 291–312. https://doi.org/10.1007/978-1-4939-3530-7_19

Bailey, S. J., Stocksley, M. A., Buckel, A., Young, C., & Slater, C. R. (2003). Voltage-gated sodium channels and ankyrinG occupy a different postsynaptic domain from acetylcholine receptors from an early stage of neuromuscular junction maturation in rats. *The Journal of Neuroscience*, *23*(6), 2102–2111. https://doi.org/10.1523/JNEUROSCI.23-06-02102.2003

Balakrishnan, M., Howard, A., Yu, S. F., Sommer, K., Nowak, S. J., & Baylies, M. K. (2021). A screen for Twist-interacting proteins identifies Twinstar as a regulator of muscle development during embryogenesis. *BioRxiv*. https://doi.org/10.1101/2021.02.10.430492

Balakrishnan, M., Sisso, W. J., & Baylies, M. K. (2021). Analyzing muscle structure and function throughout the larval instars in live Drosophila. *STAR Protocols*, *2*(1), 100291. https://doi.org/10.1016/j.xpro.2020.100291

Balakrishnan, M., Yu, S. F., Chin, S. M., Soffar, D. B., Windner, S. E., Goode, B. L., & Baylies, M. K. (2020). Cofilin Loss in Drosophila Muscles Contributes to Muscle Weakness through Defective Sarcomerogenesis during Muscle Growth. *Cell Reports*, *32*(3), 107893. https://doi.org/10.1016/j.celrep.2020.107893

Bamburg, J. R., & Bernstein, B. W. (2010). Roles of ADF/cofilin in actin polymerization and beyond. *F1000 Biology Reports*, *2*, 62. https://doi.org/10.3410/B2-62

Banerjee, S., Venkatesan, A., & Bhat, M. A. (2017). Neurexin, Neuroligin and Wishful Thinking coordinate synaptic cytoarchitecture and growth at neuromuscular junctions. *Molecular and Cellular Neurosciences*, *78*, 9–24. https://doi.org/10.1016/j.mcn.2016.11.004

Banovic, D., Khorramshahi, O., Owald, D., Wichmann, C., Riedt, T., Fouquet, W., Tian, R., Sigrist, S. J., & Aberle, H. (2010). Drosophila neuroligin 1 promotes growth and postsynaptic differentiation at glutamatergic neuromuscular junctions. *Neuron*, *66*(5), 724–738. https://doi.org/10.1016/j.neuron.2010.05.020

Bataillé, L., Boukhatmi, H., Frendo, J.-L., & Vincent, A. (2017). Dynamics of transcriptional (re)-programming of syncytial nuclei in developing muscles. *BMC Biology*, *15*(1), 48. https://doi.org/10.1186/s12915-017-0386-2

Bate, M. (1990). The embryonic development of larval muscles in Drosophila. *Development*, *110*(3), 791–804. https://doi.org/10.1242/dev.110.3.791

Baylies, M. K., & Bate, M. (1996). twist: a myogenic switch in Drosophila. *Science*, *272*(5267), 1481–1484. https://doi.org/10.1126/science.272.5267.1481

Baylies, M. K., Martinez Arias, A., & Bate, M. (1995). wingless is required for the formation of a subset of muscle founder cells during Drosophila embryogenesis. *Development*, *121*(11), 3829–3837. https://doi.org/10.1242/dev.121.11.3829

Belyantseva, I. A., Perrin, B. J., Sonnemann, K. J., Zhu, M., Stepanyan, R., McGee, J., Frolenkov, G. I., Walsh, E. J., Friderici, K. H., Friedman, T. B., & Ervasti, J. M. (2009). Gamma-actin is required for cytoskeletal maintenance but not development. *Proceedings of the National Academy of Sciences of the United States of America*, *106*(24), 9703–9708. https://doi.org/10.1073/pnas.0900221106

Berger, J., Tarakci, H., Berger, S., Li, M., Hall, T. E., Arner, A., & Currie, P. D. (2014). Loss of Tropomodulin4 in the zebrafish mutant träge causes cytoplasmic rod formation and muscle weakness reminiscent of nemaline myopathy. *Disease Models & Mechanisms*, *7*(12), 1407–1415. https://doi.org/10.1242/dmm.017376

Bergquist, S., Dickman, D. K., & Davis, G. W. (2010). A hierarchy of cell intrinsic and target-derived homeostatic signaling. *Neuron*, *66*(2), 220–234. https://doi.org/10.1016/j.neuron.2010.03.023

Berkenstadt, M., Pode-Shakked, B., Barel, O., Barash, H., Achiron, R., Gilboa, Y., Kidron, D., & Raas-Rothschild, A. (2018). LMOD3-Associated Nemaline Myopathy: Prenatal Ultrasonographic, Pathologic, and Molecular Findings. *Journal of Ultrasound in Medicine*, *37*(7), 1827–1833. https://doi.org/10.1002/jum.14520

Bernadzki, K. M., Rojek, K. O., & Prószyński, T. J. (2014). Podosomes in muscle cells and their role in the remodeling of neuromuscular postsynaptic machinery. *European Journal of Cell Biology*, *93*(10–12), 478–485. https://doi.org/10.1016/j.ejcb.2014.06.002

Bernstein, B. W., & Bamburg, J. R. (1982). Tropomyosin binding to F-actin protects the F-actin from disassembly by brain actin-depolymerizing factor (ADF). *Cell Motility*, *2*(1), 1–8.

Berthier, C., & Blaineau, S. (1997). Supramolecular organization of the subsarcolemmal cytoskeleton of adult skeletal muscle fibers. A review. *Biology of the Cell*, *89*(7), 413–434. https://doi.org/10.1016/s0248-4900(97)89313-6

Bi, P., Ramirez-Martinez, A., Li, H., Cannavino, J., McAnally, J. R., Shelton, J. M., Sánchez-Ortiz, E., Bassel-Duby, R., & Olson, E. N. (2017). Control of muscle formation by the fusogenic micropeptide myomixer. *Science*, *356*(6335), 323–327. https://doi.org/10.1126/science.aam9361

Blair, A., Tomlinson, A., Pham, H., Gunsalus, K. C., Goldberg, M. L., & Laski, F. A. (2006). Twinstar, the Drosophila homolog of cofilin/ADF, is required for planar cell polarity patterning. *Development*, *133*(9), 1789–1797. https://doi.org/10.1242/dev.02320

Bloch, R. J., & Hall, Z. W. (1983). Cytoskeletal components of the vertebrate neuromuscular junction: vinculin, alpha-actinin, and filamin. *The Journal of Cell Biology*, *97*(1), 217–223. https://doi.org/10.1083/jcb.97.1.217

Blunk, A. D., Akbergenova, Y., Cho, R. W., Lee, J., Walldorf, U., Xu, K., Zhong, G., Zhuang, X., & Littleton, J. T. (2014). Postsynaptic actin regulates active zone spacing and glutamate receptor apposition at the Drosophila neuromuscular junction. *Molecular and Cellular Neurosciences*, *61*, 241–254. https://doi.org/10.1016/j.mcn.2014.07.005

Bolaños, P., & Calderón, J. C. (2022). Excitation-contraction coupling in mammalian skeletal muscle: Blending old and last-decade research. *Frontiers in Physiology*, *13*, 989796. https://doi.org/10.3389/fphys.2022.989796

Bothe, I., & Baylies, M. K. (2016). Drosophila myogenesis. *Current Biology*, *26*(17), R786-91. https://doi.org/10.1016/j.cub.2016.07.062

Brand, A. H., & Perrimon, N. (1993). Targeted gene expression as a means of altering cell fates and generating dominant phenotypes. *Development*, *118*(2), 401–415. https://doi.org/10.1242/dev.118.2.401

Brent, J. R., Werner, K. M., & McCabe, B. D. (2009). Drosophila larval NMJ dissection. *Journal of Visualized Experiments*, *24*. https://doi.org/10.3791/1107

Brieher, W. (2013). Mechanisms of actin disassembly. *Molecular Biology of the Cell*, *24*(15), 2299–2302. https://doi.org/10.1091/mbc.E12-09-0694

Broadie, K., Prokop, A., Bellen, H. J., O'Kane, C. J., Schulze, K. L., & Sweeney, S. T. (1995). Syntaxin and synaptobrevin function downstream of vesicle docking in Drosophila. *Neuron*, *15*(3), 663–673. https://doi.org/10.1016/0896-6273(95)90154-x

Buckingham, M., & Relaix, F. (2007). The role of Pax genes in the development of tissues and organs: Pax3 and Pax7 regulate muscle

progenitor cell functions. *Annual Review of Cell and Developmental Biology*, *23*, 645–673. https://doi.org/10.1146/annurev.cellbio.23.090506.123438

Buckingham, M. (2007). Skeletal muscle progenitor cells and the role of Pax genes. *Comptes Rendus Biologies*, *330*(6–7), 530–533. https://doi.org/10.1016/j.crvi.2007.03.015

Bullard, B., Bell, J., Craig, R., & Leonard, K. (1985). Arthrin: a new actin-like protein in insect flight muscle. *Journal of Molecular Biology*, *182*(3), 443–454. https://doi.org/10.1016/0022-2836(85)90203-7

Bunnell, T. M., Burbach, B. J., Shimizu, Y., & Ervasti, J. M. (2011). β-Actin specifically controls cell growth, migration, and the G-actin pool. *Molecular Biology of the Cell*, *22*(21), 4047–4058. https://doi.org/10.1091/mbc.E11-06-0582

Caridi, C. P., Plessner, M., Grosse, R., & Chiolo, I. (2019). Nuclear actin filaments in DNA repair dynamics. *Nature Cell Biology*, *21*(9), 1068–1077. https://doi.org/10.1038/s41556-019-0379-1

Carmena, A., Bate, M., & Jiménez, F. (1995). Lethal of scute, a proneural gene, participates in the specification of muscle progenitors during Drosophila embryogenesis. *Genes & Development*, *9*(19), 2373–2383. https://doi.org/10.1101/gad.9.19.2373

Cervera-Mérida, J. F., Villa-García, I., & Ygual-Fernández, A. (2020). Speech treatment in nemaline myopathy: A single-subject experimental study. *Journal of Communication Disorders*, *88*, 106051. https://doi.org/10.1016/j.jcomdis.2020.106051

Chal, J., & Pourquié, O. (2017). Making muscle: skeletal myogenesis in vivo and in vitro. *Development*, *144*(12), 2104–2122. https://doi.org/10.1242/dev.151035

Chen, K., & Featherstone, D. E. (2005). Discs-large (DLG) is clustered by presynaptic innervation and regulates postsynaptic glutamate receptor subunit composition in Drosophila. *BMC Biology*, *3*, 1. https://doi.org/10.1186/1741-7007-3-1

Chen, K., Gracheva, E. O., Yu, S.-C., Sheng, Q., Richmond, J., & Featherstone, D. E. (2010). Neurexin in embryonic Drosophila neuromuscular junctions. *Plos One*, *5*(6), e11115. https://doi.org/10.1371/journal.pone.0011115

Chen, K., Merino, C., Sigrist, S. J., & Featherstone, D. E. (2005). The 4.1 protein coracle mediates subunit-selective anchoring of Drosophila glutamate receptors to the postsynaptic actin cytoskeleton. *The Journal of*

Neuroscience, *25*(28), 6667–6675. https://doi.org/10.1523/JNEUROSCI.1527-05.2005

Chen, X., Sanchez, G. N., Schnitzer, M. J., & Delp, S. L. (2016). Changes in sarcomere lengths of the human vastus lateralis muscle with knee flexion measured using in vivo microendoscopy. *Journal of Biomechanics*, *49*(13), 2989–2994. https://doi.org/10.1016/j.jbiomech.2016.07.013

Chiu, T. T., Patel, N., Shaw, A. E., Bamburg, J. R., & Klip, A. (2010). Arp2/3- and cofilin-coordinated actin dynamics is required for insulin-mediated GLUT4 translocation to the surface of muscle cells. *Molecular Biology of the Cell*, *21*(20), 3529–3539. https://doi.org/10.1091/mbc.E10-04-0316

Chou, V. T., Johnson, S. A., & Van Vactor, D. (2020). Synapse development and maturation at the drosophila neuromuscular junction. *Neural Development*, *15*(1), 11. https://doi.org/10.1186/s13064-020-00147-5

Christophers, B., Lopez, M. A., Gupta, V. A., Vogel, H., & Baylies, M. (2022). Pediatric nemaline myopathy: A systematic review using individual patient data. *Journal of Child Neurology*, *37*(7), 652–663. https://doi.org/10.1177/08830738221096316

Chuang, C.-H., Carpenter, A. E., Fuchsova, B., Johnson, T., de Lanerolle, P., & Belmont, A. S. (2006). Long-range directional movement of an interphase chromosome site. *Current Biology*, *16*(8), 825–831. https://doi.org/10.1016/j.cub.2006.03.059

Claeys, K. G. (2020). Congenital myopathies: an update. *Developmental Medicine and Child Neurology*, *62*(3), 297–302. https://doi.org/10.1111/dmcn.14365

Conen, P. E., Murphy, E. G., & Donohue, W. L. (1963). Light and electron microscopic studies of “myogranules” in a child with hypotonia and muscle weakness. *Canadian Medical Association Journal*, *89*, 983–986.

Coyle, I. P., Koh, Y.-H., Lee, W.-C. M., Slind, J., Fergestad, T., Littleton, J. T., & Ganetzky, B. (2004). Nervous wreck, an SH3 adaptor protein that interacts with Wsp, regulates synaptic growth in Drosophila. *Neuron*, *41*(4), 521–534. https://doi.org/10.1016/s0896-6273(04)00016-9

Craig, S. W., & Pardo, J. V. (1983). Gamma actin, spectrin, and intermediate filament proteins colocalize with vinculin at costameres, myofibril-to-sarcolemma attachment sites. *Cell Motility*, *3*(5–6), 449–462.

Cramer, A. A. W., Prasad, V., Eftestøl, E., Song, T., Hansson, K.-A., Dugdale, H. F., Sadayappan, S., Ochala, J., Gundersen, K., & Millay, D. P. (2020). Nuclear numbers in syncytial muscle fibers promote size but limit the

development of larger myonuclear domains. *Nature Communications*, *11*(1), 6287. https://doi.org/10.1038/s41467-020-20058-7

Crisp, S., Evers, J. F., Fiala, A., & Bate, M. (2008). The development of motor coordination in Drosophila embryos. *Development*, *135*(22), 3707–3717. https://doi.org/10.1242/dev.026773

Daniels, R. W., Collins, C. A., Gelfand, M. V., Dant, J., Brooks, E. S., Krantz, D. E., & DiAntonio, A. (2004). Increased expression of the Drosophila vesicular glutamate transporter leads to excess glutamate release and a compensatory decrease in quantal content. *The Journal of Neuroscience*, *24*(46), 10466–10474. https://doi.org/10.1523/JNEUROSCI.3001-04.2004

Demontis, F., & Perrimon, N. (2009). Integration of Insulin receptor/Foxo signaling and dMyc activity during muscle growth regulates body size in Drosophila. *Development*, *136*(6), 983–993. https://doi.org/10.1242/dev.027466

Deng, S., Azevedo, M., & Baylies, M. (2017). Acting on identity: Myoblast fusion and the formation of the syncytial muscle fiber. *Seminars in Cell & Developmental Biology*, *72*, 45–55. https://doi.org/10.1016/j.semcdb.2017.10.033

Deng, S., Silimon, R. L., Balakrishnan, M., Bothe, I., Juros, D., Soffar, D. B., & Baylies, M. K. (2021). The actin polymerization factor Diaphanous and the actin severing protein Flightless I collaborate to regulate sarcomere size. *Developmental Biology*, *469*, 12–25. https://doi.org/10.1016/j.ydbio.2020.09.014

Denker, A., & Rizzoli, S. O. (2010). Synaptic vesicle pools: an update. *Frontiers in Synaptic Neuroscience*, *2*, 135. https://doi.org/10.3389/fnsyn.2010.00135

De La Cruz, E. M. (2005). Cofilin binding to muscle and non-muscle actin filaments: isoform-dependent cooperative interactions. *Journal of Molecular Biology*, *346*(2), 557–564. https://doi.org/10.1016/j.jmb.2004.11.065

di Pietro, F., Herszterg, S., Huang, A., Bosveld, F., Alexandre, C., Sancéré, L., Pelletier, S., Joudat, A., Kapoor, V., Vincent, J.-P., & Bellaïche, Y. (2021). Rapid and robust optogenetic control of gene expression in Drosophila. *Developmental Cell*, *56*(24), 3393-3404.e7. https://doi.org/10.1016/j.devcel.2021.11.016

DiAntonio, A., Petersen, S. A., Heckmann, M., & Goodman, C. S. (1999). Glutamate receptor expression regulates quantal size and quantal content at the Drosophila neuromuscular junction. *The Journal of Neuroscience*, *19*(8), 3023–3032. https://doi.org/10.1523/JNEUROSCI.19-08-03023.1999

Dlugosz, A. A., Antin, P. B., Nachmias, V. T., & Holtzer, H. (1984). The relationship between stress fiber-like structures and nascent myofibrils in cultured cardiac myocytes. *The Journal of Cell Biology*, *99*(6), 2268–2278. https://doi.org/10.1083/jcb.99.6.2268

Doe, C. Q. (2017). Temporal patterning in the drosophila CNS. *Annual Review of Cell and Developmental Biology*, *33*, 219–240. https://doi.org/10.1146/annurev-cellbio-111315-125210

Dopie, J., Rajakylä, E. K., Joensuu, M. S., Huet, G., Ferrantelli, E., Xie, T., Jäälinoja, H., Jokitalo, E., & Vartiainen, M. K. (2015). Genome-wide RNAi screen for nuclear actin reveals a network of cofilin regulators. *Journal of Cell Science*, *128*(13), 2388–2400. https://doi.org/10.1242/jcs.169441

Dopie, J., Skarp, K.-P., Rajakylä, E. K., Tanhuanpää, K., & Vartiainen, M. K. (2012). Active maintenance of nuclear actin by importin 9 supports transcription. *Proceedings of the National Academy of Sciences of the United States of America*, *109*(9), E544-52. https://doi.org/10.1073/pnas.1118880109

Dubey, M., Ain, U., & Firdaus, H. (2020). An insight on Drosophila myogenesis and its assessment techniques. *Molecular Biology Reports*, *47*(12), 9849–9863. https://doi.org/10.1007/s11033-020-06006-0

Dundr, M., Ospina, J. K., Sung, M.-H., John, S., Upender, M., Ried, T., Hager, G. L., & Matera, A. G. (2007). Actin-dependent intranuclear repositioning of an active gene locus in vivo. *The Journal of Cell Biology*, *179*(6), 1095–1103. https://doi.org/10.1083/jcb.200710058

Ennis, J., Dyment, D. A., Michaud, J., & McMillan, H. J. (2015). Congenital nemaline myopathy: the value of magnetic resonance imaging of muscle. *The Canadian Journal of Neurological Sciences. Le Journal Canadien Des Sciences Neurologiques*, *42*(5), 338–340. https://doi.org/10.1017/cjn.2015.59

Fahim, M. A., Hasan, M. Y., & Alshuaib, W. B. (2000). Early morphological remodeling of neuromuscular junction in a murine model of diabetes. *Journal of Applied Physiology*, *89*(6), 2235–2240. https://doi.org/10.1152/jappl.2000.89.6.2235

Fardeau, M., & Desguerre, I. (2013). Diagnostic workup for neuromuscular diseases. *Handbook of Clinical Neurology*, *113*, 1291–1297. https://doi.org/10.1016/B978-0-444-59565-2.00001-0

Fattori, F., Fiorillo, C., Rodolico, C., Tasca, G., Verardo, M., Bellacchio, E., Pizzi, S., Ciolfi, A., Fagiolari, G., Lupica, A., Broda, P., Pedemonte, M., Moggio, M., Bruno, C., Tartaglia, M., Bertini, E., & D'Amico, A. (2018).

Expanding the histopathological spectrum of CFL2-related myopathies. *Clinical Genetics*, *93*(6), 1234–1239. https://doi.org/10.1111/cge.13240

Featherstone, David E, Rushton, E., Rohrbough, J., Liebl, F., Karr, J., Sheng, Q., Rodesch, C. K., & Broadie, K. (2005). An essential Drosophila glutamate receptor subunit that functions in both central neuropil and neuromuscular junction. *The Journal of Neuroscience*, *25*(12), 3199–3208. https://doi.org/10.1523/JNEUROSCI.4201-04.2005

Featherstone, D E, Rushton, E. M., Hilderbrand-Chae, M., Phillips, A. M., Jackson, F. R., & Broadie, K. (2000). Presynaptic glutamic acid decarboxylase is required for induction of the postsynaptic receptor field at a glutamatergic synapse. *Neuron*, *27*(1), 71–84. https://doi.org/10.1016/s0896-6273(00)00010-6

Fernandes, J. J., & Keshishian, H. (1999). Development of the adult neuromuscular system. *International Review of Neurobiology*, *43*, 221–239. https://doi.org/10.1016/S0074-7742(08)60547-4

Fertuck, H. C., & Salpeter, M. M. (1974). Localization of acetylcholine receptor by 125I-labeled alpha-bungarotoxin binding at mouse motor endplates. *Proceedings of the National Academy of Sciences of the United States of America*, *71*(4), 1376–1378. https://doi.org/10.1073/pnas.71.4.1376

Figeac, N., Daczewska, M., Marcelle, C., & Jagla, K. (2007). Muscle stem cells and model systems for their investigation. *Developmental Dynamics*, *236*(12), 3332–3342. https://doi.org/10.1002/dvdy.21345

Finsterer, J. (2020). Update Review about Metabolic Myopathies. *Life (Basel, Switzerland)*, *10*(4). https://doi.org/10.3390/life10040043

Folker, E. S., Schulman, V. K., & Baylies, M. K. (2012). Muscle length and myonuclear position are independently regulated by distinct Dynein pathways. *Development*, *139*(20), 3827–3837. https://doi.org/10.1242/dev.079178

Fukuhara, N., Yuasa, T., Tsubaki, T., Kushiro, S., & Takasawa, N. (1978). Nemaline myopathy: histological, histochemical and ultrastructural studies. *Acta Neuropathologica*, *42*(1), 33–41. https://doi.org/10.1007/BF01273264

Fyrberg, E. A., Bond, B. J., Hershey, N. D., Mixter, K. S., & Davidson, N. (1981). The actin genes of Drosophila: protein coding regions are highly conserved but intron positions are not. *Cell*, *24*(1), 107–116. https://doi.org/10.1016/0092-8674(81)90506-7

Fyrberg, E. A., Mahaffey, J. W., Bond, B. J., & Davidson, N. (1983). Transcripts of the six Drosophila actin genes accumulate in a stage- and

tissue-specific manner. *Cell*, *33*(1), 115–123. https://doi.org/10.1016/0092-8674(83)90340-9

Galkin, V. E., Orlova, A., Kudryashov, D. S., Solodukhin, A., Reisler, E., Schröder, G. F., & Egelman, E. H. (2011). Remodeling of actin filaments by ADF/cofilin proteins. *Proceedings of the National Academy of Sciences of the United States of America*, *108*(51), 20568–20572. https://doi.org/10.1073/pnas.1110109108

Ganesan, S., Karr, J. E., & Featherstone, D. E. (2011). Drosophila glutamate receptor mRNA expression and mRNP particles. *RNA Biology*, *8*(5), 771–781. https://doi.org/10.4161/rna.8.5.16014

Ganetzky, B., & Wu, C. F. (1983). Neurogenetic analysis of potassium currents in Drosophila: synergistic effects on neuromuscular transmission in double mutants. *Journal of Neurogenetics*, *1*(1), 17–28. https://doi.org/10.3109/01677068309107069

Ganetzky, B. (1984). Genetic studies of membrane excitability in Drosophila: lethal interaction between two temperature-sensitive paralytic mutations. *Genetics*, *108*(4), 897–911. https://doi.org/10.1093/genetics/108.4.897

Gardiol, A., & St Johnston, D. (2014). Staufen targets coracle mRNA to Drosophila neuromuscular junctions and regulates GluRIIA synaptic accumulation and bouton number. *Developmental Biology*, *392*(2), 153–167. https://doi.org/10.1016/j.ydbio.2014.06.007

Gerhart, J., Elder, J., Neely, C., Schure, J., Kvist, T., Knudsen, K., & George-Weinstein, M. (2006). MyoD-positive epiblast cells regulate skeletal muscle differentiation in the embryo. *The Journal of Cell Biology*, *175*(2), 283–292. https://doi.org/10.1083/jcb.200605037

Ge, S. X., Son, E. W., & Yao, R. (2018). iDEP: an integrated web application for differential expression and pathway analysis of RNA-Seq data. *BMC Bioinformatics*, *19*(1), 534. https://doi.org/10.1186/s12859-018-2486-6

Gohla, A., Birkenfeld, J., & Bokoch, G. M. (2005). Chronophin, a novel HAD-type serine protein phosphatase, regulates cofilin-dependent actin dynamics. *Nature Cell Biology*, *7*(1), 21–29. https://doi.org/10.1038/ncb1201

Gokhin, D. S., & Fowler, V. M. (2011). Cytoplasmic gamma-actin and tropomodulin isoforms link to the sarcoplasmic reticulum in skeletal muscle fibers. *The Journal of Cell Biology*, *194*(1), 105–120. https://doi.org/10.1083/jcb.201011128

Gommans, I. M. P., Davis, M., Saar, K., Lammens, M., Mastaglia, F., Lamont, P., van Duijnhoven, G., ter Laak, H. J., Reis, A., Vogels, O. J. M., Laing, N.,

van Engelen, B. G. M., & Kremer, H. (2003). A locus on chromosome 15q for a dominantly inherited nemaline myopathy with core-like lesions. *Brain: A Journal of Neurology*, *126*(Pt 7), 1545–1551. https://doi.org/10.1093/brain/awg162

Gonatas, N. K., Shy, G. M., & Godfrey, E. H. (1966). Nemaline myopathy. The origin of nemaline structures. *The New England Journal of Medicine*, *274*(10), 535–539. https://doi.org/10.1056/NEJM196603102741002

Gotti, C., Sensini, A., Zucchelli, A., Carloni, R., & Focarete, M. L. (2020). Hierarchical fibrous structures for muscle-inspired soft-actuators: A review. *Applied Materials Today*, *20*, 100772. https://doi.org/10.1016/j.apmt.2020.100772

Gunsalus, K. C., Bonaccorsi, S., Williams, E., Verni, F., Gatti, M., & Goldberg, M. L. (1995). Mutations in twinstar, a Drosophila gene encoding a cofilin/ADF homologue, result in defects in centrosome migration and cytokinesis. *The Journal of Cell Biology*, *131*(5), 1243–1259. https://doi.org/10.1083/jcb.131.5.1243

Gu, J., Lee, C. W., Fan, Y., Komlos, D., Tang, X., Sun, C., Yu, K., Hartzell, H. C., Chen, G., Bamburg, J. R., & Zheng, J. Q. (2010). ADF/cofilin-mediated actin dynamics regulate AMPA receptor trafficking during synaptic plasticity. *Nature Neuroscience*, *13*(10), 1208–1215. https://doi.org/10.1038/nn.2634

Gurniak, C. B., Chevessier, F., Jokwitz, M., Jönsson, F., Perlas, E., Richter, H., Matern, G., Boyl, P. P., Chaponnier, C., Fürst, D., Schröder, R., & Witke, W. (2014). Severe protein aggregate myopathy in a knockout mouse model points to an essential role of cofilin2 in sarcomeric actin exchange and muscle maintenance. *European Journal of Cell Biology*, *93*(5–6), 252–266. https://doi.org/10.1016/j.ejcb.2014.01.007

Hall, Z. W., Lubit, B. W., & Schwartz, J. H. (1981). Cytoplasmic actin in postsynaptic structures at the neuromuscular junction. *The Journal of Cell Biology*, *90*(3), 789–792. https://doi.org/10.1083/jcb.90.3.789

Halpern, M. E., Chiba, A., Johansen, J., & Keshishian, H. (1991). Growth cone behavior underlying the development of stereotypic synaptic connections in Drosophila embryos. *The Journal of Neuroscience*, *11*(10), 3227–3238. https://doi.org/10.1523/JNEUROSCI.11-10-03227.1991

Hasty, P., Bradley, A., Morris, J. H., Edmondson, D. G., Venuti, J. M., Olson, E. N., & Klein, W. H. (1993). Muscle deficiency and neonatal death in mice with a targeted mutation in the myogenin gene. *Nature*, *364*(6437), 501–506. https://doi.org/10.1038/364501a0

Hayakawa, K., Tatsumi, H., & Sokabe, M. (2011). Actin filaments function as a tension sensor by tension-dependent binding of cofilin to the filament. *The Journal of Cell Biology*, *195*(5), 721–727. https://doi.org/10.1083/jcb.201102039

Hayden, S. M., Miller, P. S., Brauweiler, A., & Bamburg, J. R. (1993). Analysis of the interactions of actin depolymerizing factor with G- and F-actin. *Biochemistry*, *32*(38), 9994–10004. https://doi.org/10.1021/bi00089a015

Heffernan, L. P., Rewcastle, N. B., & Humphrey, J. G. (1968). The spectrum of rod myopathies. *Archives of Neurology*, *18*(5), 529–542. https://doi.org/10.1001/archneur.1968.00470350087008

Henderson, C. A., Gomez, C. G., Novak, S. M., Mi-Mi, L., & Gregorio, C. C. (2017). Overview of the muscle cytoskeleton. *Comprehensive Physiology*, *7*(3), 891–944. https://doi.org/10.1002/cphy.c160033

Herman, I., Lopez, M. A., Marafi, D., Pehlivan, D., Calame, D. G., Abid, F., & Lotze, T. E. (2021). Clinical exome sequencing in the diagnosis of pediatric neuromuscular disease. *Muscle & Nerve*, *63*(3), 304–310. https://doi.org/10.1002/mus.27112

Hewes, R. S., Snowdeal, E. C., Saitoe, M., & Taghert, P. H. (1998). Functional redundancy of FMRFamide-related peptides at the Drosophila larval neuromuscular junction. *The Journal of Neuroscience*, *18*(18), 7138–7151. https://doi.org/10.1523/JNEUROSCI.18-18-07138.1998

Hoang, B., & Chiba, A. (2001). Single-cell analysis of Drosophila larval neuromuscular synapses. *Developmental Biology*, *229*(1), 55–70. https://doi.org/10.1006/dbio.2000.9983

Holtzer, H., Hijikata, T., Lin, Z. X., Zhang, Z. Q., Holtzer, S., Protasi, F., Franzini-Armstrong, C., & Sweeney, H. L. (1997). Independent assembly of 1.6 microns long bipolar MHC filaments and I-Z-I bodies. *Cell Structure and Function*, *22*(1), 83–93. https://doi.org/10.1247/csf.22.83

Hosoda, A., Sato, N., Nagaoka, R., Abe, H., & Obinata, T. (2007). Activity of cofilin can be regulated by a mechanism other than phosphorylation/dephosphorylation in muscle cells in culture. *Journal of Muscle Research and Cell Motility*, *28*(2–3), 183–194. https://doi.org/10.1007/s10974-007-9117-6

Huang, K., Bi, F.-F., & Yang, H. (2021). A Systematic Review and Meta-Analysis of the Prevalence of Congenital Myopathy. *Frontiers in Neurology*, *12*, 761636. https://doi.org/10.3389/fneur.2021.761636

Huehn, A. R., Bibeau, J. P., Schramm, A. C., Cao, W., De La Cruz, E. M., & Sindelar, C. V. (2020). Structures of cofilin-induced structural changes reveal local and asymmetric perturbations of actin filaments. *Proceedings of the National Academy of Sciences of the United States of America*, *117*(3), 1478–1484. https://doi.org/10.1073/pnas.1915987117

Humphreys, J. M., Duyf, B., Joiner, M. L., Phillips, J. P., & Hilliker, A. J. (1996). Genetic analysis of oxygen defense mechanisms in Drosophila melanogaster and identification of a novel behavioural mutant with a Shaker phenotype. *Genome*, *39*(4), 749–757. https://doi.org/10.1139/g96-094

Huxley, A. F., & Niedergerke, R. (1954). Structural changes in muscle during contraction; interference microscopy of living muscle fibres. *Nature*, *173*(4412), 971–973. https://doi.org/10.1038/173971a0

Huxley, A. F. (1957). Muscle structure and theories of contraction. *Progress in Biophysics and Biophysical Chemistry*, *7*, 255–318. https://doi.org/10.1016/S0096-4174(18)30128-8

Huxley, H., & Hanson, J. (1954). Changes in the cross-striations of muscle during contraction and stretch and their structural interpretation. *Nature*, *173*(4412), 973–976. https://doi.org/10.1038/173973a0

Huxley, H. E. (1963). Electron microscope studies on the structure of natural and synthetic protein filaments from striated muscle. *Journal of Molecular Biology*, *7*, 281–308. https://doi.org/10.1016/s0022-2836(63)80008-x

Ilkovski, B., Cooper, S. T., Nowak, K., Ryan, M. M., Yang, N., Schnell, C., Durling, H. J., Roddick, L. G., Wilkinson, I., Kornberg, A. J., Collins, K. J., Wallace, G., Gunning, P., Hardeman, E. C., Laing, N. G., & North, K. N. (2001). Nemaline myopathy caused by mutations in the muscle alpha-skeletal-actin gene. *American Journal of Human Genetics*, *68*(6), 1333–1343. https://doi.org/10.1086/320605

Jagla, T., Bidet, Y., Da Ponte, J. P., Dastugue, B., & Jagla, K. (2002). Cross-repressive interactions of identity genes are essential for proper specification of cardiac and muscular fates in Drosophila. *Development*, *129*(4), 1037–1047. https://doi.org/10.1242/dev.129.4.1037

Jan, L. Y., & Jan, Y. N. (1982). Antibodies to horseradish peroxidase as specific neuronal markers in Drosophila and in grasshopper embryos. *Proceedings of the National Academy of Sciences of the United States of America*, *79*(8), 2700–2704. https://doi.org/10.1073/pnas.79.8.2700

Johansen, J., Halpern, M. E., Johansen, K. M., & Keshishian, H. (1989). Stereotypic morphology of glutamatergic synapses on identified muscle cells

of Drosophila larvae. *The Journal of Neuroscience*, *9*(2), 710–725. https://doi.org/10.1523/JNEUROSCI.09-02-00710.1989

Johnston, J. J., Kelley, R. I., Crawford, T. O., Morton, D. H., Agarwala, R., Koch, T., Schäffer, A. A., Francomano, C. A., & Biesecker, L. G. (2000). A novel nemaline myopathy in the Amish caused by a mutation in troponin T1. *American Journal of Human Genetics*, *67*(4), 814–821. https://doi.org/10.1086/303089

Jungbluth, H., Ochala, J., Treves, S., & Gautel, M. (2017). Current and future therapeutic approaches to the congenital myopathies. *Seminars in Cell & Developmental Biology*, *64*, 191–200. https://doi.org/10.1016/j.semcdb.2016.08.004

Junion, G., & Jagla, K. (2022). Diversification of muscle types in Drosophila embryos. *Experimental Cell Research*, *410*(1), 112950. https://doi.org/10.1016/j.yexcr.2021.112950

Kambadur, R., Koizumi, K., Stivers, C., Nagle, J., Poole, S. J., & Odenwald, W. F. (1998). Regulation of POU genes by castor and hunchback establishes layered compartments in the Drosophila CNS. *Genes & Development*, *12*(2), 246–260. https://doi.org/10.1101/gad.12.2.246

Kaplan, W. D., & Trout, W. E. (1969). The behavior of four neurological mutants of Drosophila. *Genetics*, *61*(2), 399–409. https://doi.org/10.1093/genetics/61.2.399

Karpati, G., Carpenter, S., & Andermann, F. (1971). A new concept of childhood nemaline myopathy. *Archives of Neurology*, *24*(4), 291–304. https://doi.org/10.1001/archneur.1971.00480340023002

Kassar-Duchossoy, L., Gayraud-Morel, B., Gomès, D., Rocancourt, D., Buckingham, M., Shinin, V., & Tajbakhsh, S. (2004). Mrf4 determines skeletal muscle identity in Myf5:Myod double-mutant mice. *Nature*, *431*(7007), 466–471. https://doi.org/10.1038/nature02876

Kassar-Duchossoy, L., Giacone, E., Gayraud-Morel, B., Jory, A., Gomès, D., & Tajbakhsh, S. (2005). Pax3/Pax7 mark a novel population of primitive myogenic cells during development. *Genes & Development*, *19*(12), 1426–1431. https://doi.org/10.1101/gad.345505

Kee, A. J., Gunning, P. W., & Hardeman, E. C. (2009). Diverse roles of the actin cytoskeleton in striated muscle. *Journal of Muscle Research and Cell Motility*, *30*(5–6), 187–197. https://doi.org/10.1007/s10974-009-9193-x

Kim, J. H., Jin, P., Duan, R., & Chen, E. H. (2015). Mechanisms of myoblast fusion during muscle development. *Current Opinion in Genetics & Development*, *32*, 162–170. https://doi.org/10.1016/j.gde.2015.03.006

Kohsaka, H., Okusawa, S., Itakura, Y., Fushiki, A., & Nose, A. (2012). Development of larval motor circuits in Drosophila. *Development, Growth & Differentiation*, *54*(3), 408–419. https://doi.org/10.1111/j.1440-169X.2012.01347.x

Kohsaka, H., Takasu, E., & Nose, A. (2007). In vivo induction of postsynaptic molecular assembly by the cell adhesion molecule Fasciclin2. *The Journal of Cell Biology*, *179*(6), 1289–1300. https://doi.org/10.1083/jcb.200705154

Koper, A., Schenck, A., & Prokop, A. (2012). Analysis of adhesion molecules and basement membrane contributions to synaptic adhesion at the Drosophila embryonic NMJ. *Plos One*, *7*(4), e36339. https://doi.org/10.1371/journal.pone.0036339

Kremneva, E., Makkonen, M. H., Skwarek-Maruszewska, A., Gateva, G., Michelot, A., Dominguez, R., & Lappalainen, P. (2014). Cofilin-2 controls actin filament length in muscle sarcomeres. *Developmental Cell*, *31*(2), 215–226. https://doi.org/10.1016/j.devcel.2014.09.002

Kuo, I. Y., & Ehrlich, B. E. (2015). Signaling in muscle contraction. *Cold Spring Harbor Perspectives in Biology*, *7*(2), a006023. https://doi.org/10.1101/cshperspect.a006023

Labasse, C., Brochier, G., Taratuto, A.-L., Cadot, B., Rendu, J., Monges, S., Biancalana, V., Quijano-Roy, S., Bui, M. T., Chanut, A., Madelaine, A., Lacène, E., Beuvin, M., Amthor, H., Servais, L., de Feraudy, Y., Erro, M., Saccoliti, M., Neto, O. A., … Romero, N. B. (2022). Severe ACTA1-related nemaline myopathy: intranuclear rods, cytoplasmic bodies, and enlarged perinuclear space as characteristic pathological features on muscle biopsies. *Acta Neuropathologica Communications*, *10*(1), 101. https://doi.org/10.1186/s40478-022-01400-0

Lahey, T., Gorczyca, M., Jia, X. X., & Budnik, V. (1994). The Drosophila tumor suppressor gene dlg is required for normal synaptic bouton structure. *Neuron*, *13*(4), 823–835. https://doi.org/10.1016/0896-6273(94)90249-6

Laitila, J., & Wallgren-Pettersson, C. (2021). Recent advances in nemaline myopathy. *Neuromuscular Disorders*, *31*(10), 955–967. https://doi.org/10.1016/j.nmd.2021.07.012

Landgraf, M., Baylies, M., & Bate, M. (1999). Muscle founder cells regulate defasciculation and targeting of motor axons in the Drosophila embryo.

Current Biology, *9*(11), 589–592. https://doi.org/10.1016/s0960-9822(99)80262-0

Landgraf, M., Bossing, T., Technau, G. M., & Bate, M. (1997). The origin, location, and projections of the embryonic abdominal motorneurons of Drosophila. *The Journal of Neuroscience*, *17*(24), 9642–9655. https://doi.org/10.1523/JNEUROSCI.17-24-09642.1997

Laurichesse, Q., & Soler, C. (2020). Muscle development : a view from adult myogenesis in Drosophila. *Seminars in Cell & Developmental Biology*, *104*, 39–50. https://doi.org/10.1016/j.semcdb.2020.02.009

Leahy, S. N., Song, C., Vita, D. J., & Broadie, K. (2023). FMRP activity and control of Csw/SHP2 translation regulate MAPK-dependent synaptic transmission. *PLoS Biology*, *21*(1), e3001969. https://doi.org/10.1371/journal.pbio.3001969

Lee, C. W., Han, J., Bamburg, J. R., Han, L., Lynn, R., & Zheng, J. Q. (2009). Regulation of acetylcholine receptor clustering by ADF/cofilin-directed vesicular trafficking. *Nature Neuroscience*, *12*(7), 848–856. https://doi.org/10.1038/nn.2322

Lee, G., & Schwarz, T. L. (2016). Filamin, a synaptic organizer in Drosophila, determines glutamate receptor composition and membrane growth. *ELife*, *5*. https://doi.org/10.7554/eLife.19991

Lee, T., & Luo, L. (1999). Mosaic analysis with a repressible cell marker for studies of gene function in neuronal morphogenesis. *Neuron*, *22*(3), 451–461. https://doi.org/10.1016/s0896-6273(00)80701-1

Lemke, S. B., & Schnorrer, F. (2017). Mechanical forces during muscle development. *Mechanisms of Development*, *144*(Pt A), 92–101. https://doi.org/10.1016/j.mod.2016.11.003

Liebl, F. L. W., & Featherstone, D. E. (2005). Genes involved in Drosophila glutamate receptor expression and localization. *BMC Neuroscience*, *6*, 44. https://doi.org/10.1186/1471-2202-6-44

Liebl, F. L. W., Wu, Y., Featherstone, D. E., Noordermeer, J. N., Fradkin, L., & Hing, H. (2008). Derailed regulates development of the Drosophila neuromuscular junction. *Developmental Neurobiology*, *68*(2), 152–165. https://doi.org/10.1002/dneu.20562

Lin, J. J.-C., Eppinga, R. D., Warren, K. S., & McCrae, K. R. (2008). Human tropomyosin isoforms in the regulation of cytoskeleton functions. *Advances in Experimental Medicine and Biology*, *644*, 201–222. https://doi.org/10.1007/978-0-387-85766-4_16

Lin, S.-S., Hsieh, T.-L., Liou, G.-G., Li, T.-N., Lin, H.-C., Chang, C.-W., Wu, H.-Y., Yao, C.-K., & Liu, Y.-W. (2020). Dynamin-2 Regulates Postsynaptic Cytoskeleton Organization and Neuromuscular Junction Development. *Cell Reports*, *33*(4), 108310. https://doi.org/10.1016/j.celrep.2020.108310

Li, J., Ashley, J., Budnik, V., & Bhat, M. A. (2007). Crucial role of Drosophila neurexin in proper active zone apposition to postsynaptic densities, synaptic growth, and synaptic transmission. *Neuron*, *55*(5), 741–755. https://doi.org/10.1016/j.neuron.2007.08.002

Love, M. I., Huber, W., & Anders, S. (2014). Moderated estimation of fold change and dispersion for RNA-seq data with DESeq2. *Genome Biology*, *15*(12), 550. https://doi.org/10.1186/s13059-014-0550-8

Luxton, G. W. G., Gomes, E. R., Folker, E. S., Worman, H. J., & Gundersen, G. G. (2011). TAN lines: a novel nuclear envelope structure involved in nuclear positioning. *Nucleus (Austin, Tex.)*, *2*(3), 173–181. https://doi.org/10.4161/nucl.2.3.16243

Malfatti, E., Böhm, J., Lacène, E., Beuvin, M., Romero, N. B., & Laporte, J. (2015). A Premature Stop Codon in MYO18B is Associated with Severe Nemaline Myopathy with Cardiomyopathy. *Journal of Neuromuscular Diseases*, *2*(3), 219–227. https://doi.org/10.3233/JND-150085

Marcelle, C., Stark, M. R., & Bronner-Fraser, M. (1997). Coordinate actions of BMPs, Wnts, Shh and noggin mediate patterning of the dorsal somite. *Development*, *124*(20), 3955–3963. https://doi.org/10.1242/dev.124.20.3955

Marrus, S. B., Portman, S. L., Allen, M. J., Moffat, K. G., & DiAntonio, A. (2004). Differential localization of glutamate receptor subunits at the Drosophila neuromuscular junction. *The Journal of Neuroscience*, *24*(6), 1406–1415. https://doi.org/10.1523/JNEUROSCI.1575-03.2004

Martin, A. R. (1994). Amplification of neuromuscular transmission by postjunctional folds. *Proceedings. Biological Sciences / the Royal Society*, *258*(1353), 321–326. https://doi.org/10.1098/rspb.1994.0180

Mazumder, A., Roopa, T., Basu, A., Mahadevan, L., & Shivashankar, G. V. (2008). Dynamics of chromatin decondensation reveals the structural integrity of a mechanically prestressed nucleus. *Biophysical Journal*, *95*(6), 3028–3035. https://doi.org/10.1529/biophysj.108.132274

McDonald, C. M. (2012). Clinical approach to the diagnostic evaluation of hereditary and acquired neuromuscular diseases. *Physical Medicine and Rehabilitation Clinics of North America*, *23*(3), 495–563. https://doi.org/10.1016/j.pmr.2012.06.011

McGough, A., Pope, B., Chiu, W., & Weeds, A. (1997). Cofilin changes the twist of F-actin: implications for actin filament dynamics and cellular function. *The Journal of Cell Biology*, *138*(4), 771–781. https://doi.org/10.1083/jcb.138.4.771

Megighian, A., Scorzeto, M., Zanini, D., Pantano, S., Rigoni, M., Benna, C., Rossetto, O., Montecucco, C., & Zordan, M. (2010). Arg206 of SNAP-25 is essential for neuroexocytosis at the Drosophila melanogaster neuromuscular junction. *Journal of Cell Science*, *123*(Pt 19), 3276–3283. https://doi.org/10.1242/jcs.071316

Meng, J. L., Wang, Y., Carrillo, R. A., & Heckscher, E. S. (2020). Temporal transcription factors determine circuit membership by permanently altering motor neuron-to-muscle synaptic partnerships. *ELife*, *9*. https://doi.org/10.7554/eLife.56898

Menon, K. P., Carrillo, R. A., & Zinn, K. (2013). Development and plasticity of the Drosophila larval neuromuscular junction. *Wiley Interdisciplinary Reviews. Developmental Biology*, *2*(5), 647–670. https://doi.org/10.1002/wdev.108

Mercuri, E., Bönnemann, C. G., & Muntoni, F. (2019). Muscular dystrophies. *The Lancet*, *394*(10213), 2025–2038. https://doi.org/10.1016/S0140-6736(19)32910-1

Messineo, A. M., Gineste, C., Sztal, T. E., McNamara, E. L., Vilmen, C., Ogier, A. C., Hahne, D., Bendahan, D., Laing, N. G., Bryson-Richardson, R. J., Gondin, J., & Nowak, K. J. (2018). L-tyrosine supplementation does not ameliorate skeletal muscle dysfunction in zebrafish and mouse models of dominant skeletal muscle α-actin nemaline myopathy. *Scientific Reports*, *8*(1), 11490. https://doi.org/10.1038/s41598-018-29437-z

Millay, D. P., O'Rourke, J. R., Sutherland, L. B., Bezprozvannaya, S., Shelton, J. M., Bassel-Duby, R., & Olson, E. N. (2013). Myomaker is a membrane activator of myoblast fusion and muscle formation. *Nature*, *499*(7458), 301–305. https://doi.org/10.1038/nature12343

Miyauchi-Nomura, S., Obinata, T., & Sato, N. (2012). Cofilin is required for organization of sarcomeric actin filaments in chicken skeletal muscle cells. *Cytoskeleton*, *69*(5), 290–302. https://doi.org/10.1002/cm.21025

Mohri, K, Takano-Ohmuro, H., Nakashima, H., Hayakawa, K., Endo, T., Hanaoka, K., & Obinata, T. (2000). Expression of cofilin isoforms during development of mouse striated muscles. *Journal of Muscle Research and Cell Motility*, *21*(1), 49–57. https://doi.org/10.1023/a:1005682322132

Mohri, Kurato, Suzuki-Toyota, F., Obinata, T., & Sato, N. (2019). Chimeric Mice with Deletion of Cfl2 that Encodes Muscle-Type Cofilin (MCF or Cofilin-2) Results in Defects of Striated Muscles, Both Skeletal and Cardiac Muscles. *Zoological Science*, *36*(2), 112–119. https://doi.org/10.2108/zs180151

Moreau-Le Lan, S., Aller, E., Calabria, I., Gonzalez-Tarancon, L., Cardona-Gay, C., Martinez-Matilla, M., Aparisi, M. J., Selles, J., Sagath, L., Pitarch, I., Muelas, N., Cervera, J. V., Millan, J. M., & Pedrola, L. (2018). New mutations found by Next-Generation Sequencing screening of Spanish patients with Nemaline Myopathy. *Plos One*, *13*(12), e0207296. https://doi.org/10.1371/journal.pone.0207296

Morin, X., Daneman, R., Zavortink, M., & Chia, W. (2001). A protein trap strategy to detect GFP-tagged proteins expressed from their endogenous loci in Drosophila. *Proceedings of the National Academy of Sciences of the United States of America*, *98*(26), 15050–15055. https://doi.org/10.1073/pnas.261408198

Morrison, B. M. (2016). Neuromuscular Diseases. *Seminars in Neurology*, *36*(5), 409–418. https://doi.org/10.1055/s-0036-1586263

Morton, S. U., Joshi, M., Savic, T., Beggs, A. H., & Agrawal, P. B. (2015). Skeletal muscle microRNA and messenger RNA profiling in cofilin-2 deficient mice reveals cell cycle dysregulation hindering muscle regeneration. *Plos One*, *10*(4), e0123829. https://doi.org/10.1371/journal.pone.0123829

Mukund, K., & Subramaniam, S. (2020). Skeletal muscle: A review of molecular structure and function, in health and disease. *Wiley Interdisciplinary Reviews. Systems Biology and Medicine*, *12*(1), e1462. https://doi.org/10.1002/wsbm.1462

Musumeci, G., Castrogiovanni, P., Coleman, R., Szychlinska, M. A., Salvatorelli, L., Parenti, R., Magro, G., & Imbesi, R. (2015). Somitogenesis: From somite to skeletal muscle. *Acta Histochemica*, *117*(4–5), 313–328. https://doi.org/10.1016/j.acthis.2015.02.011

Nabeshima, Y., Hanaoka, K., Hayasaka, M., Esumi, E., Li, S., Nonaka, I., & Nabeshima, Y. (1993). Myogenin gene disruption results in perinatal lethality because of severe muscle defect. *Nature*, *364*(6437), 532–535. https://doi.org/10.1038/364532a0

Nagaoka, R., Abe, H., & Obinata, T. (1996). Site-directed mutagenesis of the phosphorylation site of cofilin: Its role in cofilin-actin interaction and cytoplasmic localization. *Cell Motility and the Cytoskeleton*.

Nair-Shalliker, V., Kee, A. J., Joya, J. E., Lucas, C. A., Hoh, J. F., & Hardeman, E. C. (2004). Myofiber adaptational response to exercise in a mouse model of nemaline myopathy. *Muscle & Nerve*, *30*(4), 470–480. https://doi.org/10.1002/mus.20138

Nakashima, K., Sato, N., Nakagaki, T., Abe, H., Ono, S., & Obinata, T. (2005). Two mouse cofilin isoforms, muscle-type (MCF) and non-muscle type (NMCF), interact with F-actin with different efficiencies. *Journal of Biochemistry*, *138*(4), 519–526. https://doi.org/10.1093/jb/mvi152

Nakata, T., Nishina, Y., & Yorifuji, H. (2001). Cytoplasmic gamma actin as a Z-disc protein. *Biochemical and Biophysical Research Communications*, *286*(1), 156–163. https://doi.org/10.1006/bbrc.2001.5353

Nakayama, M., Matsushita, F., & Hama, C. (2014). The matrix protein Hikaru genki localizes to cholinergic synaptic clefts and regulates postsynaptic organization in the Drosophila brain. *The Journal of Neuroscience*, *34*(42), 13872–13877. https://doi.org/10.1523/JNEUROSCI.1585-14.2014

Nakayama, M., Suzuki, E., Tsunoda, S., & Hama, C. (2016). The Matrix Proteins Hasp and Hig Exhibit Segregated Distribution within Synaptic Clefts and Play Distinct Roles in Synaptogenesis. *The Journal of Neuroscience*, *36*(2), 590–606. https://doi.org/10.1523/JNEUROSCI.2300-15.2016

Natera-de Benito, D., Nascimento, A., Abicht, A., Ortez, C., Jou, C., Müller, J. S., Evangelista, T., Töpf, A., Thompson, R., Jimenez-Mallebrera, C., Colomer, J., & Lochmüller, H. (2016). KLHL40-related nemaline myopathy with a sustained, positive response to treatment with acetylcholinesterase inhibitors. *Journal of Neurology*, *263*(3), 517–523. https://doi.org/10.1007/s00415-015-8015-x

Nelson, B. R., Wu, F., Liu, Y., Anderson, D. M., McAnally, J., Lin, W., Cannon, S. C., Bassel-Duby, R., & Olson, E. N. (2013). Skeletal muscle-specific T-tubule protein STAC3 mediates voltage-induced Ca2+ release and contractility. *Proceedings of the National Academy of Sciences of the United States of America*, *110*(29), 11881–11886. https://doi.org/10.1073/pnas.1310571110

Nelson, J. C., Stavoe, A. K. H., & Colón-Ramos, D. A. (2013). The actin cytoskeleton in presynaptic assembly. *Cell Adhesion & Migration*, *7*(4), 379–387. https://doi.org/10.4161/cam.24803

Nguyen, M.-A. T., Joya, J. E., Kee, A. J., Domazetovska, A., Yang, N., Hook, J. W., Lemckert, F. A., Kettle, E., Valova, V. A., Robinson, P. J., North, K. N., Gunning, P. W., Mitchell, C. A., & Hardeman, E. C. (2011). Hypertrophy and dietary tyrosine ameliorate the phenotypes of a mouse model of severe

nemaline myopathy. *Brain: A Journal of Neurology*, *134*(Pt 12), 3516–3529. https://doi.org/10.1093/brain/awr274

Nguyen, M. T., & Lee, W. (2022). MiR-141-3p regulates myogenic differentiation in C2C12 myoblasts via CFL2-YAP-mediated mechanotransduction. *BMB Reports*, *55*(2), 104–109. https://doi.org/10.5483/BMBRep.2022.55.2.142

Nguyen, M. T., Min, K.-H., Kim, D., Park, S.-Y., & Lee, W. (2020). CFL2 is an essential mediator for myogenic differentiation in C2C12 myoblasts. *Biochemical and Biophysical Research Communications*, *533*(4), 710–716. https://doi.org/10.1016/j.bbrc.2020.11.016

Nicholson, L., & Keshishian, H. (2006). Neuromuscular Development. In *Muscle development in drosophila* (pp. 113–124). Springer New York. https://doi.org/10.1007/0-387-32963-3_10

Nicolau, S., & Milone, M. (2023). Sporadic Late-Onset Nemaline Myopathy: Current Landscape. *Current Neurology and Neuroscience Reports*, *23*(11), 777–784. https://doi.org/10.1007/s11910-023-01311-0

Nikonova, E., Kao, S.-Y., & Spletter, M. L. (2020). Contributions of alternative splicing to muscle type development and function. *Seminars in Cell & Developmental Biology*, *104*, 65–80. https://doi.org/10.1016/j.semcdb.2020.02.003

Niwa, R., Nagata-Ohashi, K., Takeichi, M., Mizuno, K., & Uemura, T. (2002). Control of actin reorganization by Slingshot, a family of phosphatases that dephosphorylate ADF/cofilin. *Cell*, *108*(2), 233–246. https://doi.org/10.1016/s0092-8674(01)00638-9

Ockeloen, C. W., Gilhuis, H. J., Pfundt, R., Kamsteeg, E. J., Agrawal, P. B., Beggs, A. H., Dara Hama-Amin, A., Diekstra, A., Knoers, N. V. A. M., Lammens, M., & van Alfen, N. (2012). Congenital myopathy caused by a novel missense mutation in the CFL2 gene. *Neuromuscular Disorders*, *22*(7), 632–639. https://doi.org/10.1016/j.nmd.2012.03.008

Ohashi, K. (2015). Roles of cofilin in development and its mechanisms of regulation. *Development, Growth & Differentiation*, *57*(4), 275–290. https://doi.org/10.1111/dgd.12213

Ohta, Y., Kousaka, K., Nagata-Ohashi, K., Ohashi, K., Muramoto, A., Shima, Y., Niwa, R., Uemura, T., & Mizuno, K. (2003). Differential activities, subcellular distribution and tissue expression patterns of three members of Slingshot family phosphatases that dephosphorylate cofilin. *Genes To Cells*, *8*(10), 811–824. https://doi.org/10.1046/j.1365-2443.2003.00678.x

Oliveira, M., Fernandes, A. L., & Vargas, S. (2018). Using sevoflurane in a pediatric patient with nemaline rod myopathy. *Paediatric Anaesthesia*, *28*(8), 749–750. https://doi.org/10.1111/pan.13458

Ong, C., Yung, L.-Y. L., Cai, Y., Bay, B.-H., & Baeg, G.-H. (2015). Drosophila melanogaster as a model organism to study nanotoxicity. *Nanotoxicology*, *9*(3), 396–403. https://doi.org/10.3109/17435390.2014.940405

Ong, R. W., AlSaman, A., Selcen, D., Arabshahi, A., Yau, K. S., Ravenscroft, G., Duff, R. M., Atkinson, V., Allcock, R. J., & Laing, N. G. (2014). Novel cofilin-2 (CFL2) four base pair deletion causing nemaline myopathy. *Journal of Neurology, Neurosurgery, and Psychiatry*, *85*(9), 1058–1060. https://doi.org/10.1136/jnnp-2014-307608

Ono, K., Parast, M., Alberico, C., Benian, G. M., & Ono, S. (2003). Specific requirement for two ADF/cofilin isoforms in distinct actin-dependent processes in Caenorhabditis elegans. *Journal of Cell Science*, *116*(Pt 10), 2073–2085. https://doi.org/10.1242/jcs.00421

Ono, S, Minami, N., Abe, H., & Obinata, T. (1994). Characterization of a novel cofilin isoform that is predominantly expressed in mammalian skeletal muscle. *The Journal of Biological Chemistry*, *269*(21), 15280–15286. https://doi.org/10.1016/S0021-9258(17)36603-6

Ono, Shoichiro, Baillie, D. L., & Benian, G. M. (1999). UNC-60B, an ADF/Cofilin Family Protein, Is Required for Proper Assembly of Actin into Myofibrils in*Caenorhabditis elegans* Body Wall Muscle. *The Journal of Cell Biology*, *145*(3), 491–502. https://doi.org/10.1083/jcb.145.3.491

Ono, Shoichiro. (2003). Regulation of actin filament dynamics by actin depolymerizing factor/cofilin and actin-interacting protein 1: new blades for twisted filaments. *Biochemistry*, *42*(46), 13363–13370. https://doi.org/10.1021/bi034600x

Ott, M. O., Bober, E., Lyons, G., Arnold, H., & Buckingham, M. (1991). Early expression of the myogenic regulatory gene, myf-5, in precursor cells of skeletal muscle in the mouse embryo. *Development*, *111*(4), 1097–1107. https://doi.org/10.1242/dev.111.4.1097

Papponen, H., Kaisto, T., Leinonen, S., Kaakinen, M., & Metsikkö, K. (2009). Evidence for gamma-actin as a Z disc component in skeletal myofibers. *Experimental Cell Research*, *315*(2), 218–225. https://doi.org/10.1016/j.yexcr.2008.10.021

Pardo, J. V., Pittenger, M. F., & Craig, S. W. (1983). Subcellular sorting of isoactins: Selective association of γ actin with skeletal muscle mitochondria. *Cell*, *32*(4), 1093–1103. https://doi.org/10.1016/0092-8674(83)90293-3

Parker, F., Baboolal, T. G., & Peckham, M. (2020). Actin mutations and their role in disease. *International Journal of Molecular Sciences*, *21*(9). https://doi.org/10.3390/ijms21093371

Pelin, K., Ridanpää, M., Donner, K., Wilton, S., Krishnarajah, J., Laing, N., Kolmerer, B., Millevoi, S., Labeit, S., de la Chapelle, A., & Wallgren-Petterson, C. (1997). Refined localisation of the genes for nebulin and titin on chromosome 2q allows the assignment of nebulin as a candidate gene for autosomal recessive nemaline myopathy. *European Journal of Human Genetics*, *5*(4), 229–234.

Perkins, L. A., Holderbaum, L., Tao, R., Hu, Y., Sopko, R., McCall, K., Yang-Zhou, D., Flockhart, I., Binari, R., Shim, H.-S., Miller, A., Housden, A., Foos, M., Randkelv, S., Kelley, C., Namgyal, P., Villalta, C., Liu, L.-P., Jiang, X., … Perrimon, N. (2015). The transgenic rnai project at harvard medical school: resources and validation. *Genetics*, *201*(3), 843–852. https://doi.org/10.1534/genetics.115.180208

Petersen, S. A., Fetter, R. D., Noordermeer, J. N., Goodman, C. S., & DiAntonio, A. (1997). Genetic analysis of glutamate receptors in Drosophila reveals a retrograde signal regulating presynaptic transmitter release. *Neuron*, *19*(6), 1237–1248. https://doi.org/10.1016/s0896-6273(00)80415-8

Pielage, J., Fetter, R. D., & Davis, G. W. (2006). A postsynaptic spectrin scaffold defines active zone size, spacing, and efficacy at the Drosophila neuromuscular junction. *The Journal of Cell Biology*, *175*(3), 491–503. https://doi.org/10.1083/jcb.200607036

Poliacikova, G., Maurel-Zaffran, C., Graba, Y., & Saurin, A. J. (2021). Hox proteins in the regulation of muscle development. *Frontiers in Cell and Developmental Biology*, *9*, 731996. https://doi.org/10.3389/fcell.2021.731996

Pollard, T. D. (2016). Actin and Actin-Binding Proteins. *Cold Spring Harbor Perspectives in Biology*, *8*(8). https://doi.org/10.1101/cshperspect.a018226

Prokop, A. (2006). Organization of the efferent system and structure of neuromuscular junctions in Drosophila. *International Review of Neurobiology*, *75*, 71–90. https://doi.org/10.1016/S0074-7742(06)75004-8

Proszynski, T. J., Gingras, J., Valdez, G., Krzewski, K., & Sanes, J. R. (2009). Podosomes are present in a postsynaptic apparatus and participate in its maturation. *Proceedings of the National Academy of Sciences of the United States of America*, *106*(43), 18373–18378. https://doi.org/10.1073/pnas.0910391106

Qin, G., Schwarz, T., Kittel, R. J., Schmid, A., Rasse, T. M., Kappei, D., Ponimaskin, E., Heckmann, M., & Sigrist, S. J. (2005). Four different subunits are essential for expressing the synaptic glutamate receptor at neuromuscular junctions of Drosophila. *The Journal of Neuroscience*, *25*(12), 3209–3218. https://doi.org/10.1523/JNEUROSCI.4194-04.2005

Quijano-Roy, S., & Carlier, R. Y. (2014). Congenital myopathies and congenital muscular dystrophies. The value of muscle imaging in current diagnostic approaches. *Medecine Therapeutique Pediatrie*, *17*(3), 160–169.

Ramachandran, P., & Budnik, V. (2010). Dissection of Drosophila larval body-wall muscles. *Cold Spring Harbor Protocols*, *2010*(8), pdb.prot5469. https://doi.org/10.1101/pdb.prot5469

Rasse, T. M., Fouquet, W., Schmid, A., Kittel, R. J., Mertel, S., Sigrist, C. B., Schmidt, M., Guzman, A., Merino, C., Qin, G., Quentin, C., Madeo, F. F., Heckmann, M., & Sigrist, S. J. (2005). Glutamate receptor dynamics organizing synapse formation in vivo. *Nature Neuroscience*, *8*(7), 898–905. https://doi.org/10.1038/nn1484

Ravenscroft, G., Miyatake, S., Lehtokari, V.-L., Todd, E. J., Vornanen, P., Yau, K. S., Hayashi, Y. K., Miyake, N., Tsurusaki, Y., Doi, H., Saitsu, H., Osaka, H., Yamashita, S., Ohya, T., Sakamoto, Y., Koshimizu, E., Imamura, S., Yamashita, M., Ogata, K., … Laing, N. G. (2013). Mutations in KLHL40 are a frequent cause of severe autosomal-recessive nemaline myopathy. *American Journal of Human Genetics*, *93*(1), 6–18. https://doi.org/10.1016/j.ajhg.2013.05.004

Rebbeck, R. T., Karunasekara, Y., Board, P. G., Beard, N. A., Casarotto, M. G., & Dulhunty, A. F. (2014). Skeletal muscle excitation-contraction coupling: who are the dancing partners? *The International Journal of Biochemistry & Cell Biology*, *48*, 28–38. https://doi.org/10.1016/j.biocel.2013.12.001

Reedy, M. C., & Beall, C. (1993). Ultrastructure of developing flight muscle in Drosophila. I. Assembly of myofibrils. *Developmental Biology*, *160*(2), 443–465. https://doi.org/10.1006/dbio.1993.1320

Relaix, F., Rocancourt, D., Mansouri, A., & Buckingham, M. (2005). A Pax3/Pax7-dependent population of skeletal muscle progenitor cells. *Nature*, *435*(7044), 948–953. https://doi.org/10.1038/nature03594

Ritzenthaler, S., & Chiba, A. (2003). Myopodia (postsynaptic filopodia) participate in synaptic target recognition. *Journal of Neurobiology*, *55*(1), 31–40. https://doi.org/10.1002/neu.10180

Romero-Pozuelo, J., Dason, J. S., Atwood, H. L., & Ferrús, A. (2007). Chronic and acute alterations in the functional levels of Frequenins 1 and 2 reveal their roles in synaptic transmission and axon terminal morphology. *The European Journal of Neuroscience*, *26*(9), 2428–2443. https://doi.org/10.1111/j.1460-9568.2007.05877.x

Roos, J., Hummel, T., Ng, N., Klämbt, C., & Davis, G. W. (2000). Drosophila Futsch regulates synaptic microtubule organization and is necessary for synaptic growth. *Neuron*, *26*(2), 371–382. https://doi.org/10.1016/s0896-6273(00)81170-8

Röper, K., Mao, Y., & Brown, N. H. (2005). Contribution of sequence variation in Drosophila actins to their incorporation into actin-based structures in vivo. *Journal of Cell Science*, *118*(Pt 17), 3937–3948. https://doi.org/10.1242/jcs.02517

Rosen, S. M., Joshi, M., Hitt, T., Beggs, A. H., & Agrawal, P. B. (2020). Knockin mouse model of the human CFL2 p.A35T mutation results in a unique splicing defect and severe myopathy phenotype. *Human Molecular Genetics*, *29*(12), 1996–2003. https://doi.org/10.1093/hmg/ddaa035

Ross, J. A., Levy, Y., Ripolone, M., Kolb, J. S., Turmaine, M., Holt, M., Lindqvist, J., Claeys, K. G., Weis, J., Monforte, M., Tasca, G., Moggio, M., Figeac, N., Zammit, P. S., Jungbluth, H., Fiorillo, C., Vissing, J., Witting, N., Granzier, H., … Ochala, J. (2019). Impairments in contractility and cytoskeletal organisation cause nuclear defects in nemaline myopathy. *Acta Neuropathologica*, *138*(3), 477–495. https://doi.org/10.1007/s00401-019-02034-8

Rudnicki, M. A., Schnegelsberg, P. N., Stead, R. H., Braun, T., Arnold, H. H., & Jaenisch, R. (1993). MyoD or Myf-5 is required for the formation of skeletal muscle. *Cell*, *75*(7), 1351–1359. https://doi.org/10.1016/0092-8674(93)90621-v

Ruggiero, C., & Lalli, E. (2021). Targeting the cytoskeleton against metastatic dissemination. *Cancer Metastasis Reviews*, *40*(1), 89–140. https://doi.org/10.1007/s10555-020-09936-0

R Core Team. (2021). *R: A Language and Environment for Statistical Computing* (4.0.2) [Computer software]. R Foundation for Statistical Computing.

Ruiz-Cañada, C., & Budnik, V. (2006). Synaptic cytoskeleton at the neuromuscular junction. *International Review of Neurobiology*, *75*, 217–236. https://doi.org/10.1016/S0074-7742(06)75010-3

Rybakova, I. N., Patel, J. R., & Ervasti, J. M. (2000). The dystrophin complex forms a mechanically strong link between the sarcolemma and costameric actin. *The Journal of Cell Biology*, *150*(5), 1209–1214. https://doi.org/10.1083/jcb.150.5.1209

Sahin, S., Oncel, M. Y., Bidev, D., Okur, N., Talim, B., & Oguz, S. S. (2019). Nemaline rod myopathy treated with L-tyrosine to relieve symptoms in a neonate. *Archivos Argentinos de Pediatria*, *117*(4), E382–E385.

Sambuughin, N., Yau, K. S., Olivé, M., Duff, R. M., Bayarsaikhan, M., Lu, S., Gonzalez-Mera, L., Sivadorai, P., Nowak, K. J., Ravenscroft, G., Mastaglia, F. L., North, K. N., Ilkovski, B., Kremer, H., Lammens, M., van Engelen, B. G. M., Fabian, V., Lamont, P., Davis, M. R., … Goldfarb, L. G. (2010). Dominant mutations in KBTBD13, a member of the BTB/Kelch family, cause nemaline myopathy with cores. *American Journal of Human Genetics*, *87*(6), 842–847. https://doi.org/10.1016/j.ajhg.2010.10.020

Sandmann, T., Girardot, C., Brehme, M., Tongprasit, W., Stolc, V., & Furlong, E. E. M. (2007). A core transcriptional network for early mesoderm development in Drosophila melanogaster. *Genes & Development*, *21*(4), 436–449. https://doi.org/10.1101/gad.1509007

Schmid, A., Hallermann, S., Kittel, R. J., Khorramshahi, O., Frölich, A. M. J., Quentin, C., Rasse, T. M., Mertel, S., Heckmann, M., & Sigrist, S. J. (2008). Activity-dependent site-specific changes of glutamate receptor composition in vivo. *Nature Neuroscience*, *11*(6), 659–666. https://doi.org/10.1038/nn.2122

Schröder, J. M., Durling, H., & Laing, N. (2004). Actin myopathy with nemaline bodies, intranuclear rods, and a heterozygous mutation in ACTA1 (Asp154Asn). *Acta Neuropathologica*, *108*(3), 250–256. https://doi.org/10.1007/s00401-004-0888-1

Schulman, V. K., Dobi, K. C., & Baylies, M. K. (2015). Morphogenesis of the somatic musculature in Drosophila melanogaster. *Wiley Interdisciplinary Reviews. Developmental Biology*, *4*(4), 313–334. https://doi.org/10.1002/wdev.180

Schulman, V. K., Folker, E. S., Rosen, J. N., & Baylies, M. K. (2014). Syd/JIP3 and JNK signaling are required for myonuclear positioning and muscle function. *PLoS Genetics*, *10*(12), e1004880. https://doi.org/10.1371/journal.pgen.1004880

Schuster, C. M., Ultsch, A., Schloss, P., Cox, J. A., Schmitt, B., & Betz, H. (1991). Molecular cloning of an invertebrate glutamate receptor subunit

expressed in Drosophila muscle. *Science*, *254*(5028), 112–114. https://doi.org/10.1126/science.1681587

Schweitzer, R., Zelzer, E., & Volk, T. (2010). Connecting muscles to tendons: tendons and musculoskeletal development in flies and vertebrates. *Development*, *137*(17), 2807–2817. https://doi.org/10.1242/dev.047498

Scott, R. W., & Olson, M. F. (2007). LIM kinases: function, regulation and association with human disease. *Journal of Molecular Medicine*, *85*(6), 555–568. https://doi.org/10.1007/s00109-007-0165-6

Sewry, C. A., Laitila, J. M., & Wallgren-Pettersson, C. (2019). Nemaline myopathies: a current view. *Journal of Muscle Research and Cell Motility*, *40*(2), 111–126. https://doi.org/10.1007/s10974-019-09519-9

Shishmarev, D. (2020). Excitation-contraction coupling in skeletal muscle: recent progress and unanswered questions. *Biophysical Reviews*, *12*(1), 143–153. https://doi.org/10.1007/s12551-020-00610-x

Shukla, V. K., Maheshwari, D., Jain, A., Tripathi, S., Kumar, D., & Arora, A. (2018). Structure, dynamics, and biochemical characterization of ADF/cofilin Twinstar from Drosophilamelanogaster. *Biochimica et Biophysica Acta. Proteins and Proteomics*, *1866*(8), 885–898. https://doi.org/10.1016/j.bbapap.2018.04.010

Shy, G. M., Engel, W. K., Somers, J. E., & Wanko, T. (1963). NEMALINE MYOPATHY. A NEW CONGENITAL MYOPATHY. *Brain: A Journal of Neurology*, *86*, 793–810. https://doi.org/10.1093/brain/86.4.793

Sigrist, S. J., Reiff, D. F., Thiel, P. R., Steinert, J. R., & Schuster, C. M. (2003). Experience-dependent strengthening of Drosophila neuromuscular junctions. *The Journal of Neuroscience*, *23*(16), 6546–6556. https://doi.org/10.1523/JNEUROSCI.23-16-06546.2003

Sigrist, S. J., Thiel, P. R., Reiff, D. F., & Schuster, C. M. (2002). The postsynaptic glutamate receptor subunit DGluR-IIA mediates long-term plasticity in Drosophila. *The Journal of Neuroscience*, *22*(17), 7362–7372. https://doi.org/10.1523/JNEUROSCI.22-17-07362.2002

Simon, A. F., Daniels, R., Romero-Calderón, R., Grygoruk, A., Chang, H.-Y., Najibi, R., Shamouelian, D., Salazar, E., Solomon, M., Ackerson, L. C., Maidment, N. T., Diantonio, A., & Krantz, D. E. (2009). Drosophila vesicular monoamine transporter mutants can adapt to reduced or eliminated vesicular stores of dopamine and serotonin. *Genetics*, *181*(2), 525–541. https://doi.org/10.1534/genetics.108.094110

Slater, C. R. (2015). The functional organization of motor nerve terminals. *Progress in Neurobiology*, *134*, 55–103. https://doi.org/10.1016/j.pneurobio.2015.09.004

Smith, B. K., Bleiweis, M. S., Zauhar, J., & Martin, A. D. (2011). Inspiratory muscle training in a child with nemaline myopathy and organ transplantation. *Pediatric Critical Care Medicine*, *12*(2), e94-8. https://doi.org/10.1097/PCC.0b013e3181dde680

Soler, C., Laddada, L., & Jagla, K. (2016). Coordinated Development of Muscles and Tendon-Like Structures: Early Interactions in the Drosophila Leg. *Frontiers in Physiology*, *7*, 22. https://doi.org/10.3389/fphys.2016.00022

Song, C., Leahy, S. N., Rushton, E. M., & Broadie, K. (2022). RNA-binding FMRP and Staufen sequentially regulate the Coracle scaffold to control synaptic glutamate receptor and bouton development. *Development*, *149*(9). https://doi.org/10.1242/dev.200045

Sonnemann, K. J., Fitzsimons, D. P., Patel, J. R., Liu, Y., Schneider, M. F., Moss, R. L., & Ervasti, J. M. (2006). Cytoplasmic gamma-actin is not required for skeletal muscle development but its absence leads to a progressive myopathy. *Developmental Cell*, *11*(3), 387–397. https://doi.org/10.1016/j.devcel.2006.07.001

Soreq, H., & Seidman, S. (2001). Acetylcholinesterase--new roles for an old actor. *Nature Reviews. Neuroscience*, *2*(4), 294–302. https://doi.org/10.1038/35067589

Sun, Y., Li, M., Geng, J., Meng, S., Tu, R., Zhuang, Y., Sun, M., Rui, M., Ou, M., Xing, G., Johnson, T. K., & Xie, W. (2023). Neuroligin 2 governs synaptic morphology and function through RACK1-cofilin signaling in Drosophila. *Communications Biology*, *6*(1), 1056. https://doi.org/10.1038/s42003-023-05428-3

Suzuki, M. (2006). The Drosophila tweety family: molecular candidates for large-conductance Ca2+-activated Cl- channels. *Experimental Physiology*, *91*(1), 141–147. https://doi.org/10.1113/expphysiol.2005.031773

Sztal, T. E., McKaige, E. A., Williams, C., Oorschot, V., Ramm, G., & Bryson-Richardson, R. J. (2018). Testing of therapies in a novel nebulin nemaline myopathy model demonstrate a lack of efficacy. *Acta Neuropathologica Communications*, *6*(1), 40. https://doi.org/10.1186/s40478-018-0546-9

Tajbakhsh, S., & Cossu, G. (1997). Establishing myogenic identity during somitogenesis. *Current Opinion in Genetics & Development*, *7*(5), 634–641. https://doi.org/10.1016/s0959-437x(97)80011-1

Tajbakhsh, S., Rocancourt, D., Cossu, G., & Buckingham, M. (1997). Redefining the genetic hierarchies controlling skeletal myogenesis: Pax-3 and Myf-5 act upstream of MyoD. *Cell*, *89*(1), 127–138. https://doi.org/10.1016/s0092-8674(00)80189-0

Talbot, J., & Maves, L. (2016). Skeletal muscle fiber type: using insights from muscle developmental biology to dissect targets for susceptibility and resistance to muscle disease. *Wiley Interdisciplinary Reviews. Developmental Biology*, *5*(4), 518–534. https://doi.org/10.1002/wdev.230

Tan, P., Briner, J., Boltshauser, E., Davis, M. R., Wilton, S. D., North, K., Wallgren-Pettersson, C., & Laing, N. G. (1999). Homozygosity for a nonsense mutation in the alpha-tropomyosin slow gene TPM3 in a patient with severe infantile nemaline myopathy. *Neuromuscular Disorders*, *9*(8), 573–579. https://doi.org/10.1016/s0960-8966(99)00053-x

Tanaka, K., Takeda, S., Mitsuoka, K., Oda, T., Kimura-Sakiyama, C., Maéda, Y., & Narita, A. (2018). Structural basis for cofilin binding and actin filament disassembly. *Nature Communications*, *9*(1), 1860. https://doi.org/10.1038/s41467-018-04290-w

Thirion, C., Stucka, R., Mendel, B., Gruhler, A., Jaksch, M., Nowak, K. J., Binz, N., Laing, N. G., & Lochmüller, H. (2001). Characterization of human muscle type cofilin (CFL2) in normal and regenerating muscle. *European Journal of Biochemistry / FEBS*, *268*(12), 3473–3482. https://doi.org/10.1046/j.1432-1327.2001.02247.x

Tobin, J. F., & Celeste, A. J. (2005). Myostatin, a negative regulator of muscle mass: implications for muscle degenerative diseases. *Current Opinion in Pharmacology*, *5*(3), 328–332. https://doi.org/10.1016/j.coph.2005.01.011

Torroja, L., Packard, M., Gorczyca, M., White, K., & Budnik, V. (1999). The Drosophila beta-amyloid precursor protein homolog promotes synapse differentiation at the neuromuscular junction. *The Journal of Neuroscience*, *19*(18), 7793–7803. https://doi.org/10.1523/JNEUROSCI.19-18-07793.1999

Toshima, J., Toshima, J. Y., Amano, T., Yang, N., Narumiya, S., & Mizuno, K. (2001). Cofilin phosphorylation by protein kinase testicular protein kinase 1 and its role in integrin-mediated actin reorganization and focal adhesion formation. *Molecular Biology of the Cell*, *12*(4), 1131–1145. https://doi.org/10.1091/mbc.12.4.1131

Tran, & Smith. (2017). Anesthetic consideration for patients with nemaline rod myopa- thy: a literature review. *Pediatric Anesthesia & Critical Care Journal*.

Tran, N. H., & Chhibber, A. (2016). Anesthetic management of a pediatric patient with NEB1-Genotype Nemaline Rod Myopathy for cleft palate repair. *PEDIATRIC ANESTHESIA AND CRITICAL CARE JOURNAL*, *4*(2), 78–82.

Vandekerckhove, J., & Weber, K. (1978). At least six different actins are expressed in a higher mammal: an analysis based on the amino acid sequence of the amino-terminal tryptic peptide. *Journal of Molecular Biology*, *126*(4), 783–802. https://doi.org/10.1016/0022-2836(78)90020-7

van der Plas, M. C., Pilgram, G. S. K., Plomp, J. J., de Jong, A., Fradkin, L. G., & Noordermeer, J. N. (2006). Dystrophin is required for appropriate retrograde control of neurotransmitter release at the Drosophila neuromuscular junction. *The Journal of Neuroscience*, *26*(1), 333–344. https://doi.org/10.1523/JNEUROSCI.4069-05.2006

Van Troys, M., Huyck, L., Leyman, S., Dhaese, S., Vandekerkhove, J., & Ampe, C. (2008). Ins and outs of ADF/cofilin activity and regulation. *European Journal of Cell Biology*, *87*(8–9), 649–667. https://doi.org/10.1016/j.ejcb.2008.04.001

Varland, S., Vandekerckhove, J., & Drazic, A. (2019). Actin Post-translational Modifications: The Cinderella of Cytoskeletal Control. *Trends in Biochemical Sciences*, *44*(6), 502–516. https://doi.org/10.1016/j.tibs.2018.11.010

Vartiainen, M. K., Mustonen, T., Mattila, P. K., Ojala, P. J., Thesleff, I., Partanen, J., & Lappalainen, P. (2002). The three mouse actin-depolymerizing factor/cofilins evolved to fulfill cell-type-specific requirements for actin dynamics. *Molecular Biology of the Cell*, *13*(1), 183–194. https://doi.org/10.1091/mbc.01-07-0331

Venuti, J. M., Morris, J. H., Vivian, J. L., Olson, E. N., & Klein, W. H. (1995). Myogenin is required for late but not early aspects of myogenesis during mouse development. *The Journal of Cell Biology*, *128*(4), 563–576. https://doi.org/10.1083/jcb.128.4.563

Vignier, N., Chatzifrangkeskou, M., Pinton, L., Wioland, H., Marais, T., Lemaitre, M., Le Dour, C., Peccate, C., Cardoso, D., Schmitt, A., Wu, W., Biferi, M.-G., Naouar, N., Macquart, C., Beuvin, M., Decostre, V., Bonne, G., Romet-Lemonne, G., Worman, H. J., … Muchir, A. (2021). The non-muscle ADF/cofilin-1 controls sarcomeric actin filament integrity and force production in striated muscle laminopathies. *Cell Reports*, *36*(8), 109601. https://doi.org/10.1016/j.celrep.2021.109601

Viswanathan, M. C., Blice-Baum, A. C., Schmidt, W., Foster, D. B., & Cammarato, A. (2015). Pseudo-acetylation of K326 and K328 of actin disrupts Drosophila melanogaster indirect flight muscle structure and

performance. *Frontiers in Physiology*, *6*, 116. https://doi.org/10.3389/fphys.2015.00116

von der Hagen, M., Kress, W., Hahn, G., Brocke, K. S., Mitzscherling, P., Huebner, A., Müller-Reible, C., Stoltenburg-Didinger, G., & Kaindl, A. M. (2008). Novel RYR1 missense mutation causes core rod myopathy. *European Journal of Neurology*, *15*(4), e31–e32. https://doi.org/10.1111/j.1468-1331.2008.02094.x

Wagh, D. A., Rasse, T. M., Asan, E., Hofbauer, A., Schwenkert, I., Dürrbeck, H., Buchner, S., Dabauvalle, M.-C., Schmidt, M., Qin, G., Wichmann, C., Kittel, R., Sigrist, S. J., & Buchner, E. (2006). Bruchpilot, a protein with homology to ELKS/CAST, is required for structural integrity and function of synaptic active zones in Drosophila. *Neuron*, *49*(6), 833–844. https://doi.org/10.1016/j.neuron.2006.02.008

Wagner, C. R., Mahowald, A. P., & Miller, K. G. (2002). One of the two cytoplasmic actin isoforms in Drosophila is essential. *Proceedings of the National Academy of Sciences of the United States of America*, *99*(12), 8037–8042. https://doi.org/10.1073/pnas.082235499

Wallgren-Pettersson, C, & Laing, N. G. (2000). Report of the 70th ENMC International Workshop: nemaline myopathy, 11-13 June 1999, Naarden, The Netherlands. *Neuromuscular Disorders*, *10*(4–5), 299–306. https://doi.org/10.1016/s0960-8966(99)00129-7

Wallgren-Pettersson, C, Sainio, K., & Salmi, T. (1989). Electromyography in congenital nemaline myopathy. *Muscle & Nerve*, *12*(7), 587–593. https://doi.org/10.1002/mus.880120710

Wallgren-Pettersson, Carina, Bushby, K., Mellies, U., Simonds, A., & ENMC. (2004). 117th ENMC workshop: ventilatory support in congenital neuromuscular disorders -- congenital myopathies, congenital muscular dystrophies, congenital myotonic dystrophy and SMA (II) 4-6 April 2003, Naarden, The Netherlands. *Neuromuscular Disorders*, *14*(1), 56–69. https://doi.org/10.1016/j.nmd.2003.09.003

Wallgren-Pettersson, Carina, Donner, K., Sewry, C., Bijlsma, E., Lammens, M., Bushby, K., Giovannucci Uzielli, M. L., Lapi, E., Odent, S., Akcoren, Z., Topaloğlu, H., & Pelin, K. (2002). Mutations in the nebulin gene can cause severe congenital nemaline myopathy. *Neuromuscular Disorders*, *12*(7–8), 674–679. https://doi.org/10.1016/s0960-8966(02)00065-2

Wang, C.-T., Bai, J., Chang, P. Y., Chapman, E. R., & Jackson, M. B. (2006). Synaptotagmin-Ca2+ triggers two sequential steps in regulated exocytosis in rat PC12 cells: fusion pore opening and fusion pore dilation. *The Journal*

of Physiology, *570*(Pt 2), 295–307. https://doi.org/10.1113/jphysiol.2005.097378

Wang, C. H., Dowling, J. J., North, K., Schroth, M. K., Sejersen, T., Shapiro, F., Bellini, J., Weiss, H., Guillet, M., Amburgey, K., Apkon, S., Bertini, E., Bonnemann, C., Clarke, N., Connolly, A. M., Estournet-Mathiaud, B., Fitzgerald, D., Florence, J. M., Gee, R., … Yuan, N. (2012). Consensus statement on standard of care for congenital myopathies. *Journal of Child Neurology*, *27*(3), 363–382. https://doi.org/10.1177/0883073812436605

Wang, D., Zhang, L., Zhao, G., Wahlström, G., Heino, T. I., Chen, J., & Zhang, Y. Q. (2010). Drosophila twinfilin is required for cell migration and synaptic endocytosis. *Journal of Cell Science*, *123*(Pt 9), 1546–1556. https://doi.org/10.1242/jcs.060251

Wang, S. J. H., Tsai, A., Wang, M., Yoo, S., Kim, H.-Y., Yoo, B., Chui, V., Kisiel, M., Stewart, B., Parkhouse, W., Harden, N., & Krieger, C. (2014). Phospho-regulated Drosophila adducin is a determinant of synaptic plasticity in a complex with Dlg and PIP2 at the larval neuromuscular junction. *Biology Open*, *3*(12), 1196–1206. https://doi.org/10.1242/bio.20148342

White, R. B., Biérinx, A.-S., Gnocchi, V. F., & Zammit, P. S. (2010). Dynamics of muscle fibre growth during postnatal mouse development. *BMC Developmental Biology*, *10*, 21. https://doi.org/10.1186/1471-213X-10-21

Wickham, H. (2009). *ggplot2: Elegant Graphics for Data Analysis* (Version 978-0-387-98140-6) [Computer software]. Springer-Verlag.

Wickham, H. (2016). ggplot2: Elegant Graphics for Data Analysis. *Springer-Verlag New York*.

Wilkinson, K. A. (2021). Methodological advances for studying gamma motor neurons. *Current Opinion in Physiology*, *19*, 135–140. https://doi.org/10.1016/j.cophys.2020.10.002

Windner, S. E., Manhart, A., Brown, A., Mogilner, A., & Baylies, M. K. (2019). Nuclear Scaling Is Coordinated among Individual Nuclei in Multinucleated Muscle Fibers. *Developmental Cell*, *49*(1), 48-62.e3. https://doi.org/10.1016/j.devcel.2019.02.020

Wioland, H., Jegou, A., & Romet-Lemonne, G. (2019). Torsional stress generated by ADF/cofilin on cross-linked actin filaments boosts their severing. *Proceedings of the National Academy of Sciences of the United States of America*, *116*(7), 2595–2602. https://doi.org/10.1073/pnas.1812053116

Xing, G., Li, M., Sun, Y., Rui, M., Zhuang, Y., Lv, H., Han, J., Jia, Z., & Xie, W. (2018). Neurexin-Neuroligin 1 regulates synaptic morphology and functions via the WAVE regulatory complex in Drosophila neuromuscular junction. *ELife*, *7*. https://doi.org/10.7554/eLife.30457

Yin, X., Pu, C., Wang, Z., Li, K., & Wang, H. (2021). Clinico-pathological features and mutational spectrum of 16 nemaline myopathy patients from a Chinese neuromuscular center. *Acta Neurologica Belgica*. https://doi.org/10.1007/s13760-020-01542-9

Yoshihara, M., Rheuben, M. B., & Kidokoro, Y. (1997). Transition from growth cone to functional motor nerve terminal in Drosophila embryos. *The Journal of Neuroscience*, *17*(21), 8408–8426. https://doi.org/10.1523/JNEUROSCI.17-21-08408.1997

Zapater I Morales, C., Carman, P. J., Soffar, D. B., Windner, S. E., Dominguez, R., & Baylies, M. K. (2023). Drosophila Tropomodulin is required for multiple actin-dependent processes within developing myofibers. *Development*, *150*(6). https://doi.org/10.1242/dev.201194

Zhang, B., & Stewart, B. (2010). Voltage-clamp analysis of synaptic transmission at the Drosophila larval neuromuscular junction. *Cold Spring Harbor Protocols*, *2010*(9), pdb.prot5488. https://doi.org/10.1101/pdb.prot5488

Zheng, K., Kitazato, K., Wang, Y., & He, Z. (2016). Pathogenic microbes manipulate cofilin activity to subvert actin cytoskeleton. *Critical Reviews in Microbiology*, *42*(5), 677–695. https://doi.org/10.3109/1040841X.2015.1010139

Zhou, Q., Xiao, M. Y., & Nicoll, R. A. (2001). Contribution of cytoskeleton to the internalization of AMPA receptors. *Proceedings of the National Academy of Sciences*, *98*(3), 1261–1266. https://doi.org/10.1073/pnas.98.3.1261

Zhu, H., Yang, H., Zhao, S., Zhang, J., Liu, D., Tian, Y., Shen, Z., & Su, Y. (2018). Role of the cofilin 2 gene in regulating the myosin heavy chain genes in mouse myoblast C2C12 cells. *International Journal of Molecular Medicine*, *41*(2), 1096–1102. https://doi.org/10.3892/ijmm.2017.3272

Zito, K., Fetter, R. D., Goodman, C. S., & Isacoff, E. Y. (1997). Synaptic clustering of Fascilin II and Shaker: essential targeting sequences and role of Dlg. *Neuron*, *19*(5), 1007–1016. https://doi.org/10.1016/s0896-6273(00)80393-1

Zito, K., Parnas, D., Fetter, R. D., Isacoff, E. Y., & Goodman, C. S. (1999). Watching a synapse grow: noninvasive confocal imaging of synaptic growth

in Drosophila. *Neuron*, *22*(4), 719–729. https://doi.org/10.1016/s0896-6273(00)80731-x

Zuccaro, E., Piol, D., Basso, M., & Pennuto, M. (2021). Motor neuron diseases and neuroprotective peptides: A closer look to neurons. *Frontiers in Aging Neuroscience*, *13*, 723871. https://doi.org/10.3389/fnagi.2021.723871

Zwart, M. F., Randlett, O., Evers, J. F., & Landgraf, M. (2013). Dendritic growth gated by a steroid hormone receptor underlies increases in activity in the developing Drosophila locomotor system. *Proceedings of the National Academy of Sciences of the United States of America*, *110*(40), E3878-87. https://doi.org/10.1073/pnas.1311711110